Effects of grain size and Mg contents on deformation behavior and strengthening mechanisms in Al-Mg alloys

2021

LAN XIAODONG

Effects of grain size and Mg contents on deformation behavior and strengthening mechanisms in Al-Mg alloys

LAN XIAODONG

Department of Materials Science and Engineering

Graduate School of Engineering

Kyoto University

2021

Contents

Chapter 1 Introduction

1.1 Background

The continued pursuit for structural materials with superior mechanical properties, and the increasing necessity to save energy and reduce emissions, have posed high demands on material scientists to research, not only into the development of established materials and processing routes, but also the design of novel alloys and advanced processing techniques. In automotive and aviation industry, reducing structural weight is one of the major ways to meet the stringent requirements for reduced emissions and improved fuel economy. On the other hand, improving the performance and service life of structural components used in automobiles and aircrafts are essential demands to guarantee the consumers' safety, which should always be the first priority. Therefore, there is an increasing trend to use lightweight structural materials like aluminum alloys for various commercial applications due to their high specific strength, good formability and decent machinability [1–3]. A thorough understanding of the mechanical behaviors and strengthening mechanisms in aluminum alloys will be very important for guiding the structural design of novel alloys with high strength and large ductility which will find a wide range of applications.

1.2 Aluminum alloys and general properties

Aluminum is the third most abundant element in the earth's crust, and the most abundant metallic element. It has a face-centered cubic (FCC) crystal structure and a density of 2.7 g/cm^3, around one-third that of iron or copper, which makes it one of the lightest commercially available metals. The substantial strength to weight ratio makes it of especially good use where light materials with good mechanical properties are needed. Pure aluminum is soft and ductile. However, most commercial applications require higher strength than pure aluminum can afford. The addition of alloying elements like copper, manganese, silicon, magnesium and zinc can increase the

strength properties of aluminum and produce an alloy with properties tailored to particular applications. To characterize the different aluminum alloys, they are grouped by their respective production process and alloying elements. The roughest differentiation exists between wrought and cast aluminum alloys. The main difference between wrought and cast aluminum alloys is the microstructures that the production process generates. Both sets can be further divided into heat-treatable and non-heat-treatable alloys. This dissertation deals only with wrought aluminum, the properties of cast aluminum will not be mentioned further. Wrought aluminum alloys are typically divided into 7 series with each series corresponding to specific alloying elements, as listed in Table 1-1.

Table 1-1 Wrought aluminum alloy designation system.

Series	Major alloying elements	Heat treatable or not
1xxx	Al ≥ 99%	Non-heat-treatable
2xxx	Cu	Heat-treatable
3xxx	Mn	Non-heat-treatable
4xxx	Si	Non-heat-treatable
5xxx	Mg	Non-heat-treatable
6xxx	Mg + Si	Heat-treatable
7xxx	Zn + Mg + Cu	Heat-treatable

The initial strength of heat-treatable aluminum alloys (2xxx, 6xxx and 7xxx series) is enhanced by the addition of alloying elements. Further strengthening can be achieved through the precipitation of a special hardening phase during heat treatment or aging. Therefore, the mechanical properties of heat-treatable aluminum alloys can be adjusted after forming, which makes for superior fabricability. Non-heat-treatable aluminum alloys (1xxx, 3xxx, 4xxx and 5xxx series) show no significant precipitation hardening and are mostly strengthened via working

hardening or solid solution hardening. Fig. 1.1 shows the relationship between the tensile strength and elongation in various types of aluminum alloys [4,5], where a trade-off relationship between the strength and ductility can be observed. In this graph, the heat-treatable aluminum alloys, for example, the 2xxx and 7xxx series exhibit very high tensile strength but limited ductility. In contrast, the non-heat-treatable 1xxx and 3xxx series show low tensile strength but large ductility. It is noteworthy that 5xxx series (Al-Mg alloys) possess a relatively good balance between strength and ductility, compared with other aluminum alloys. The simultaneous increase in both strength and ductility is highly required, because high strength allows structural components to carry high load and large ductility is essential to prevent catastrophic failure.

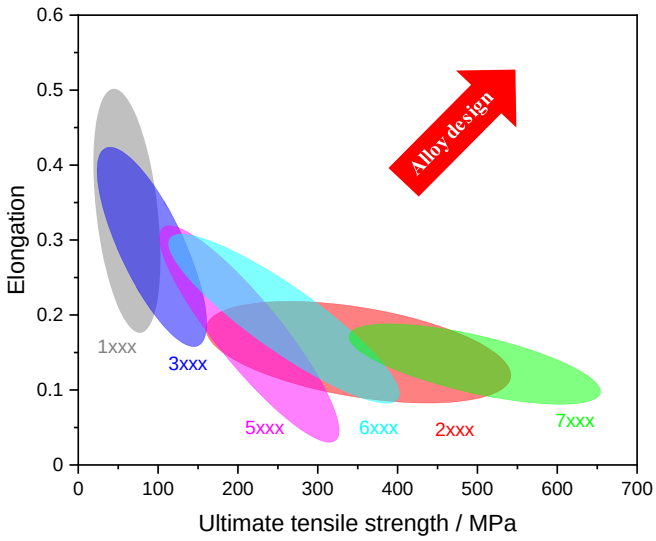

Fig. 1.1 General relationship between tensile strength and elongation in various types of aluminum alloys [4,5].

It's noted that different alloying elements contribute to significantly different mechanical properties of aluminum alloys. One of the underlying principles for alloying is that alloying elements influence the microscopic deformation mechanism that governs the macroscopic mechanical behavior. Fig. 1.2 shows the true tress-strain curves for three representative aluminum alloys (1100-Al [4], Al-5Mg [6] and 7075-T6 alloy [7]). The stress-strain behaviors clearly show

that, heat-treatable aluminum alloy exhibits high yield strength but low work hardening and limited ductility, whereas non-heat-treatable Al-Mg alloy shows relatively low yield strength but excellent work hardening and favorable ductility. The relatively good balance between strength and ductility in Al-Mg alloys results from the excellent work-hardening ability. As a material with single-phase structure, the outstanding work-hardening ability of Al-Mg alloys is believed to be induced by Mg addition. Meanwhile, adding Mg can further reduce the density of the alloy, which is desirable for weight reduction. It is therefore of value to investigate Al-Mg alloys with different Mg contents as candidates that lead to more enhanced mechanical properties.

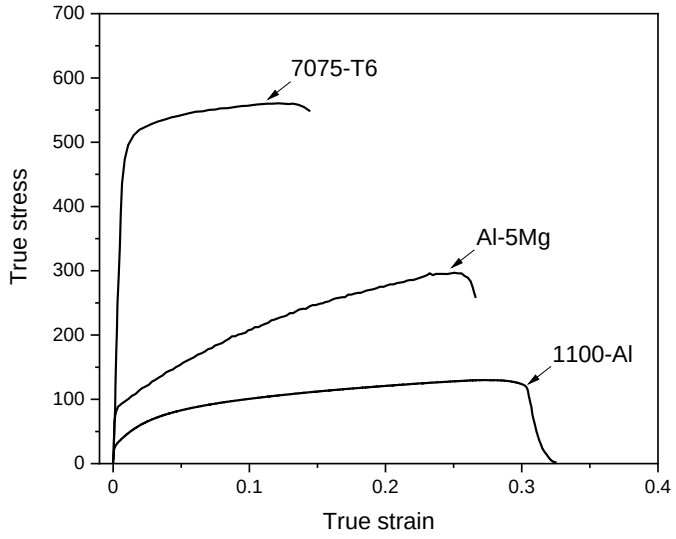

Fig. 1.2 True tress-strain curves for three representative aluminum alloys.

1.3 Al-Mg alloys and strengthening mechanisms

Al-Mg alloys constitute an important class of lightweight structural materials which find wide applications in automotive and aviation industry. The high solubility of Mg in Al at elevated temperatures (maximum 15 wt.% at 450 ℃) and the large atomic size mismatch (12%) between Al and Mg atoms make Mg one of the alloying elements that can provide effective enhancement of strength, while maintaining a high specific strength and a relatively low production cost. The

constant demand for a reduction in the weight of structural components, coupled with an increase in strength-ductility synergy, has focused attention on the development of Al-Mg alloys with high strength and large ductility. Thus, further improvements in the understanding of mechanical properties and strengthening mechanisms in Al-Mg alloys are highly required.

As an important class of non-heat-treatable aluminum alloys, Al-Mg alloys are mostly strengthened by solid solution hardening, grain boundary strengthening, work hardening, or, the combination of these methods. Strength and ductility are two of the most important mechanical properties of structural materials. However, the strength-ductility synergy has never been achieved in coarse-grained metallic materials. It is well-known that grain refinement can effectively improve the yield strength of metallic materials without changing the chemical composition, as described by the Hall-Petch relationship [8]:

$$\sigma_{YS} = \sigma_0 + k_{HP} d^{-1/2} \qquad (1-1)$$

where σ_{YS} is the yield strength, σ_0 is the friction stress, k_{HP} (Hall-Petch slope) is a constant that describes the relative strengthening contribution of grain boundaries and d is the mean grain size of the material. Significant grain size refinement can be achieved by various severe plastic deformation processes [9], which leads to ultra-high strength according to the Hall-Petch relationship. Unfortunately, the ductility is usually deteriorated when the grain size decreases down to ultrafine range, as shown in Fig. 1.3 [10], which is known as the trade-off relationship between strength and ductility. The poor tensile ductility, especially the limited uniform elongation of ultrafine-grained materials, severely limits their applications in the industry. The uniform elongation of a material during tensile deformation is determined by the plastic instability condition:

$$\sigma \geq \frac{\mathrm{d}\sigma}{\mathrm{d}\varepsilon} \qquad (1-2)$$

where σ is flow stress, ε is true strain, and dσ/dε is work-hardening rate. According to the plastic instability condition, necking will occur when the flow stress becomes larger than the work-hardening rate. The yield stress increases with decreasing grain size without any accompanying increase in work-hardening rate, leading to the occurrence of plastic instability at very early stage of tensile test in the ultrafine-grained materials. In order to obtain enough uniform elongation in the ultrafine-grained materials, in turn, the Eq. (1-2) also suggests that it is necessary to enhance the work hardening of the material by any means. Improving the uniform elongation of ultrafine-grained materials has been a challenging issue for industrial applications.

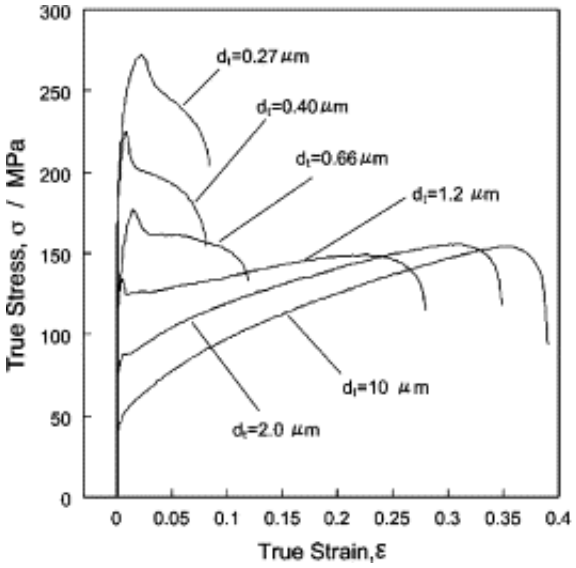

Fig. 1.3 True stress-strain curves of the 1100-Al with various grain sizes produced by accumulative roll-bonding and subsequent annealing [10].

On the other hand, many studies have shown that increasing Mg content in Al-Mg alloys leads to an enhancement of both yield strength and work-hardening capacity without significantly sacrificing the ductility [11,12], as shown in Fig. 1.4. Therefore, it's reasonable to anticipate that high strength and large ductility could be achieved through combining optimized grain refinement with Mg addition. Furthermore, it should be noted that the effects of grain size and Mg content on the mechanical properties of Al-Mg alloys may be far more complicated since some researchers

have reported that solute segregation during annealing can have significant effect on the mechanical properties and deformation behaviors of structural materials [13,14]. Murdoch and Schuh [15] have reported that Mg has a positive enthalpy of segregation in Al and would therefore have an energetic preference to segregate to the grain boundaries. It seems possible that grain boundary segregation may occur in Al-Mg alloys during annealing and alter the structure of the grain boundary. And it has already been noticed that the Hall-Petch slope for Al-Mg alloy is significantly larger than that of pure Al [16–18], which suggests that the addition of solute Mg contributes not only to solid solution hardening but also to enhanced grain boundary strengthening. These results indicate that there are some possibilities to further improve the mechanical properties of Al-Mg alloys. However, there are still lack of details about the underlying physics of yielding phenomenon that relates to solute segregation and the relationship between Hall-Petch slope and global Mg content. Thus, it is necessary to investigate the combined effects of grain size and Mg content on the mechanical properties and strengthening mechanisms in Al-Mg alloys, for managing both high strength and large ductility.

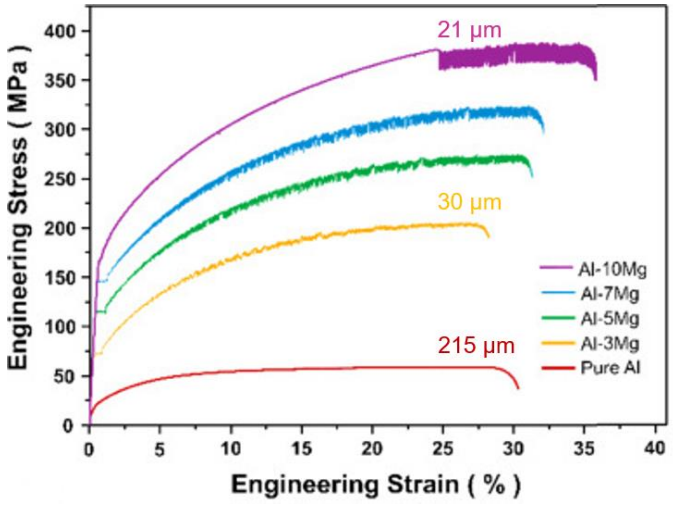

Fig. 1.4 Engineering stress-strain curves of Al-Mg alloys with different Mg contents [11].

1.4 High work hardening in Al-Mg alloys

Work hardening is one of the most important factors in the evaluation of plastic deformation, and it is critical for the stability of plastic flow against strain localization. The tensile strength and ductility of materials are closely related to the work-hardening capacity [19]. Therefore, a thorough understanding of the work-hardening behavior in terms of the fundamental mechanisms has attracted tremendous interest for its importance in advanced manufacturing processes and novel alloy design. As mentioned in the previous section, increasing Mg content can significantly increase the work-hardening ability of Al-Mg alloys, resulting in a better strength-ductility balance. But the underlying mechanism of the improved strength-ductility synergy has not been fully explored. It has been believed that work hardening is governed by the evolution of dislocation structures and the extent of work hardening with increments in the dislocation density can be well described by the Bailey-Hirsch relationship [20]. The dislocation density is determined by two competing processes: one is athermal storage of forest dislocations and the other is dynamic recovery due to thermally activated dislocation rearrangements and annihilation. The effect of Mg atoms on the work hardening of Al-Mg alloys should be attributed to their effects on these two processes.

The most frequently quoted explanation for the enhanced work-hardening rate with increasing Mg content is based on a viewpoint of stacking fault energy (SFE). It is well known that pure Al is a high SFE material, dynamic recovery can easily take place through the cross slip of dislocations during deformation, facilitating the formation of dislocation cell structures [11,21]. This cell structure has a low dislocation storage capacity, that's why pure Al exhibits low work hardening during tensile deformation [11]. Intensive investigations have been carried out on the microstructure evolution and work hardening in Al-Mg alloys [21–24]. It has been shown that the

addition of solute Mg can inhibit cell structure formation and result in a higher work-hardening rate, which is often considered to be attributed to Mg addition reduces the SFE [11,25–27], as shown in Fig. 1.5. The conventional view considers that the SFE decreases with increasing Mg content, which results in the recombination of partial dislocations becoming difficult, thus limiting dislocation cross slip. Note that the judgment is mainly based on theoretical calculation, while direct experimental data are not available.

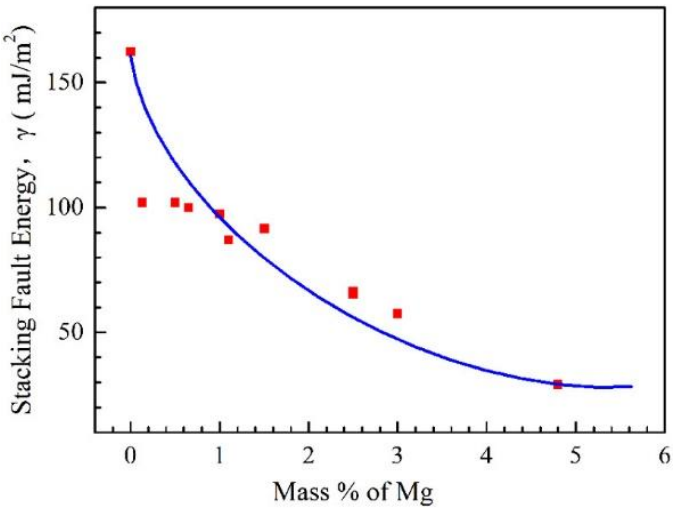

Fig. 1.5 Effect of Mg content on stacking fault energy in aluminum alloys [26,27].

Despite there are some published results showing that stacking faults and micro twins can be observed in some severely deformed Al-Mg alloys [28,29] or shock-loaded Al-Mg alloys at low temperature [30], the dislocation dissociation is so weak that no direct experimental evidence has ever shown stacking faults or deformation twins in Al-Mg alloys under quasi-static tensile deformation at room temperature. Therefore, it is believed that the SFE should still be remarkably high in Al-Mg alloys. In addition, a comparative study on the work hardening of Al-Mg and Al-Cu alloys revealed no significant difference in dislocation structures and work-hardening behaviors, in spite of the opposite effects of Mg and Cu on the SFE of Al matrix [31]. If the explanation based on SFE were established, adding Cu should increase the SFE of Al and therefore

well-defined cell structures would occur in Al-Cu alloy. But the dislocation structure in Al-Cu alloy is very similar to that observed in Al-Mg alloy. These experimental evidence suggest that the reduction of SFE induced by Mg addition may not be the main cause that is responsible for the high work-hardening ability of Al-Mg alloys. Thus, an alternative interpretation is proposed that the microstructure evolution in aluminum alloys is controlled by solute-dislocation interactions rather than the stacking fault-induced barriers for cross slip [31]. But the detailed mechanism for the enhanced work-hardening rate by increasing Mg content has not been perfectly clarified yet. A thorough understanding of this mechanism is indispensable for designing new, improved alloys.

1.5 Heterogeneous deformation in Al-Mg alloys

In general, due to solid solution hardening and enhanced work hardening, an increase in Mg content leads to higher yield strength and ultimate tensile strength in Al-Mg alloys. Meanwhile, the deformation behavior changes with increasing Mg content, manifested by the serrated flow in the stress-strain curve, as shown in Fig. 1.4. The serrated flow is also understood in terms of the Portevin-Le Chatelier (PLC) effect [32–34]. PLC effect is a commonly observed heterogeneous deformation behavior in Al-Mg alloys. The most distinct features of PLC effect are the localized deformation bands and the motion of these bands along the specimen with increasing stress, as schematically illustrated in Fig. 1.6. Upon deformation at room temperature, Al-Mg alloys exhibit undesirable deformation traces on the as-formed sheet surface as a result of strain localization, which create undesired optical effects and limit sheet-forming applications. Understanding the fundamental features of the PLC effect is crucial for the effective use of Al-Mg alloys, and therefore more attention should be devoted to the heterogeneous deformation in Al-Mg alloys.

The PLC effect has been studied extensively since its discovery. Various types of deformation bands induced by the PLC effect are known to exist. In general, the PLC bands can be classified

into three types (assigned as type A, type B, and type C) based on the morphologies of serrations that appear in the stress-strain curve of materials during constant strain rate tensile tests, and their characteristics are well documented [35]. Fig. 1.6 shows the schematics of motion, spatiotemporal appearances and stress-strain curve characteristics of these PLC bands [36]. The nucleation and propagation behaviors of PLC bands are directly related to the morphologies of the serrations in the stress-strain curve. Type A serrations are associated with repetitive continuous propagation of deformation bands along the gauge part of the sample and are often nucleated at one end of gauge part. Type B serrations correspond to a hopping propagation of localized bands in the axial tensile direction of the sample. Type C serrations are characterized by random nucleation of localized non-propagating bands accompanied by large stress drops. The appearance of the PLC bands can change from type A to type B and then to type C, either with decreasing strain rate or increasing temperature [37,38]. The PLC effect affects most material properties. Dynamic strain aging has generally been known to cause blue brittleness that deteriorates ductility at high temperatures or low strain rates [39,40]. On the other hand, the work hardening of materials is significantly enhanced under dynamic strain aging conditions [41]. If the serrated flow is properly controlled based on fundamental understanding of its mechanism, good work hardening is expected to be achieved, leading to high strength and large ductility of the material.

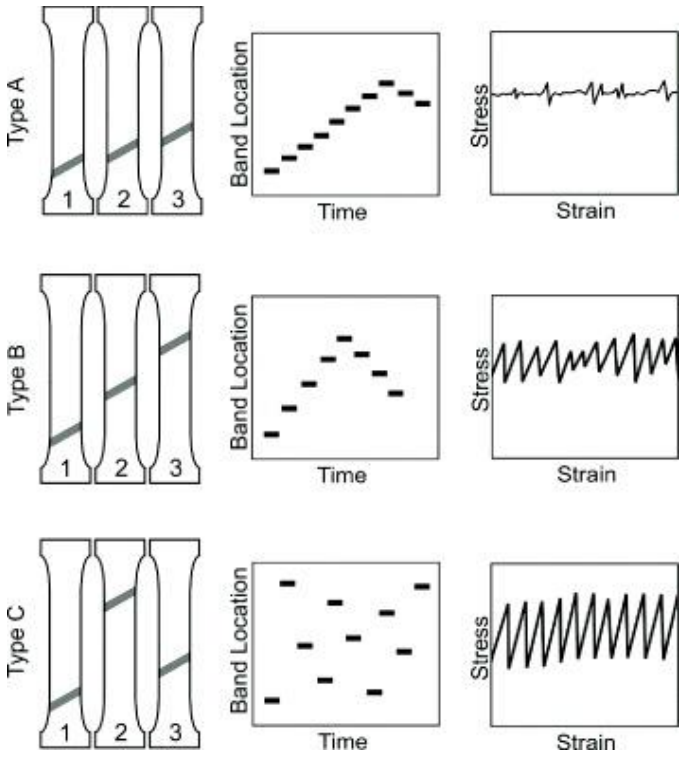

Fig. 1.6 Schematics of motion, spatiotemporal appearances and strain-controlled tensile curve characteristics of the PLC bands [41].

Several models have been proposed to explain different types of PLC instabilities occurring during plastic flow, the most commonly accepted explanation is based on a model called dynamic strain aging [42–44], which is defined as interaction between the moving dislocations and solute atoms. The mobile dislocations act as carriers of the plastic deformation according to this mechanism, and move unsteadily among the obstacles formed by other defects. There are two main solute-dislocation interaction models for dynamic strain aging in substitutional alloys: (I) PLC effect occurs with the fast long-range diffusion (lattice diffusion) of solute atoms at a rate faster than the speed of the moving dislocations so as to catch and lock them [45]; (II) Another consideration is that the diffusion of solute atoms might occur along the dislocation core (pipe diffusion) during the residence time of dislocations at obstacles [34,46,47]. The underlying atomistic interaction mechanisms between solute atoms and dislocations are still under debate. All

models agree on attributing the jerky dislocation motion and the resulting serrated flow pattern to a dynamic solute-dislocation interaction. In this perception, dislocation motion is assumed to be hindered by solute atoms that segregate to them. The dislocations are then assumed to overcome the obstacles collectively at a slightly higher resolved shear stress, resulting in negative strain sensitivity, leading to flow instability, i.e. the PLC effect [34].

However, there is still a gap between atomic-scale solute-dislocation interactions and macroscopic band behaviors during tensile deformation. It is hypothesized that the change of localized deformation behaviors is due to transition in operative dynamic strain aging mechanisms based on relative differences between the diffusion rate of the solute atoms and the velocity of the mobile dislocations throughout the dynamic strain aging domain. Nevertheless, the solute-dislocation interaction models suggest that the Mg content does play an important role, as shown in Fig. 1.4, since high solute content can provide more abundant atoms for pinning arrested dislocations. In addition, recent studies on the PLC effect in substitutional alloys have shown that the behavior of serrated flow is also dependent on grain size. Experimental results on A1-Mg [48,49] and Cu-Zn [50] alloys have shown that the critical strain for the onset of serrated flow increases with increasing grain size. The serration amplitude was also found to decrease with increasing grain size in an Al-Mg-Si alloy [51], as shown in Fig. 1.7. Some consideration has been proposed that dynamic strain aging may occur preferentially at grain boundaries [52]. If dynamic strain aging does occur preferentially at grain boundaries, then it has been argued that this trend would provide a reasonable explanation of why fine-grained materials have enhanced dynamic strain aging properties. It is possibly useful to visualize grain boundaries as one specific form of local obstacles to dislocation motion at which the enhanced aging of dislocations takes place. Intensive studies have been carried out to investigate the effects of strain rate and temperature on

the nature of PLC effect, there has been no systematic study of the effects of solute content and grain size on the localized deformation behaviors so far. This becomes an important issue since Mg addition and grain refinement are the main methods to further improve the comprehensive mechanical properties of Al-Mg alloys. The investigation will provide new insights into localized deformation behaviors, and may contribute to the understanding of the macro-deformation mechanism induced by dynamic strain aging.

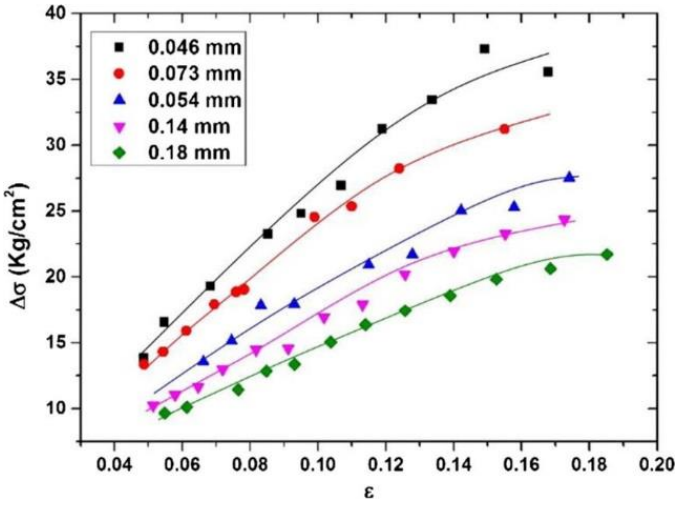

Fig. 1.7 The effect of grain size on the strain dependence of serration amplitude in the Al-Mg-Si alloy [51].

1.6 Purpose of the present study

The main purposes of the present study are as follows:

(1) To clarify the combined effects of grain size and Mg content on the mechanical properties and strengthening mechanisms in Al-Mg alloys, for managing both high strength and large ductility.

(2) To investigate the effect of solute Mg on the evolution of dislocation density during tensile deformation and the mechanism of high work-hardening ability in Al-Mg alloys.

(3) To understand the fundamental features of the serrated flow and the relevant mechanisms of heterogeneous deformation in Al-Mg alloys.

1.7 Dissertation outline

The dissertation is composed of five chapters.

In Chapter 1, the background and purpose of this study were introduced.

In Chapter 2, the combined effects of grain size and Mg content on the mechanical properties and strengthening mechanisms in Al-Mg alloys were systematically investigated. Systematic tensile tests confirmed the accurate and reliable Hall-Petch relationships, where extra-hardening phenomena accompanying with discontinuous yielding behaviors were observed in the fine-grained alloys. It was found that the addition of solute Mg contributed not only to solid solution hardening, but also to enhanced grain boundary strengthening due to an increased Hall-Petch slope. In addition, increasing Mg content could postpone the occurrence of drastic loss of ductility induced by the enhanced early plastic instability associated with the occurrence of discontinuous yielding behavior in ultrafine-grained alloys.

In Chapter 3, the effects of solute Mg on the microstructure evolution and work hardening in Al-Mg alloys having similar grain size were investigated. The tensile results showed that Al-Mg alloys with higher Mg contents exhibited higher work-hardening rate, as well as better strength-ductility balance than those with lower Mg contents. The in-situ synchrotron XRD results showed that the dislocation density accumulated much faster with strain in Al-Mg alloys with higher Mg contents. TEM observations revealed that the addition of solute Mg could hinder dislocation cross slip and promote a transition from wavy slip to planar slip. It was concluded that the excellent tensile properties and work-hardening ability of the Al-Mg alloys were mainly caused by the high dislocation density induced by the solute Mg-dislocation interactions.

In chapter 4, the spatiotemporal characteristics associated with heterogeneous deformation behaviors in Al-Mg alloys were investigated to reveal the relevant mechanisms. It was found that

the characteristics of PLC bands depended strongly on Mg content and grain size. The local rearrangement of solute Mg by cross-core diffusion could be applied as a partial mechanism to explain the PLC effect, and detailed analysis suggested that both dynamic strain aging and intensive dislocation interactions were necessary prerequisites to produce the PLC instabilities.

In chapter 5, the main research accomplishments and final conclusions of the dissertation are summarized.

References

[1] T. Dursun, C. Soutis, Recent developments in advanced aircraft aluminium alloys, Mater. Des. 56 (2014) 862–871. https://doi.org/https://doi.org/10.1016/j.matdes.2013.12.002.

[2] Y. Liu, M. Liu, X. Chen, Y. Cao, H.J. Roven, M. Murashkin, R.Z. Valiev, H. Zhou, Effect of Mg on microstructure and mechanical properties of Al-Mg alloys produced by high pressure torsion, Scr. Mater. 159 (2019) 137–141.

[3] H. Aboulfadl, J. Deges, P. Choi, D. Raabe, Dynamic strain aging studied at the atomic scale, Acta Mater. 86 (2015) 34–42. https://doi.org/https://doi.org/10.1016/j.actamat.2014.12.028.

[4] 紙川尚也, 繰り返し重ね接合圧延 (ARB) による構造用金属材料の結晶粒超微細化, (2006).

[5] H. Hosono, Y. Mishima, H. Takezoe, K.J.D. MacKenzie, Nanomaterials: Research Towards Applications, Elsevier, 2006.

[6] D.H. Jang, Y.B. Park, W.J. Kim, Significant strengthening in superlight Al-Mg alloy with an exceptionally large amount of Mg (13 wt%) after cold rolling, Mater. Sci. Eng. A. 744 (2019) 36–44. https://doi.org/https://doi.org/10.1016/j.msea.2018.11.132.

[7] D.-N. Zhang, Q.-Q. Shangguan, C.-J. Xie, F. Liu, A modified Johnson–Cook model of dynamic tensile behaviors for 7075-T6 aluminum alloy, J. Alloys Compd. 619 (2015) 186–194. https://doi.org/https://doi.org/10.1016/j.jallcom.2014.09.002.

[8] N.J. Petch, The cleavage strength of polycrystals, J. Iron Steel Inst. 174 (1953) 25–28.

[9] R.Z. Valiev, R.K. Islamgaliev, I. V Alexandrov, Bulk nanostructured materials from severe plastic deformation, Prog. Mater. Sci. 45 (2000) 103–189. https://doi.org/https://doi.org/10.1016/S0079-6425(99)00007-9.

[10] N. Tsuji, Y. Ito, Y. Saito, Y. Minamino, Strength and ductility of ultrafine grained aluminum and iron produced by ARB and annealing, Scr. Mater. 47 (2002) 893–899. https://doi.org/https://doi.org/10.1016/S1359-6462(02)00282-8.

[11] B.-H. Lee, S.-H. Kim, J.-H. Park, H.-W. Kim, J.-C. Lee, Role of Mg in simultaneously improving the strength and ductility of Al–Mg alloys, Mater. Sci. Eng. A. 657 (2016) 115–122. https://doi.org/https://doi.org/10.1016/j.msea.2016.01.089.

[12] Ø. Ryen, B. Holmedal, O. Nijs, E. Nes, E. Sjölander, H.-E. Ekström, Strengthening mechanisms in solid solution aluminum alloys, Metall. Mater. Trans. A. 37 (2006) 1999–2006.

[13] M. Kuzmina, M. Herbig, D. Ponge, S. Sandlöbes, D. Raabe, Linear complexions: Confined chemical and structural states at dislocations, Science (80-.). 349 (2015) 1080 LP – 1083. https://doi.org/10.1126/science.aab2633.

[14] D. Akama, N. Nakada, T. Tsuchiyama, S. Takaki, A. Hironaka, Discontinuous yielding induced by the addition of nickel to interstitial-free steel, Scr. Mater. 82 (2014) 13–16. https://doi.org/https://doi.org/10.1016/j.scriptamat.2014.03.012.

[15] H.A. Murdoch, C.A. Schuh, Estimation of grain boundary segregation enthalpy and its role in stable nanocrystalline alloy design, J. Mater. Res. 28 (2013) 2154–2163. https://doi.org/DOI: 10.1557/jmr.2013.211.

[16] D.J. Lloyd, H. Jin, Inhomogeneous yielding and work hardening of a fine grained Al–Mg alloy, Mater. Sci. Eng. A. 585 (2013) 455–459. https://doi.org/https://doi.org/10.1016/j.msea.2013.07.044.

[17] N. Kamikawa, X. Huang, N. Tsuji, N. Hansen, Strengthening mechanisms in nanostructured high-purity aluminium deformed to high strain and annealed, Acta Mater.

57 (2009) 4198–4208. https://doi.org/https://doi.org/10.1016/j.actamat.2009.05.017.

[18] D. Zhou, H. Wang, D.W. Saxey, O. Muránsky, H. Geng, W.D.A. Rickard, Z. Quadir, C. Yang, S.M. Reddy, D. Zhang, Hall–Petch Slope in Ultrafine Grained Al-Mg Alloys, Metall. Mater. Trans. A. 50 (2019) 4047–4057. https://doi.org/10.1007/s11661-019-05329-3.

[19] M.A. Meyers, K.K. Chawla, Mechanical behavior of materials, Cambridge university press, 2008.

[20] J.E. Bailey, P.B. Hirsch, The dislocation distribution, flow stress, and stored energy in cold-worked polycrystalline silver, Philos. Mag. A J. Theor. Exp. Appl. Phys. 5 (1960) 485–497. https://doi.org/10.1080/14786436008238300.

[21] J. Gubicza, N.Q. Chinh, Z. Horita, T.G. Langdon, Effect of Mg addition on microstructure and mechanical properties of aluminum, Mater. Sci. Eng. A. 387–389 (2004) 55–59. https://doi.org/https://doi.org/10.1016/j.msea.2004.03.076.

[22] D.A. Hughes, Microstructural evolution in a non-cell forming metal: Al□Mg, Acta Metall. Mater. 41 (1993) 1421–1430. https://doi.org/https://doi.org/10.1016/0956-7151(93)90251-M.

[23] G.W.J. Waldron, A study by transmission electron microscopy of the tensile and fatigue deformation of aluminum-magnesium alloys, Acta Metall. 13 (1965) 897–906. https://doi.org/https://doi.org/10.1016/0001-6160(65)90081-7.

[24] M. Jobba, R.K. Mishra, M. Niewczas, Flow stress and work-hardening behaviour of Al–Mg binary alloys, Int. J. Plast. 65 (2015) 43–60.

[25] T.C. Schulthess, P.E.A. Turchi, A. Gonis, T.-G. Nieh, Systematic study of stacking fault energies of random Al-based alloys, Acta Mater. 46 (1998) 2215–2221.

https://doi.org/https://doi.org/10.1016/S1359-6454(97)00432-1.

[26] T. Morishige, T. Hirata, T. Uesugi, Y. Takigawa, M. Tsujikawa, K. Higashi, Effect of Mg content on the minimum grain size of Al–Mg alloys obtained by friction stir processing, Scr. Mater. 64 (2011) 355–358. https://doi.org/https://doi.org/10.1016/j.scriptamat.2010.10.033.

[27] M. Muzyk, Z. Pakiela, K.J. Kurzydlowski, Ab initio calculations of the generalized stacking fault energy in aluminium alloys, Scr. Mater. 64 (2011) 916–918. https://doi.org/https://doi.org/10.1016/j.scriptamat.2011.01.034.

[28] M.P. Liu, H.J. Roven, High density hexagonal and rhombic shaped nanostructures in a fcc aluminum alloy induced by severe plastic deformation at room temperature, Appl. Phys. Lett. 90 (2007) 83115. https://doi.org/10.1063/1.2696540.

[29] X.Z. Liao, J.Y. Huang, Y.T. Zhu, F. Zhou, E.J. Lavernia, Nanostructures and deformation mechanisms in a cryogenically ball-milled Al-Mg alloy, Philos. Mag. 83 (2003) 3065–3075. https://doi.org/10.1080/1478643031000152799.

[30] G.T. Gray, Deformation twinning in Al-4.8 wt% Mg, Acta Metall. 36 (1988) 1745–1754. https://doi.org/https://doi.org/10.1016/0001-6160(88)90242-8.

[31] N.Y. Zolotorevsky, A.N. Solonin, A.Y. Churyumov, V.S. Zolotorevsky, Study of work hardening of quenched and naturally aged Al–Mg and Al–Cu alloys, Mater. Sci. Eng. A. 502 (2009) 111–117. https://doi.org/https://doi.org/10.1016/j.msea.2008.10.010.

[32] P.G. McCormigk, A model for the Portevin-Le Chatelier effect in substitutional alloys, Acta Metall. 20 (1972) 351–354. https://doi.org/https://doi.org/10.1016/0001-6160(72)90028-4.

[33] A. van den Beukel, Theory of the effect of dynamic strain aging on mechanical properties,

Phys. Status Solidi. 30 (1975) 197–206. https://doi.org/https://doi.org/10.1002/pssa.2210300120.

[34] R.A. Mulford, U.F. Kocks, New observations on the mechanisms of dynamic strain aging and of jerky flow, Acta Metall. 27 (1979) 1125–1134. https://doi.org/https://doi.org/10.1016/0001-6160(79)90130-5.

[35] H. Halim, D.S. Wilkinson, M. Niewczas, The Portevin–Le Chatelier (PLC) effect and shear band formation in an AA5754 alloy, Acta Mater. 55 (2007) 4151–4160. https://doi.org/https://doi.org/10.1016/j.actamat.2007.03.007.

[36] K. Chihab, Y. Estrin, L.P. Kubin, J. Vergnol, The kinetics of the Portevin-Le Chatelier bands in an Al-5at%Mg alloy, Scr. Metall. 21 (1987) 203–208. https://doi.org/https://doi.org/10.1016/0036-9748(87)90435-2.

[37] H. Ait-Amokhtar, C. Fressengeas, Crossover from continuous to discontinuous propagation in the Portevin–Le Chatelier effect, Acta Mater. 58 (2010) 1342–1349. https://doi.org/https://doi.org/10.1016/j.actamat.2009.10.038.

[38] Y. Zhang, J.P. Liu, S.Y. Chen, X. Xie, P.K. Liaw, K.A. Dahmen, J.W. Qiao, Y.L. Wang, Serration and noise behaviors in materials, Prog. Mater. Sci. 90 (2017) 358–460. https://doi.org/https://doi.org/10.1016/j.pmatsci.2017.06.004.

[39] B.J. Brindley, The effect of dynamic strain-ageing on the ductile fracture process in mild steel, Acta Metall. 18 (1970) 325–329. https://doi.org/https://doi.org/10.1016/0001-6160(70)90147-1.

[40] M. Koyama, Y. Shimomura, A. Chiba, E. Akiyama, K. Tsuzaki, Room-temperature blue brittleness of Fe-Mn-C austenitic steels, Scr. Mater. 141 (2017) 20–23. https://doi.org/https://doi.org/10.1016/j.scriptamat.2017.07.017.

[41] A. Yilmaz, The Portevin–Le Chatelier effect: a review of experimental findings, Sci. Technol. Adv. Mater. 12 (2011) 63001. https://doi.org/10.1088/1468-6996/12/6/063001.

[42] A.H. Cottrell, B.A. Bilby, Dislocation Theory of Yielding and Strain Ageing of Iron, Proc. Phys. Soc. Sect. A. 62 (1949) 49–62. https://doi.org/10.1088/0370-1298/62/1/308.

[43] F.R.N. Nabarro, Theory of crystal dislocations, (1967).

[44] G. Gremaud, Overview on dislocation-point defect interaction: the brownian picture of dislocation motion, Mater. Sci. Eng. A. 370 (2004) 191–198. https://doi.org/https://doi.org/10.1016/j.msea.2003.04.005.

[45] A.H. Cottrell, M.A. Jaswon, N.F. Mott, Distribution of solute atoms round a slow dislocation, Proc. R. Soc. London. Ser. A. Math. Phys. Sci. 199 (1949) 104–114. https://doi.org/10.1098/rspa.1949.0128.

[46] R.C. Picu, D. Zhang, Atomistic study of pipe diffusion in Al–Mg alloys, Acta Mater. 52 (2004) 161–171. https://doi.org/https://doi.org/10.1016/j.actamat.2003.09.002.

[47] J. Schlipf, On the kinetics of static and dynamic strain aging, Scr. Metall. Mater. 31 (1994) 909–914. https://doi.org/https://doi.org/10.1016/0956-716X(94)90501-0.

[48] B.J. Brindley, P.J. Worthington, Serrated yielding in Aluminium-3% Magnesium, Acta Metall. 17 (1969) 1357–1361. https://doi.org/https://doi.org/10.1016/0001-6160(69)90153-9.

[49] M. Wagenhofer, M. Erickson-Natishan, R.W. Armstrong, F.J. Zerilli, Influences of strain rate and grain size on yield and serrated flow in commercial Al-Mg alloy 5086, Scr. Mater. 41 (1999) 1177–1184. https://doi.org/https://doi.org/10.1016/S1359-6462(99)00265-1.

[50] W. Charnock, The influence of grain size on the nature of portevin-lechatelier yielding,

Philos. Mag. A J. Theor. Exp. Appl. Phys. 18 (1968) 89–99. https://doi.org/10.1080/14786436808227311.

[51] P.G. Mccormick, Effect of grain size on serrated yielding in an Al-Mg-Si alloy, Philos. Mag. A J. Theor. Exp. Appl. Phys. 23 (1971) 949–956. https://doi.org/10.1080/14786437108216997.

[52] J.M. Robinson, M.P. Shaw, Microstructural and mechanical influences on dynamic strain aging phenomena, Int. Mater. Rev. 39 (1994) 113–122. https://doi.org/10.1179/imr.1994.39.3.113.

Chapter 2 Effects of grain size and Mg contents on the mechanical properties of Al-Mg alloys

2.1 Introduction

Al-Mg alloys are increasingly being used as structural materials in automotive and aviation industry because of their good combination of high specific strength, favorable formability and excellent work-hardening ability [1–3]. As an important class of non-heat-treatable aluminum alloys, Al-Mg alloys are mostly strengthened by solid solution hardening, grain boundary strengthening and work hardening since the Al_3Mg_2 precipitates have no significant particle strengthening effect [4–6]. Structural materials with high strength and large ductility are desirable for industrial applications because high strength allows structural components to carry high load and large ductility is essential to prevent catastrophic failure. To achieve a superior strength and ductility balance is an ultimate goal for structural materials research and development. However, the combination of high strength and large ductility has never been achieved in coarse-grained (CG) metallic materials. Grain refinement can effectively improve the yield strength of pure Al according to the Hall-Petch effect, but the ductility (especially the uniform elongation) is usually deteriorated when the grain size decreases down to ultrafine range due to the lack of work-hardening ability, which is known as a trade-off relationship between strength and ductility [7–9]. On the other hand, many studies have shown that increasing Mg content in Al-Mg alloys leads to an enhancement of both yield strength and work-hardening capacity without significantly sacrificing the ductility [10,11]. Therefore, it's reasonable to anticipate that high strength and large ductility could be achieved through combining optimized grain refinement with Mg addition. Numerous studies have been carried out on Al-Mg alloys, but little work has been reported on the

combined effects of grain size and Mg contents on the mechanical properties and strengthening mechanisms in Al-Mg alloys so far.

A clear understanding of the mechanical response of this alloy system will be very important for guiding the structural design of new, improved Al-Mg alloys. The main purpose of this chapter is to systematically investigate the combined effects of grain size and Mg contents on the mechanical properties and strengthening mechanisms in Al-Mg alloys, for managing both high strength and large ductility.

2.2 Materials and experimental methods

2.2.1 Starting materials

Al-xMg (x = 2.5, 5, 7.5 and 10 wt.%) alloys were selected as model alloys in this study and their chemical compositions are listed in Table 2-1. For Al-2.5, 5 and 7.5Mg alloys, the as-received materials were firstly heated at 500 °C (above the solvus temperatures) for 2 hours to ensure homogenization, followed by water quench to get supersaturated solid solutions with single-phase structure. For Al-10Mg alloy, a cylindrical sample with 39 mm in diameter was cut from the as-received ingot and then extruded at 400 ℃ with an extrusion ratio of 10.6. The as-extruded rod was then heat treated at 450 ℃ for 30 min to remove the second phase, and immediately cooled in water. These as-homogenized Al-Mg alloys were used as starting materials for the proceeding experiments carried out in the present study.

Table 2-2 Chemical compositions of the Al-Mg alloys used in this study (wt.%).

Composition	Si	Fe	Cu	Mn	Mg	Cr	Zn	Ti	Be	Al
Al-2.5Mg	0.11	0.25	0.03	0.06	2.5	0.19	0.02	0.02	0	Bal.
Al-5Mg	0.009	0	0.005	0.001	5.24	0	0.001	0.046	0.003	Bal.
Al-7.5Mg	0.011	0	0.004	0.002	7.74	0	0.001	0.045	0.003	Bal.
Al-10Mg	0.03	0.06	0	0.01	9.88	0	0	0	0	Bal.

2.2.2 Materials processing

Two thermomechanical processing routes were conducted to fabricate samples with grain sizes ranging from ultrafine scale to coarse scale. In route I, the as-homogenized materials were cold rolled to a final thickness of 1 mm. Disks with 10 mm in diameter and 0.8 mm in thickness were machined from the rolled sheets and then heavily deformed by high-pressure torsion (HPT) process at room temperature. All the disks were processed up to 5 rotations under a compressive pressure of 6 GPa at a speed of 0.2 rotation per minute (Fig. 2.1 (a)). The shear strain, γ, applied to the disk samples during the HPT process can be calculated as:

$$\gamma = \frac{2\pi Nr}{t} \qquad (2-1)$$

where r is the radial position in the disk, N is the number of rotations and t is the thickness of the disk. Based on Eq. (2-1), the maximum shear strain applied to the materials by five rotations of HPT process can be as large as γ = 196. After HPT process, the samples were annealed at temperatures ranging from 175 ℃ to 400 ℃ for various holding time ranging from 5 s to 1.8 ks, and then immediately cooled in water. In route II, the as-homogenized materials were cold rolled by 84~96% reduction in thickness to 1 mm or 2 mm, then annealed at 350 ℃ to 500 ℃ for 30 s to 3.6 ks to obtain CG samples.

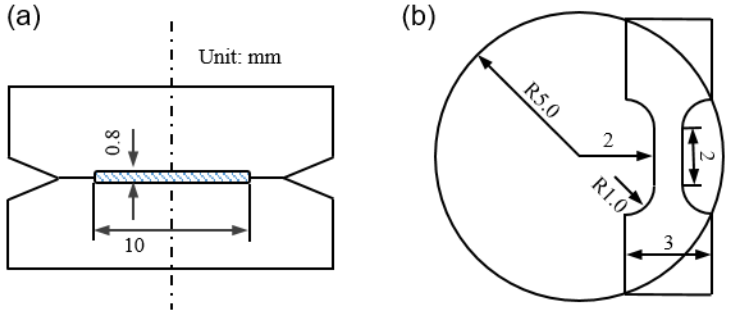

Fig. 2.1 Schematic illustration of (a) constrained high-pressure torsion (HPT) process and (b) tensile sample cut from HPT-processed disk.

2.2.3 Microstructural characterizations

After annealing, microstructural characterizations were undertaken by using a field-emission scanning electron microscope (FE-SEM, JEOL, JSM-7800F) equipped with backscattered electron (BSE) detectors operated at an accelerating voltage of 15 kV. The transverse sections of the HPT disks (containing the shear direction SD and the normal direction ND) and the rolled sheets (containing the rolling direction RD and the normal direction ND) were observed. For the HPT processed samples, the microstructures were studied at the areas of which distance from the center was larger than 2 mm to avoid microstructural inhomogeneity. All the samples for microstructural observation were firstly mechanical polished by using SiC abrasive grinding papers to achieve a mirror finish. Afterward, these samples were electrically polished in an electrolyte of 10% $HClO_4$ and 90% CH_3OH with a voltage of 20 V at about −30 ℃. The mean grain sizes of the annealed samples were measured by a line intercept method on the BSE images.

2.2.4 Tensile tests

For the samples fabricated by HPT and annealing, tensile samples with gauge length of 2 mm, width of 1 mm and thickness of 0.5 mm were cut from the HPT disks (as illustrated in Fig. 2.1 (b)). The gauge part of the tensile sample was coincided to the position larger than 2 mm from the center of the disks to avoid microstructural inhomogeneity in the near center region. For the CG samples prepared by cold rolling and annealing, tensile samples with gauge length of 10 mm, width of 5 mm and thickness of 1 mm or 2 mm were cut from the cold-rolled sheets. Tensile tests were conducted on a Shimadzu AG-X plus system with an initial strain rate of 8.3×10^{-4} s^{-1} at room temperature, and two samples were tested for each condition. Digital image correlation (DIC) method was used to precisely measure tensile strain in the tensile tests. The DIC technique was also used to analyze local deformation in the samples. Surfaces of the tensile samples were

decorated with finely sprayed black and white paint speckles which act as markers to track local displacement in the DIC analysis. During the tensile tests, images of the tensile samples were captured by a charge-coupled device (CCD) camera at a sampling rate of 10 frames per second. After tensile tests, the captured images were analyzed by using VIC-2D commercial software.

2.3 Results

2.3.1 Microstructures and microstructural evolution

Fig. 2.2 – Fig. 2.5 exhibit the representative microstructures of Al-Mg alloys obtained by BSE observations. Fully recrystallized specimens having relatively homogeneous microstructures and different mean grain sizes were successfully fabricated. It is of value to note that the grain sizes fall into wide ranges. For Al-2.5Mg alloy, as shown in Fig. 2.2, the grain size steadily increased with increasing annealing temperature. UFG microstructures with mean grain size smaller than 1 μm were easily attained, which suggested that high-density nucleation sites for recrystallization were introduced by the HPT process. The Al-2.5Mg samples fabricated in the present study all showed FCC single-phase. By contrast, for Al-5Mg alloy annealed at 225 ℃ which was below the solvus temperature (255 ℃), many precipitates appeared at the grain boundary (GB) regions, as indicated in Fig. 2.3 (a). The minimum grain size achieved was 0.61 μm (single-phase structure, as shown in Fig. 2.3 (b)) when annealed at 260 ℃ for 30 s since recrystallized grains grew fast under heat treatment. As the annealing temperature increased, the grain size quickly increased. As for Al-7.5Mg (Fig. 2.4) and Al-10Mg (Fig. 2.5) alloys, the development of recrystallized microstructures was very similar to that of Al-5Mg alloy. When annealing temperature was below the solvus temperature (310 ℃ for Al-7.5Mg and 355 ℃ for Al-10Mg), large amounts of precipitates appeared at GB regions. When annealing temperature was higher than the solvus temperature, the precipitates disappeared and the grains grew explosively.

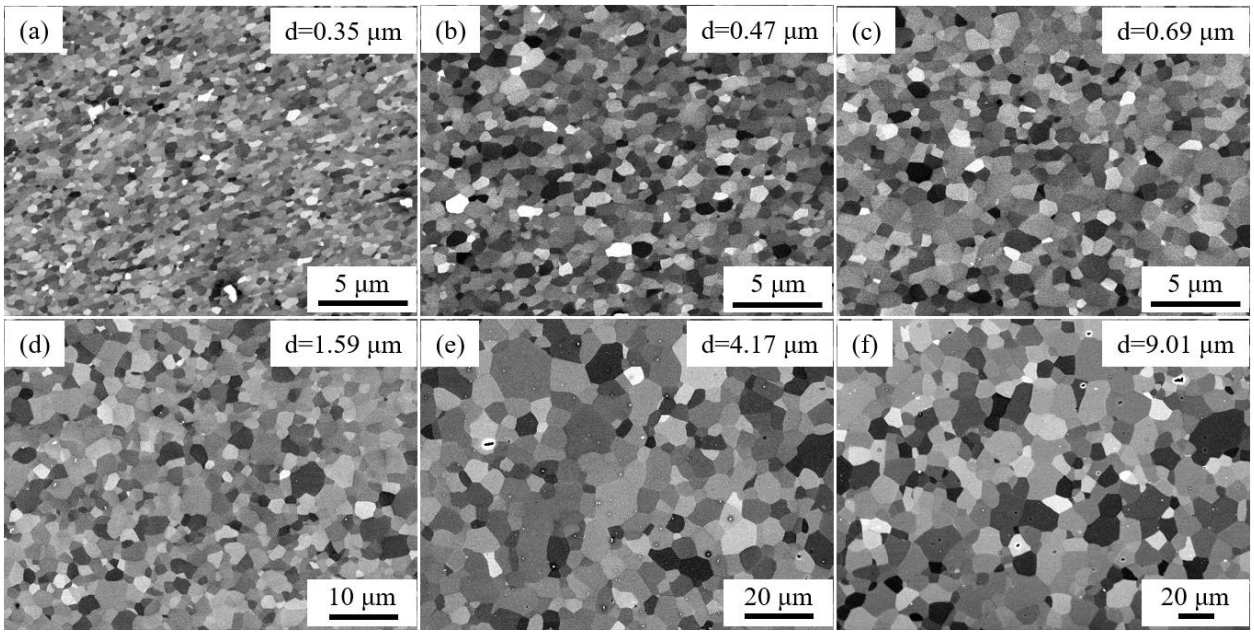

Fig. 2.2 Representative BSE micrographs of the Al-2.5Mg alloy processed by HPT and subsequently annealed under different conditions. (a) HPT + 200 ℃ for 1.8 ks, (b) HPT + 225 ℃ for 1.8 ks, (c) HPT + 250 ℃ for 1.8 ks, (d) HPT + 275 ℃ for 1.8 ks, (e) HPT + 300 ℃ for 1.8 ks and (f) HPT + 325 ℃ for 1.8 ks.

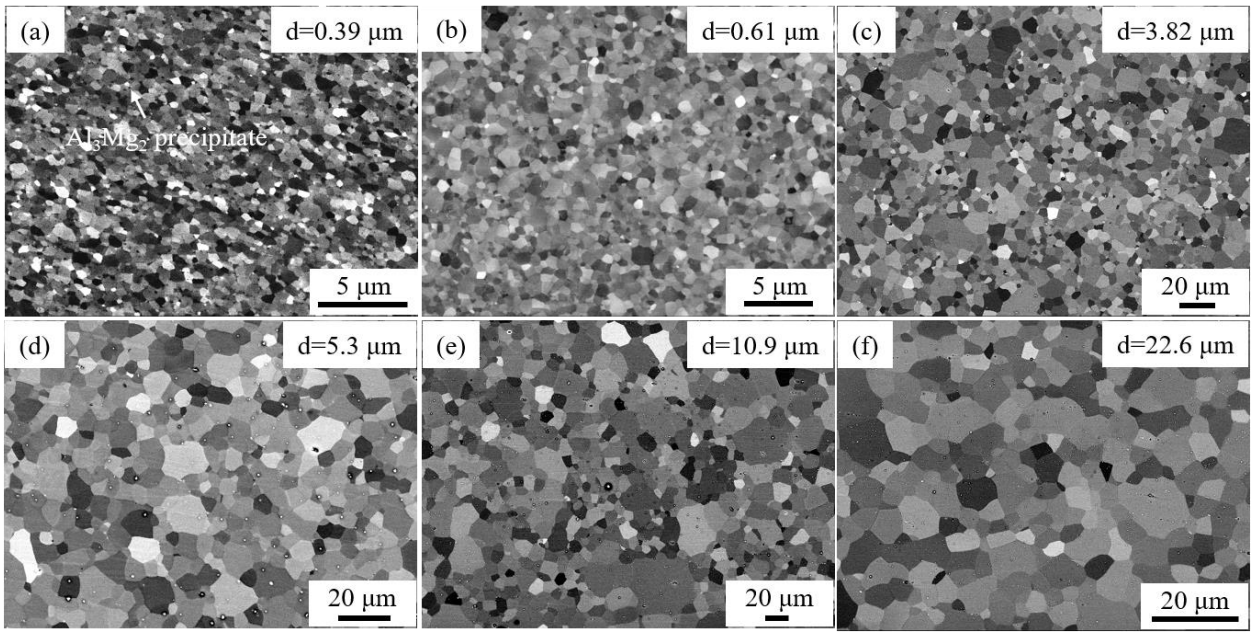

Fig. 2.3 Representative BSE micrographs of the Al-5Mg alloy processed by HPT/cold rolling and annealed under different conditions. (a) HPT + 225 ℃ for 1.8 ks, (b) HPT + 260 ℃ for 30 s, (c) HPT + 300 ℃ for 1.8 ks, (d) HPT + 325 ℃ for 1.8 ks, (e) HPT + 350 ℃ for 1.8 ks and (f) HPT + 400 ℃ for 1.8 ks.

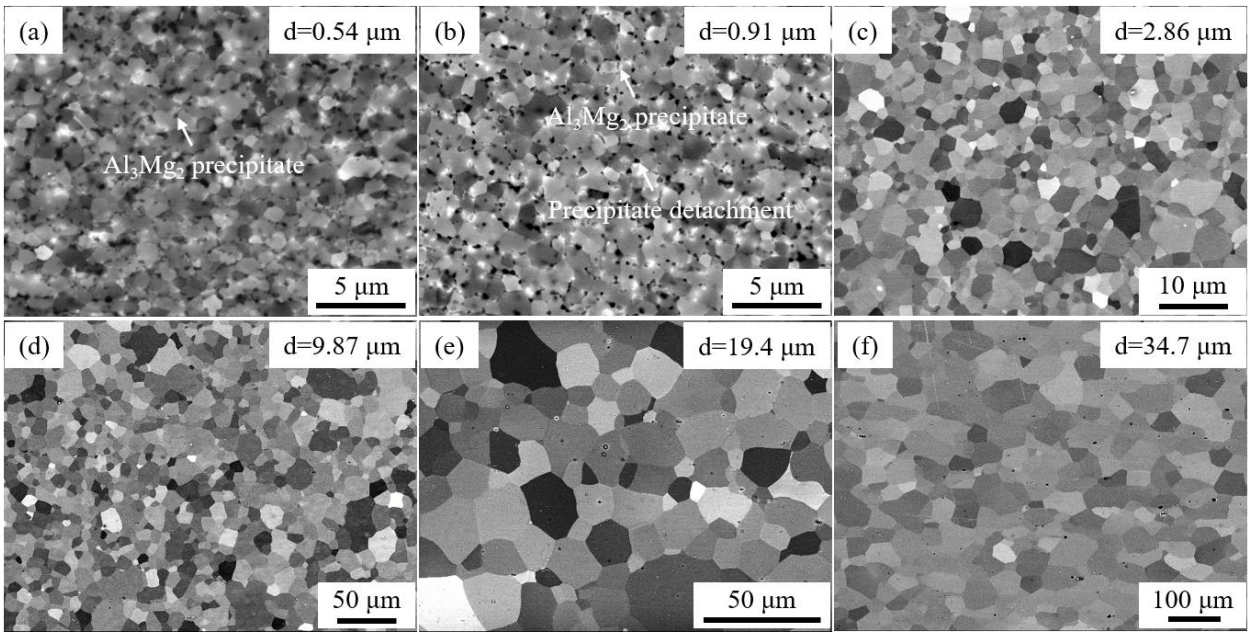

Fig. 2.4 Representative BSE micrographs of the Al-7.5Mg alloy processed by HPT/cold rolling and annealed under different conditions. (a) HPT + 275 ℃ for 1.8 ks, (b) HPT + 300 ℃ for 1.8 ks, (c) HPT + 325 ℃ for 10 s, (d) HPT + 325 ℃ for 1.8 ks, (e) HPT + 400 ℃ for 1.8 ks and (f) 90% CR + 400 ℃ for 1.8 ks.

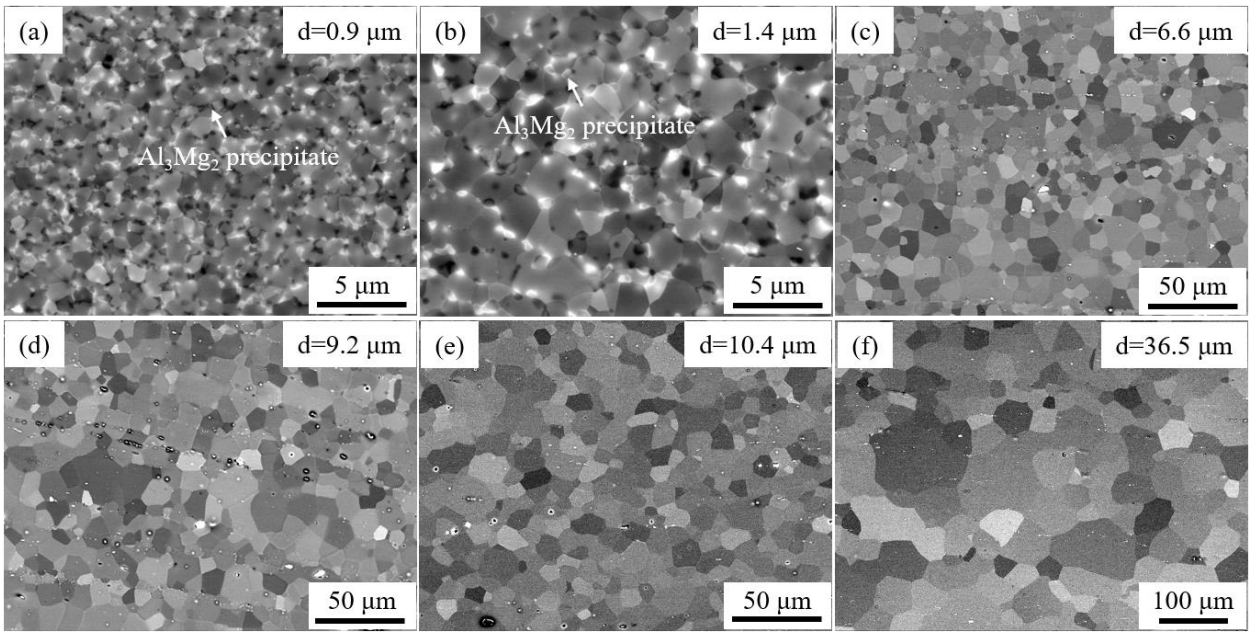

Fig. 2.5 Representative BSE micrographs of the Al-10Mg alloy processed by HPT/cold rolling and annealed under different conditions. (a) HPT + 325 ℃ for 1.8 ks, (b) HPT + 350 ℃ for 1.8 ks, (c) HPT + 375 ℃ for 30 s, (d) HPT + 375 ℃ for 120 s, (e) 90% CR + 380 ℃ for 30 s and (f) 90% CR + 500 ℃ for 1.8 ks.

To investigate the effect of annealing temperature and Mg content on recrystallization of severely deformed Al-Mg alloys, the as-HPT processed samples were annealed at temperatures ranging from 175 ℃ to 375 ℃ for 1.8 ks and the structural evolution was examined. The evolution of mean grain size as a function of annealing temperature is plotted in Fig. 2.6. Note that the open symbols represent samples with precipitates. The mean grain size of Al-10Mg alloy annealed at 375 ℃ for 120 s (indicated by the arrow in Fig. 2.6) is also included for comparison. It was found that the grain growth of Al-2.5Mg alloy was relatively slow when annealed at 275 ℃ or below, UFG structures could be easily attained by changing the annealing temperature and holding time. However, when annealed at temperatures higher than 275 ℃, the grain growth was significantly accelerated. By contrast, for Al-5Mg, Al-7.5Mg and Al-10Mg alloys, when the samples were annealed below the solvus temperatures, the grains grew rather slow since the precipitates could act as barriers to grain boundaries (GBs) migration. It should be noted that the solvus temperature for Al-Mg alloy increases with increasing Mg content and therefore a higher annealing temperature is indispensable for preparing precipitate-free samples. However, the annealing temperature has a dramatic influence on the rate of recrystallization. When annealing temperature was slightly higher than the solvus temperature, the grains grew explosively, even when annealed for a very short period (as indicated by the arrow), making it difficult to obtain UFG structures with single phase.

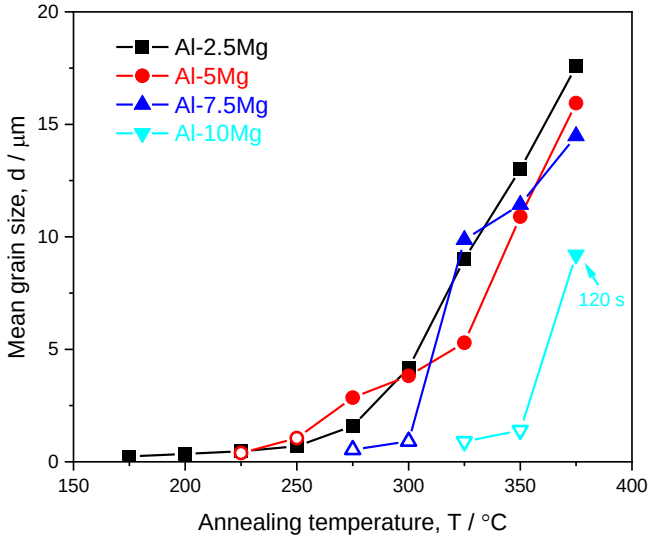

Fig. 2.6 Mean grain size of Al-Mg alloys processed by HPT and subsequently annealed at various temperatures for 1.8 ks. The open symbols represent samples with precipitates and the grain size of Al-10Mg alloy annealed at 375 ℃ for 120 s (indicated by the arrow) is also included for comparison.

2.3.2 Mechanical properties

Fig. 2.7 (a) – (d) shows the tensile nominal stress-strain curves of Al-2.5, 5, 7.5 and 10Mg alloys with different mean grain sizes, respectively. The yield strength (0.2% proof stress), ultimate tensile strength (UTS) and uniform elongation (UE) were determined from the nominal stress-strain curves. Generally, there is a trade-off relationship between strength and ductility in metallic materials, and the Al-Mg alloys in this study also show the same tendency.

For the Al-2.5Mg samples, the yield strength increased with decreasing the mean grain size, which is the well-known Hall-Petch effect [12,13]. The as-HPT processed sample with the minimum grain size exhibited very high strength (670 MPa) but limited uniform elongation (1.7%), which was a typical feature of severely deformed metallic materials due to the high dislocation density that limited work-hardening ability [8]. When the grain size was 0.24 μm, a decrease in both tensile strength (480 MPa) and ductility (0.5%) had been observed compared to the as-

deformed condition. This behavior was opposite to that in conventional materials since it was commonly accepted that annealing normally led to a decrease in strength and an increase in ductility, which could be attributed to the removal of mobile dislocations during annealing at 175 ℃ [14]. The tensile stress-strain curves for samples having grain sizes of 0.35 μm and 0.47 μm exhibited high UTS at a small tensile strain, a sharp drop of the stress (yield drop phenomenon) and a gradual decrease in the flow stress were observed in samples having grain sizes of 0.35 μm and 0.47 μm, respectively, due to early necking of these samples. When the grain size increased to 0.69 μm, an unprecedentedly large Lüders strain around 0.2 was found. In addition, this sample regained relatively good work-hardening ability, manifested by a small portion of uniform elongation after Lüders deformation. So that necking was significantly postponed, indicating a good balance between strength and ductility could be achieved in this UFG sample. When the grain size furthermore increased to 1.59 μm or 4.17 μm, the yield point phenomenon still appeared but the Lüders strain decreased with increasing grain size, which suggested that the Lüders strain had an inverse dependence on the grain size [15]. The yield point phenomenon and Lüders deformation disappeared when the grain size became coarser than 4.2 μm, which was a typical stress-strain behavior in CG Al-Mg alloys. It was noteworthy that the yielding behavior changed from continuous yielding to discontinuous yielding with Lüders deformation, with decreasing the grain size. Meanwhile, the tensile ductility slightly increased when the grain size decreased from 9.01 μm to 1.59 μm, then abruptly dropped when the grain size became smaller than 0.5 μm.

Similarly, for the Al-5Mg, Al-7.5Mg and Al-10Mg samples, the yield strength also increased with refining the grain size. The nominal stress-strain curves obtained also exhibited remarkable transitions of yielding behavior and Lüders deformation, with decreasing the grain size. No early necking phenomenon was observed since the minimum grain sizes of these fully recrystallized

materials with single-phase structure were larger than 0.6 μm, due to the rapid grain growth under heat treatment. These recrystallized grains provide sufficient space for dislocation storage, resulting in good work-hardening capability and promising tensile ductility. It is therefore reasonable to anticipate large Lüders deformation and even early necking in these materials under the prerequisite that such small recrystallized grain size can be achieved. For those tensile samples with Al_3Mg_2 precipitates, as indicated in the figures, there was no significant particle strengthening effect, which could be concluded from the comparison of stress levels between Al-10Mg samples having grain size of 1.4 μm (with precipitates) and 4.1 μm. These two samples exhibited similar stress level although the grain sizes were quite different. It is generally accepted that for Al-Mg samples having similar grain size, the stress level is expected to decrease at the presence of Al_3Mg_2 precipitates due to the Mg-rich precipitates dilute the solute content within the grains and therefore decrease the contribution from solid solution hardening. Accordingly, the mechanical properties of Al-Mg samples having precipitates were not used for the proceeding analysis.

Several characteristic deformation behaviors can be observed in Al-Mg alloys having different Mg contents. One is that a well-defined yield point phenomenon, in some cases followed by Lüders deformation, has been observed. It should be noted here that the yield point phenomenon appears in coarser grained samples with increasing Mg content. It is also noteworthy that the work-hardening capacity increases with increasing Mg content, but the detailed mechanism has not been perfectly clarified yet. Another interesting phenomenon is that serrated flow is commonly observed in tensile deformation of Al-Mg alloys, which is also understood in terms of the PLC effect. The features of serrated flow also exhibit remarkable dependence on grain size and Mg content. Understanding the mechanisms of serrated flow is essential but beyond the scope of this chapter, detailed investigation will be introduced in Chapter 4.

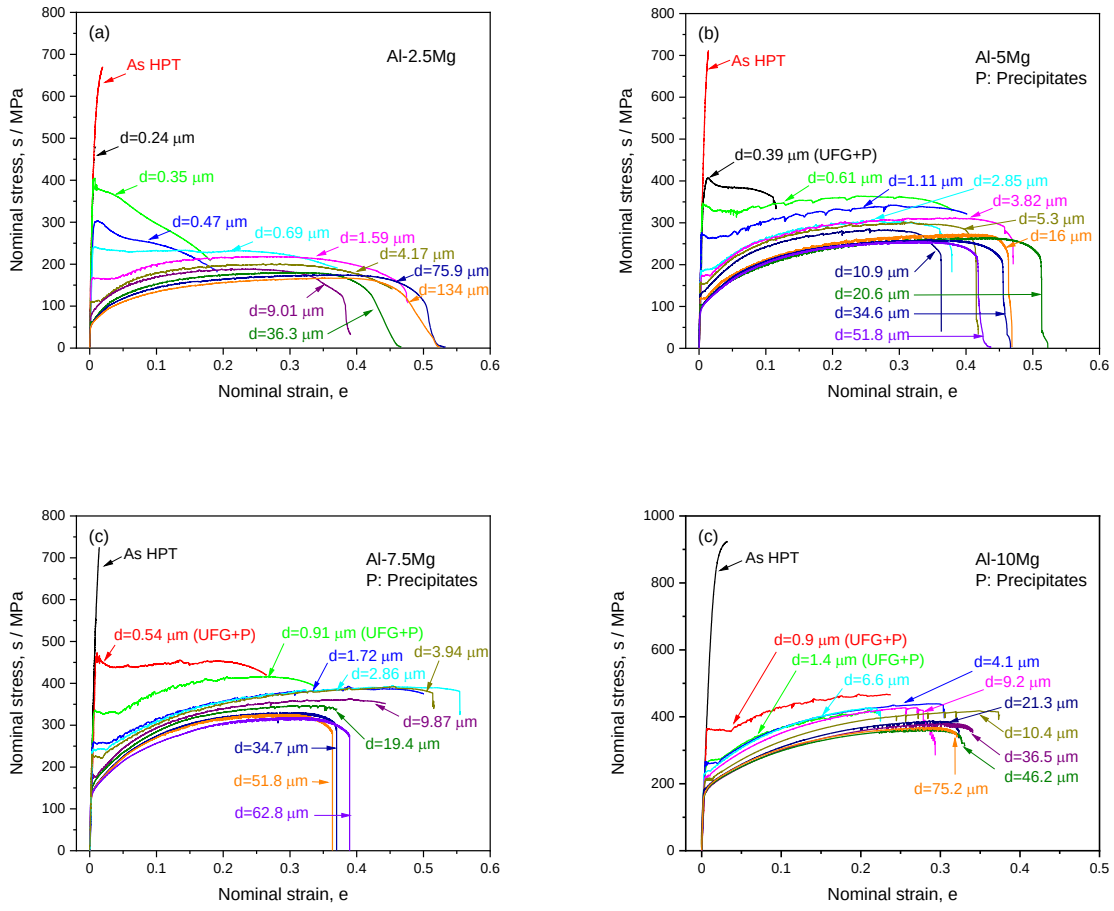

Fig. 2.7 Nominal stress-strain curves of the studied alloys with different mean grain sizes, obtained by tensile tests at room temperature. (a) Al-2.5Mg, (b) Al-5Mg, (c) Al-7.5Mg and (d) Al-10Mg.

2.3.3 Hall-Petch relationship for yield stress

The strength-structure relationship was evaluated via the Hall-Petch relationship by relating the yield strength to the reciprocal square root of grain size:

$$\sigma_{YS} = \sigma_0 + k_{HP} d^{-1/2} \qquad (2-2)$$

where σ_{YS} is the yield strength, σ_0 is the friction stress, k_{HP} (the Hall-Petch slope) is a constant that describes the relative strengthening contribution of GBs and d is the mean grain size of the material. When the σ_{YS} of Al-Mg alloys obtained from tensile tests at room temperature were plotted as a function of $d^{-1/2}$, the Hall-Petch relationship could be well described, as shown in Fig. 2.8 (a) – (d).

The friction stress and Hall-Petch slope for each material were determined by fitting the experimental data with Eq. (2-2). Note that the open symbols represent specimens with precipitates and the corresponding data points are not included for fitting. In order to make a more intuitive comparison, the Hall-Petch plots of Al-Mg alloys having different Mg contents are summarized in Fig. 2.8 (e), in which the data of pure Al (99.2 wt.%, defined as 2N Al) [16] obtained by accumulative roll-bonding/cold rolling and annealing are also plotted.

Characteristic features of the Hall-Petch plots can be seen in Fig. 2.8 (e), and three conclusions can be obtained accordingly. Firstly, the σ_{YS} and $d^{-1/2}$ for each Al-Mg alloy can be correlated with a two-stage Hall-Petch relationship. Although the Hall-Petch relationship has been widely verified in various materials, multi-stage Hall-Petch relationships were detected only in some special materials with well recrystallized structures or low-density defects, i.e. Al [17], IF steels [18] and Cu [19]. Two distinct Hall-Petch relations are obtained depending on the average grain size range, discontinuous yielding behavior resulted a much higher Hall-Petch slope than continuous yielding. The positive deviation of the yield strength became more pronounced as the mean grain size further decreased, which is also known as extra hardening phenomenon [20]. In particular, the Hall-Petch slope in fine grain-size regime is about two times that in coarse grain-size regime for all Al-Mg alloys studied here. Secondly, there exists a critical grain size which divides the Hall-Petch relationship into two stages and the magnitude of the critical grain size increases with increasing Mg content. Thirdly, it should be noted that the data points for Al-Mg alloys deviate from the Hall-Petch relation for 2N Al and can be fitted to give higher Hall-Petch slopes and friction stresses in the CG regime. Mg content-dependent Hall-Petch relationships were observed, indicating that adding Mg atoms to Al matrix is effective in enhancing both friction stress and GB strengthening due to an increased Hall-Petch slope (as shown in Fig. 2.8 (e)). Therefore, the effects of solute Mg

on the Hall-Petch slope and friction stress must be evaluated separately when considering the yield strength of polycrystalline Al-Mg alloys, even if the grain size can be controlled to be same.

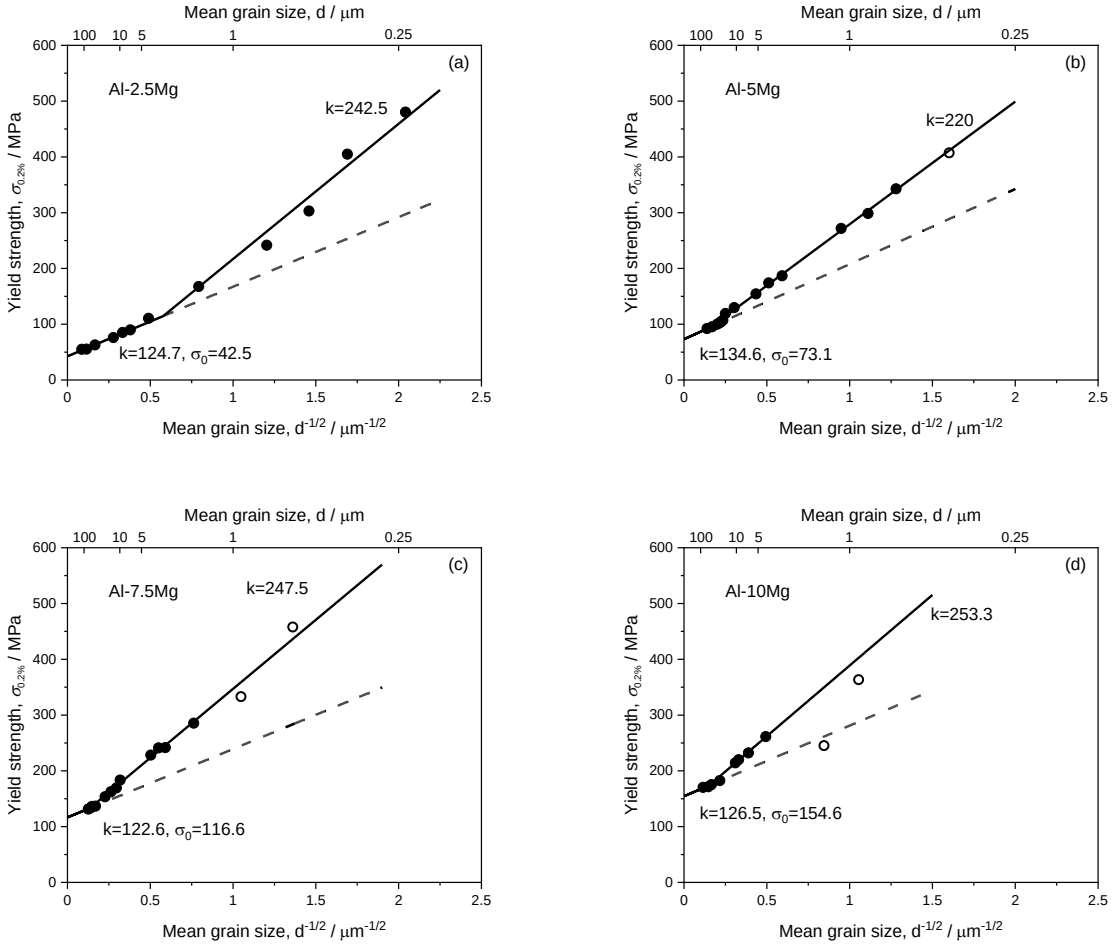

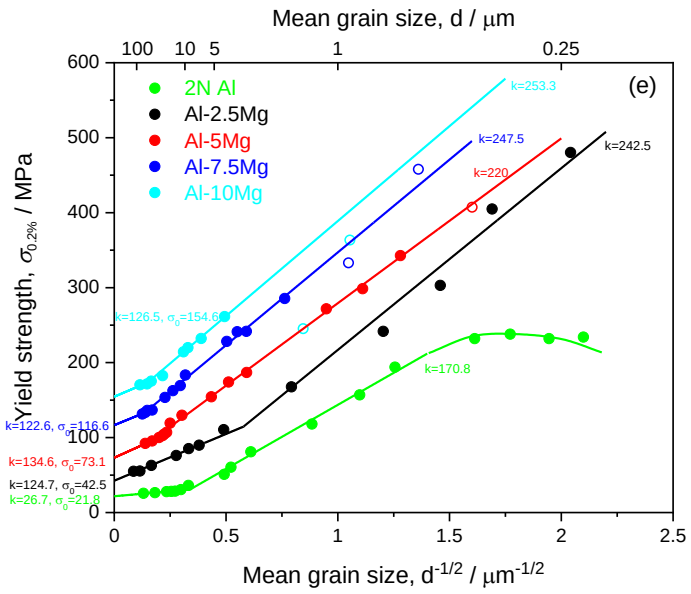

Fig. 2.8 Hall-Petch relationships of the alloys studied: (a) Al-2.5Mg, (b) Al-5Mg, (c) Al-7.5Mg, (d) Al-10Mg and (e) all alloys. Note: Open symbols represent specimens with precipitates.

To develop a complete picture of solid solution hardening, the relative contributions of GB strengthening and solid solution hardening were extracted. The friction stress σ_0 obtained from Hall-Petch plots at CG regimes are the combined contributions of lattice friction of pure Al and solid solution hardening from solute atoms, in which the GB strengthening is not included. For the 99.999 wt.% Al, the friction stress σ_{Al} = 5.5 MPa was experimentally determined for pure Al [21]. Thus, an estimation of the solid solution strengthening owing to Mg addition can be obtained from the variation of friction stress σ_0 for different Al-Mg alloys, as shown in Fig. 2.9. The friction stress increases almost linearly with an increase in Mg content, indicating linear solid solution hardening. And the solid solution strengthening due to Mg addition can be expressed as:

$$\sigma_{ss} = \sigma_0 - \sigma_{Al} = HC_0 \qquad (2-3)$$

where σ_{ss} is strength contribution from solute atoms, H is an experimental constant (= 14.9 MPa / wt.% Mg, which is almost the same as that reported by Lloyd and Court [22]) and C_0 is the content of the solute Mg in weight percent. The linear relationship obtained in this study would be valuable

to evaluate the strength contribution of solid solution strengthening in Al-Mg alloys at room temperature under quasi-static deformation.

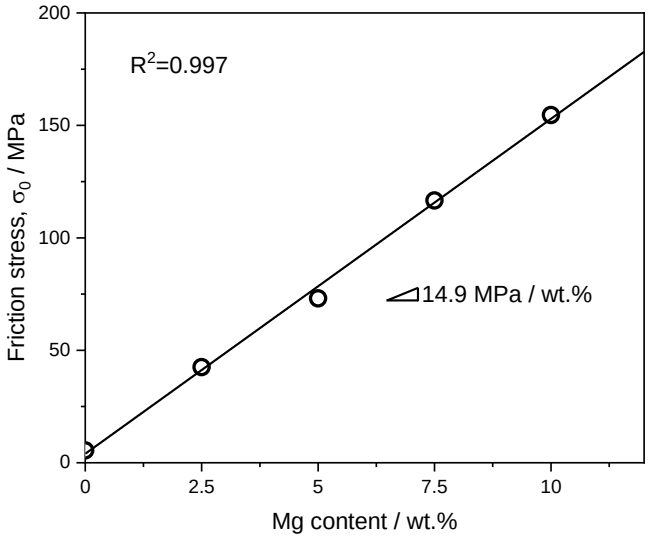

Fig. 2.9 Effect of Mg content on friction stress in Al-Mg alloys at room temperature under quasi-static deformation.

On the other hand, complicated effect of Mg contents on the Hall-Petch slopes in Al-Mg alloys were observed, as shown in Fig. 2.10. The Hall-Petch slope is as small as 26.7 MPa·μm$^{1/2}$ for 2N Al, but it increases to 124.7 MPa·μm$^{1/2}$ by only a minor addition of Mg atoms up to 2.5 wt.%, indicating that the presence of solute Mg atoms significantly enhances the GB strengthening effect. This influence of alloying elements on Hall-Petch slope in Al-Mg alloys was in agreement with the results from certain Cu-base alloys [24] and Fe-base alloys [25,26]. However, no further increase in Hall-Petch slope was found as Mg content increased from 2.5 to 10 wt.% and the Hall-Petch slope exhibited a practically constant value, which was the case for both coarse grain-size regime (continuous yielding) and fine grain-size regime (discontinuous yielding). This means that a small amount of Mg addition can lead to a large increase in the Hall-Petch slope of Al-Mg alloys, but the effect of Mg atoms on GB strengthening may have already reached saturation in Al-2.5Mg

alloy. It can be concluded that other strengthening mechanism must operate in addition to GB strengthening.

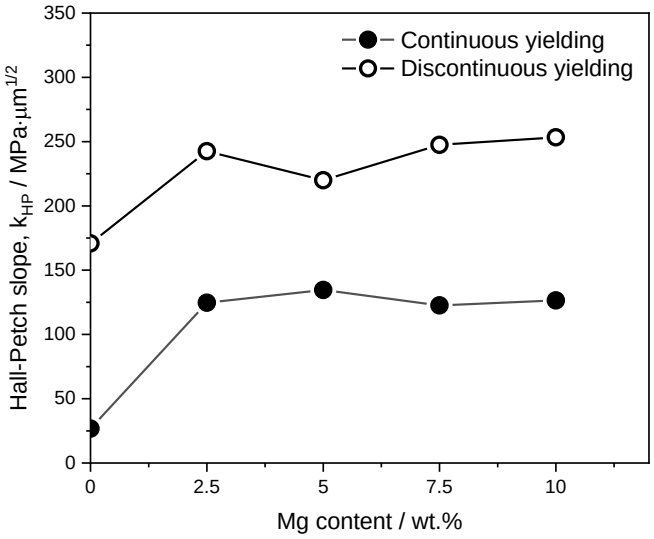

Fig. 2.10 Relationship between Hall-Petch slope and Mg content.

2.3.4 Hall-Petch relationship for flow stress

The flow stress σ(ε) at a particular strain is also related to the grain size by the equation:

$$\sigma(\varepsilon) = \sigma_0(\varepsilon) + k(\varepsilon)d^{-1/2} \qquad (2-4)$$

where $\sigma_0(\varepsilon)$ and $k(\varepsilon)$ are constants at a given true strain. Fig. 2.11 (a) – (d) show the yield stress and flow stress at selected strains (ε=0.05, 0.1, 0.15 and 0.2) plotted against the reciprocal square root of the grain size for Al-2.5, 5, 7.5 and 10Mg alloys. The flow stress for some UFG samples are not included due to the uniform elongation is too small to measure the flow stress from the true stress-strain curves. It is apparent that there is a large decrease in the Hall-Petch slope immediately after yield comparing to the Hall-Petch slope for the yield stress in the fine grain-size range. Due to the higher Hall-Petch slope for the yield stress in the fine grain-size range, the yield stress increases more rapidly than the flow stress with decreasing the grain size. When the yield stress

exceeds the extrapolated flow stress, a strain localization occurs at the onset of yielding, which corresponds to the discontinuous yielding in the present study.

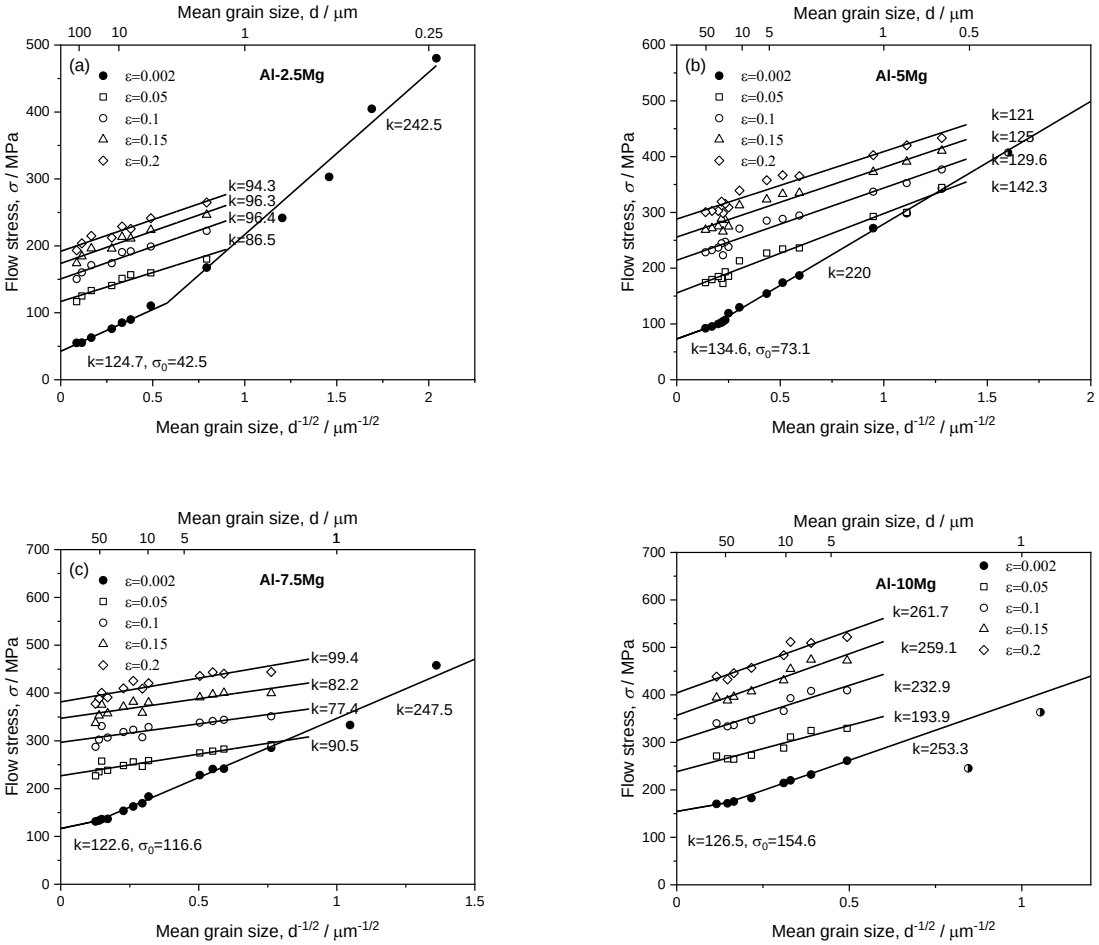

Fig. 2.11 Hall-Petch plots at different strains for (a) Al-2.5Mg, (b) Al-5Mg. (c) Al-7.5Mg and (d) Al-10Mg.

The effects of Mg contents on the Hall-Petch slope values of Al-Mg alloys for flow stresses over a range of strains were also investigated, as shown in Fig. 2.12. For Al-2.5, 5 and 7.5Mg alloys, the Hall-Petch slope shows a decrease after yield, but then remains practically constant up to true strain of 0.2, indicating that the strain dependence is quite low. Moreover, it was noteworthy that increasing Mg content does not have a significant effect on the Hall-Petch slopes for flow stresses in Al-2.5, 5 and 7.5Mg alloys. Whereas the measurements on Al-10Mg alloy provide a contrast in the effect of strain on the Hall-Petch slope: there is a gradual increase as deformation

proceeds. The variations in Hall-Petch slope may have their cause in strengthening mechanisms that contribute to the flow stress in addition to GB strengthening. This result indicates that the tensile response of Al-10Mg alloy is quite different with those of Al-Mg alloys having lower Mg contents, and the peculiarity can also be confirmed in the stress-strain curves of Al-10Mg (Fig. 2.7 (d)), there is no pronounced serrated flow at small and intermediate strains.

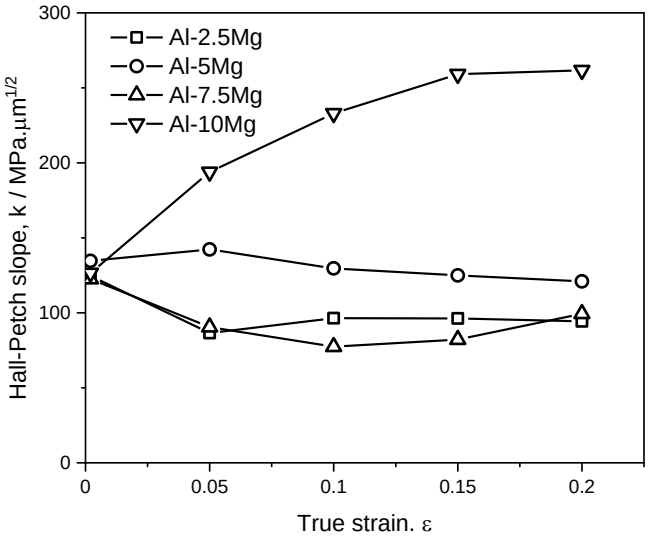

Fig. 2.12 Variation in Hall-Petch slope for different strains in Al-Mg alloys.

2.3.5 Uniform elongation and work-hardening behavior

Fig. 2.7 has clearly shown the trade-off relationship between strength and ductility in Al-Mg alloys. The change of the tensile elongation especially the uniform elongation in the fine grain-size regime is difficult to predict due to a drastic drop of uniform elongation accompanying with early plastic instability. It is thus important to determine an optimal grain size at which superior strength-ductility balance can be achieved. Since no early necking was observed in Al-5, 7.5 and 10Mg alloys having single-phase structure (limited by the minimum grain size fabricated), Al-2.5Mg alloy was selected as a representative to discuss the effect of gain size and solute Mg on the uniform elongation of Al-Mg alloys by comparing with 2N Al. The uniform elongation and Lüders

strain of Al-2.5Mg and 2N Al samples are plotted as a function of the reciprocal square root of grain size, as shown in Fig. 2.14 (a). For Al-2.5Mg alloy, the uniform elongation slightly increased first and then continuously decreased with decreasing the mean grain size from 9.01 μm to 0.69 μm. A drastic drop in the uniform elongation occurred when the grain size became smaller than 0.5 μm. When the grain size was smaller than 0.5 μm, the uniform elongation became very low, smaller than 0.01. Meanwhile, Lüders deformation appeared in samples having grain size smaller than 4.17 μm, and the Lüders strain increased with decreasing grain size. The Lüders strain slightly increased when the mean grain size decreased from 4.17 μm to 1.59 μm. When the grain size furtherly decreased to around 0.69 μm, the Lüders strain dramatically increased and became nearly the same as uniform elongation. However, as the grain size drops below 0.5 μm, early necking occurred immediately after yielding so that Lüders deformation was not observed. The sudden drop occurred in a very narrow grain size range (between 0.69 μm and 0.47 μm). The uniform elongation and Lüders strain in 2N Al exhibits similar tendency with decreasing the mean grain size. The sudden drop in uniform elongation has also been found in 2N Al. However, early necking occurred in sample having grain size around 1.2 μm. The critical grain size for the appearance of abrupt drop in uniform elongation decreased with increasing Mg content. Al-Mg alloys with higher Mg contents and finer grain sizes will be fabricated in the future to verify the predictive results.

As mentioned in the previous part that the drastic loss in uniform elongation of the UFG samples was related to the early plastic instability associated with the occurrence of discontinuous yielding behavior. The strain localization of Al-2.5Mg samples at the selected stages during tensile deformation was characterized by the DIC technique to confirm the relation between the Lüders deformation and uniform elongation. The stress-strain response of four representative samples and corresponding strain distribution maps at various global tensile strains obtained from DIC

measurements are shown in Fig. 2.13 (b) and Fig. 2.13 (c), respectively. One can easily realize the strain distribution at selected strain stage in the tensile deformation from the contour map. The measured average strain along the gauge length does not represent the actual strain experienced in the deformed region. The DIC analysis showed that the strain localization became more and more severe with decreasing grain size. At the grain size around 0.69 μm, the strain at which the flat part with a constant flow stress ended was notably high in this sample and the Lüders strain became nearly the same as uniform elongation. It can be expected that the Lüders strain will continue to increase when the grain size becomes smaller than 0.69 μm and finally becomes higher than the uniform elongation, leading to a drastic drop in the uniform elongation. And actually it is the case, in the sample having grain size of 0.47 um, as indicated in Fig. 2.13 (b), the local strain exceeds the uniform elongation at the inflection point (e = 0.05, within this strain range the localized deformation could be treated as nucleation and propagation of a Lüders band). The DIC results suggest that the way plastic strain is accommodated has a strong influence on the tensile elongation.

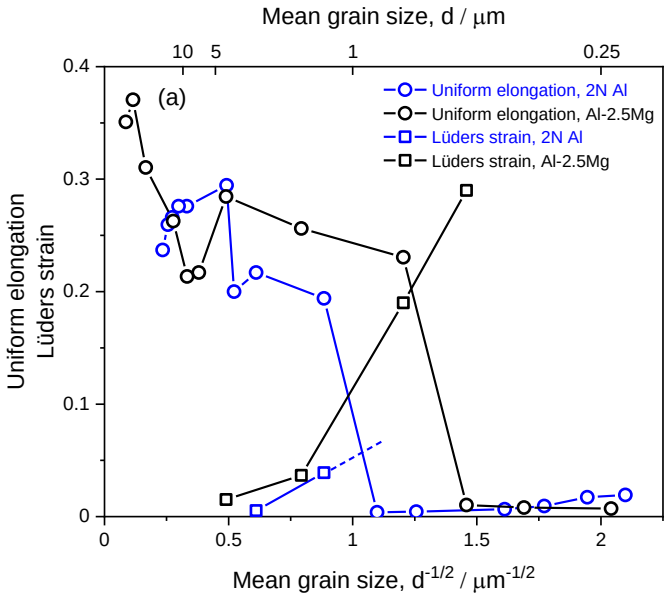

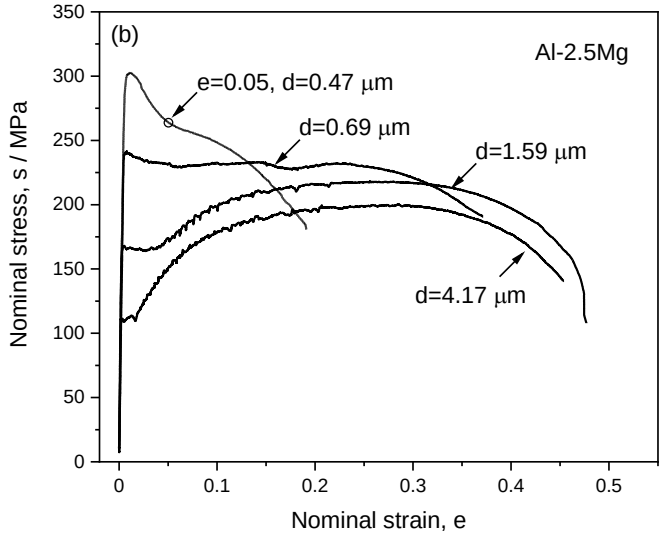
(b)
Al-2.5Mg
e=0.05, d=0.47 μm
d=0.69 μm
d=1.59 μm
d=4.17 μm
Nominal stress, s / MPa
Nominal strain, e
0
50
100
150
200
250
300
350
0
0.1
0.2
0.3
0.4
0.5

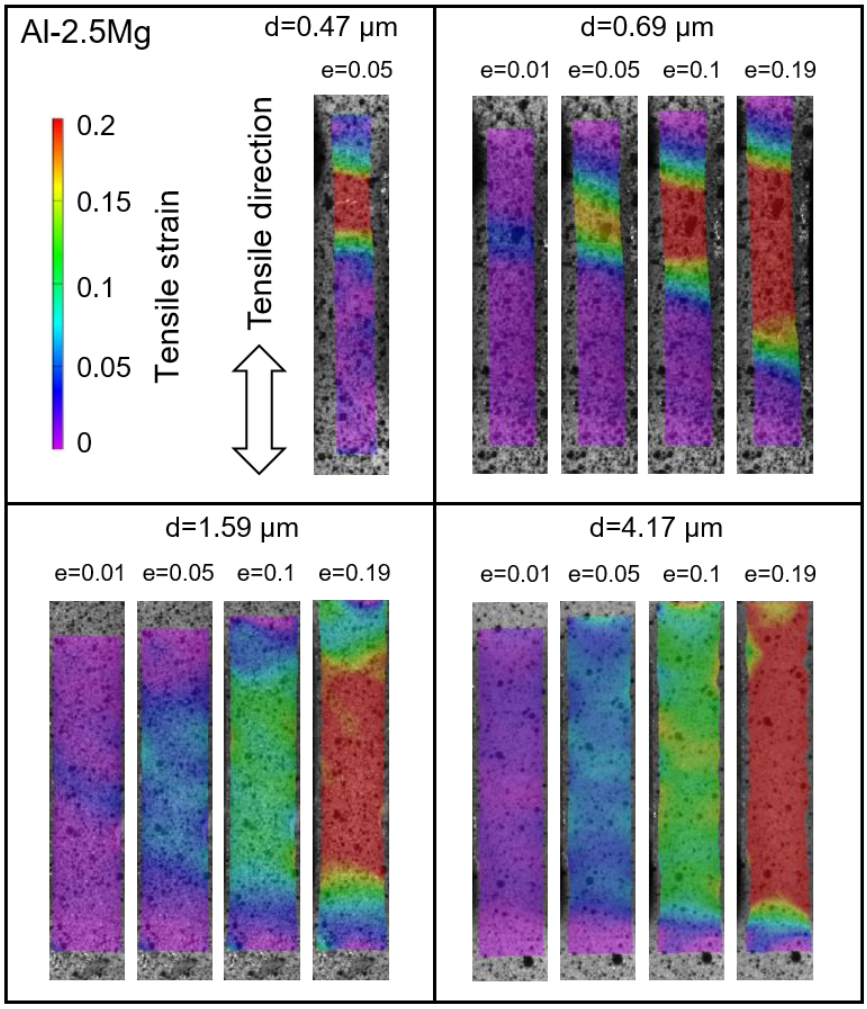

Fig. 2.13 (a) Uniform elongation and Lüders strain of the Al-2.5Mg and 2N Al samples plotted as a function of the reciprocal square root of grain size. (b) Representative nominal stress-strain curves of Al-2.5Mg samples showing discontinuous yielding behavior; (c) Strain distribution maps at the selected stages during tensile deformation of the Al-2.5Mg samples.

To investigate why adding solute Mg atoms leads to improved strength and ductility synergy, the tensile response of Al-2.5Mg and 2N Al samples having similar grain sizes are compared, as displayed in Fig. 2.14 (a). It is evident that the Al-2.5Mg samples show larger tensile ductility, as well as higher tensile strength than those of 2N Al having similar grain sizes. Especially for Al-2.5Mg alloy with grain size of 0.69 μm, a large Lüders strain around 0.2 was observed, followed by a small portion of uniform elongation, leading to large elongation. By contrast, for 2N Al with

similar grain size (d = 0.83 μm), the tensile stress-strain curve exhibited a sharp drop of the stress and then gradually decreased in the flow stress due to early necking of the sample. As a result, the elongation was much smaller than that of Al-2.5Mg alloy. It is well known that tensile strength and tensile elongation (especially, uniform elongation) are significantly affected by the work-hardening rate. Thus, the work-hardening behaviors of Al-2.5Mg alloy and 2N Al having similar grain size were investigated, as exhibited in Fig. 2.14 (b). It was notable that the work-hardening rate significantly increased with Mg addition, resulting in large uniform elongation.

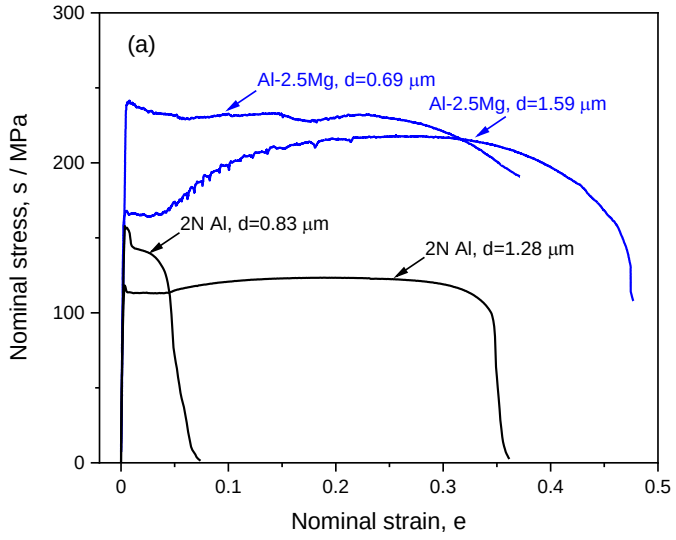

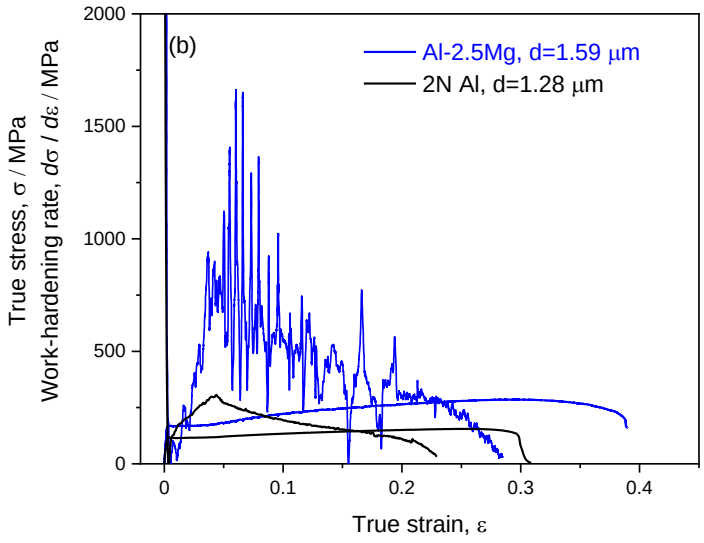

Fig. 2.14 (a) Nominal stress-strain curves, (b) true stress-strain curves and corresponding work-hardening curves of the Al-2.5Mg and 2N Al alloys with similar grain sizes.

2.4 Discussion

2.4.1 Strengthening mechanisms in Al-Mg alloys

The results obtained from present study have shown that both grain refinement and Mg addition could effectively enhance the yield strength of Al-Mg alloys. It is reasonable to consider that the yield strength of fully recrystallized Al-Mg alloys can be determined by adding the contribution of solid solution strengthening and GB strengthening to the lattice friction of pure Al, since particle strengthening and dislocation strengthening can be neglected in these fully recrystallized samples with single-phase structure. The yield strength of Al-Mg alloys can therefore be expressed as:

$$\sigma_{YS} = \sigma_{Al} + \sigma_{SS} + \sigma_{GB} \qquad (2-5)$$

where σ_{Al}, σ_{SS} and σ_{GB} are strength contributions from the lattice friction, solute atoms and GBs, respectively.

In conventional dislocation theory, it is considered that solute atoms in a crystal lattice act as obstacles for dislocation motion, mainly due to elastic fields around them. There are a number of

theories describing the traditional solid solution strengthening mechanism, such as the classical Fleischer theory [27], which applies mostly for dilute alloys; the Labusch theory [28], which extends the analysis to more concentrated solutions, etc. Any of these models is sufficient to offer a basic physical view of solid solution strengthening. Note that these models are strictly valid for solid solution hardening at 0 K. Solute atoms influence the elastic energy of a dislocation due to both local size and modulus changes and act as obstacles to dislocation motion. Thus, the friction stress of metallic materials is composed of two components, thermal component which increases with lowering temperature and non-thermal component which is changeable depending on solute contents (a dependence on $c^{1/2}$ for Fleischer model and $c^{2/3}$ for Labusch model, respectively). A simpler model is preferred in order to calculate the solid solution strengthening at room temperature. Fig. 2.9 shows the relationship between the friction stress σ_0 obtained from Hall-Petch plots and Mg contents. The solid black line is a fitting line with a correlation of more than 0.997. The linear relationship (Eq. (2-3)) is found to be applicable and more convenient to evaluate the strength contribution of solid solution strengthening in Al-Mg alloys at room temperature under quasi-static deformation.

GBs also act as barriers to dislocation motion. The contribution of the GB strengthening to the strength depends on the spacing between boundaries and their resistance to dislocation glide. The strength increment by grain size refinement is well described by the Hall-Petch relationship, as shown in Fig. 2.8. Extra hardening phenomena were observed in Al-Mg alloys and 2N Al with decreasing the grain size, discontinuous yielding behavior resulted a much higher Hall-Petch slope than continuous yielding. Extra hardening phenomenon is relevant to the discontinuous yielding behavior, which is generally induced by the shortage of mobile dislocations in recrystallized grains [9]. In the case of UFG structure, the density of GBs is significantly higher in contrast to the CG

counterpart, in parallel, dislocation sources exist generally in the grain boundaries since the finite grain interior is short of dislocations. In this case, high stress is required to activate the dislocation sources. Once activated, lower stress is capable of gliding these generated dislocations. Such plastic deformation should initiate in a local region and therefore the yield point phenomenon appears. As a result, the measured yield strength deviates from the value as predicted by conventional Hall-Petch relationship, exhibiting extra hardening behavior. Based on the cooperation of solid solution hardening and GB strengthening mechanisms, a good combination of strength and ductility in Al-Mg alloys could be achieved through combining optimized grain refinement with Mg addition. It is also noteworthy that precise measurement of the Hall-Petch slopes in Al-Mg alloys and 2N Al shows a lower Hall-Petch slope in the latter, where other strengthening mechanism must operate in addition to GB strengthening.

2.4.2 Effect of solute Mg on Hall-Petch slope for yield stress

The addition of Mg atoms contributes not only to solid solution strengthening but also to enhanced GB strengthening due to the increase in Hall-Petch slope, as shown in Fig. 2.10. It is generally accepted that the dislocation pile-up theory can explain the yielding phenomenon in CG polycrystalline metals. Following the pioneering work by Hall [12] and Petch [13], many experimental and theoretical studies have been conducted to show the linear relationship between yield stress and reciprocal square root of grain size, as shown in Eq. (2-2). In the dislocation pile-up model, the Hall-Petch slope k_{HP} can be expressed as following equation:

$$k_{HP} = M\sqrt{\frac{2\tau_c \mu b}{\pi k}} \qquad (2-6)$$

where M is the Taylor factor, τ_c is the critical stress to activate the Frank-Read source of neighboring grain, μ is the shear modulus, b is the Burgers vector, and k is a constant depending

on the character of dislocation (edge/screw). GBs act as barriers against dislocations generated from a Frank-Read source, at the same time they work as dislocation sources when the pile-up stress has exceeded τ_c. In the present study, comparing to pure Al, the addition of Mg atoms significantly enhances the strengthening effect of GBs. According to Eq. (2-6), the increase in k_{HP} should be derived from the increment of τ_c because the other parameters, μ and b, are almost independent of the addition of solute Mg [29]. That is to say, the addition of solute Mg enhances the resistance of GB to plastic deformation. It was noteworthy that the values of k_{HP} reaches a plateau when the global Mg content exceeds 2.5 wt.%. The critical stress to activate the Frank-Read source of a neighboring grain should increase with increasing Mg content according to the general scaling law describing the strength of a metal pertains to the spacing and strength of obstacles encountered by dislocations. Therefore, the Hall-Petch slope should also increase with increasing Mg content, but this does not explain the experimental results. The subsequent plateau of k_{HP} values suggests that GB strengthening may have reached saturation despite the continued increase in global Mg content. Measurements of larger Hall-Petch slope values might be interpreted in terms of the solute atoms segregating to the GB regions analogous to the situation for adding Ni to IF steel [26]. Akama et al [30] also reported that the Hall-Petch slope, significantly increases with increasing carbon content up to 60 ppm in ferritic steel, and explained that this was caused by the segregation of carbon at the GB regions. On the other hand, Murdoch and Schuh [31] had reported that Mg has a positive enthalpy of segregation in Al and would therefore have an energetic preference to segregate to the GBs. These reports enable us to consider that Mg atoms may segregate to GBs during annealing, which enhance the stability of the dislocation emission site at GBs.

According to the modified Langmuir-McLean segregation isotherm [32,33], the equilibrium GB segregation level (X_i^{GB}) in Al-Mg binary alloy can be given by:

$$\frac{X_i^{GB}}{X_i^{GB*} - X_i^{GB}} = \frac{X_i}{1 - X_i} \exp\left(-\frac{\Delta G_{i,T}}{kT}\right) \qquad (2-7)$$

where X_i^{GB*} is the saturation limit of the GB, X_i is the atomic fraction of solute atoms in the matrix, $\Delta G_{i,T}$ is the Gibbs energy of segregation of solute atoms at GB, k is the Boltzmann constant and T is the given temperature. Note that this equation is generally believed to be well accordance with the GB segregation levels in sufficiently annealed alloys since the validity has been experimentally demonstrated [32]. However, in practical annealing situations, the solute atoms seldom have sufficient time to reach full equilibrium GB segregation level. To calculate the GB segregation levels in Al-Mg alloys, the following assumptions were made: (I) there is little effect from other trace elements and the samples were taken as Al-Mg binary alloys; (II) all samples in this study have reached equilibrium GB segregation during annealing. It must be pointed out that experimental examinations have demonstrated the remarkable and complex effects of GB misorientation/types on GB segregation of solutes [32,34]. GB structures typically exhibit a diverse set of atomic environments, and thus a wide spectrum of segregation energies. Therefore, the calculated GB segregation levels should reflect the average value of all GBs. Due to the difficulties in calculating the average GB segregation while taking different GB structures into account, a special GB is selected to represent the tendency of GB segregation behavior. The values of the parameters for calculating GB segregation levels are listed in Table. 2-2.

Table 3-2 Summarized values of the parameters for calculating GB segregation in this work.

Grain boundary	X_i^{GB*}	$\Delta G_{i,T}$ / eV	Ref.
Σ17(530)[001] tilt	0.166	0.281	[35]

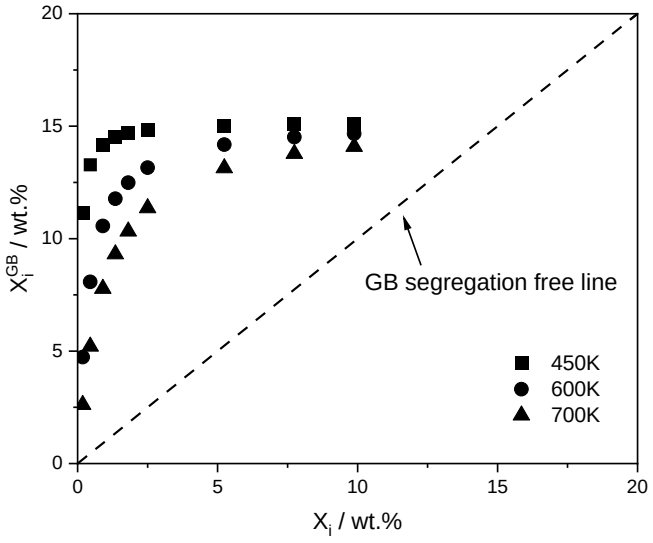

Fig. 2.15 The calculated GB segregation levels corresponding to the experimental conditions in which Hall-Petch relationship is determined

Fig. 2.15 summarizes the calculated GB segregation levels under the experimental conditions in which the Hall-Petch relationships were determined. The deviations from the GB segregation free line reflect the magnitude of GB segregation. It is indicated that Mg atoms show clear GB segregation. At a given annealing temperature, a sharp increase in the solute content at GB regions occurred over the global composition range of 0~2.5 wt.% Mg, indicating that Mg atoms predominately segregate to GBs with only a few Mg atoms apparent within the grains at low solute contents. Further increase in the global concentration toward a plateau of solute content at GBs, which suggests that GB segregation has reached maximum. The temperature dependence shows that a lower annealing temperature can increase GB segregation levels, which further decreases the global concentration needed to reach GB saturation since Al-Mg alloys with lower Mg contents were annealed at relatively lower temperatures. The majority of the Mg atoms initially segregate to the GBs at low solute contents, and subsequent Mg additions are accommodated in the grain interiors due to solute saturation of the GBs. This tendency is consistent with the solute-dependent

Hall-Petch slope exhibited in Fig. 8. The GB strengthening increments due to Mg addition can thus be understood in the context of solute segregation altering the nature of the GBs and enhancing the GB resistance against dislocation glide.

The Hall-Petch slope for fine-grained Al-Mg samples exhibits similar trend as that in CG counterparts. Although the dislocation pile-up model has been frequently quoted to explain the Hall-Petch relationship, there exist some limitations of this model that pile-up was not frequently observed, especially in UFG metallic materials. These led Li to propose the GB source model [36]. As described by the GB source model, dislocations are generated at GB ledges and all these dislocations form dislocation forests in grain interiors. Accordingly, the Hall-Petch relationship can be written as:

$$\sigma_Y = \sigma_0 + M\alpha\mu b(8m/\pi)^{1/2}d^{-1/2} \qquad (2-8)$$

Hence, the Hall-Petch slope k_{HP} based on the grain boundary source model is expressed as:

$$k_{HP} = M\alpha\mu b(8m/\pi)^{1/2} \qquad (2-9)$$

where M is the Taylor factor, α is a constant, μ is the shear modulus, b is the magnitude of Burgers vector and m is the GB ledge density. According to Eq. (2-9), the increase of k_{HP} by the addition of Mg atoms should result from the increment of m because the other parameters, α, μ and b, are almost independent of the addition of Mg. Fig. 10 shows that there is an increase in Hall-Petch slope for the fine grain-size range, but continued increase in Mg content does not lead to further increase in Hall-Petch slope. Based on the GB source model, the GB ledge density might have already reached saturation in Al-2.5Mg alloy. In polycrystalline Al-Mg alloys, it is probable that yielding starts by dislocation emission at GBs and that Mg has a significant influence on the mechanism of GB strengthening. However, regarding the discussion of the Hall-Petch relation in UFG materials, the grain-size dependence of GB segregation behavior of alloying elements and

GB ledge density should be taken into consideration. The solute concentration at GB regions will decrease drastically with decreasing grain size, because the GB area per unit volume increases with decreasing grain size. Whereas the GB ledge density is expected to increase with decreasing grain size. These two factors make it much more complicated interpret the changes in Hall-Petch slope.

The mechanism of enhanced GB strengthening due to solutes segregation has not been fully clarified yet, especially in UFG materials, further experimental and theoretical investigations need to be done in the future clarify the mechanism of yielding phenomenon in Al-Mg alloys.

2.4.3 Hall-Petch slope for flow stress

Fig. 11 has shown that the grain size dependence of the yield stress is stronger than that of the flow stress at strains beyond yield. This feature has been noted previously in Al-Mg alloys exhibiting yield point phenomena [22]. The strong grain size dependence of the yield stress primarily reflects difficulty in initiating plastic flow and Lüders band propagation. The strength-structure relationship expressed in Eq. (2-4) is based on the grain size as the strength-determining structural parameter, without considering other structural features influencing the strength such as dislocations. For Al-2.5, 5 and 7.5Mg alloys, the Hall-Petch slope for flow stress decreases to a value around 100 $MPa \cdot \mu m^{1/2}$ after yield and remains practically constant up to 0.2 strain. In this case, the main effect of strain is simply an increase in intercept stress $\sigma_0(\varepsilon)$ which is independent of the grain size. It indicates that, in spite of the development of obstacles within a grain as strain proceeds, the grain boundary resistance to slip band formation remains an important factor in the flow stress and dislocation locking induced by solute Mg continues to determine the grain boundary strength even after considerable plastic deformation. By contrast, in the case of Al-10Mg alloy, the gradual increase in Hall-Petch slope represents an effect of work hardening. The high

work-hardening rate in Al-10Mg alloy increases the difficulty of operating a dislocation source and so Hall-Petch slope increases as deformation proceeds.

2.4.4 Drastic drop in uniform elongation

In this study, it has been found that the uniform elongation of Al-2.5Mg alloy abruptly drops below 0.01 as the mean grain size decreases down to values smaller than 0.5 μm, as shown in Fig. 13 (a). The limited uniform elongation of UFG samples can be attributed to the low work-hardening ability and explained in terms of plastic instability. Plastic instability condition is expressed as:

$$\sigma \geq \frac{d\sigma}{d\varepsilon} \qquad (2-10)$$

where σ is flow stress, ε is true strain, and dσ/dε is work-hardening rate. According to the plastic instability condition, necking will occur when the flow stress becomes larger than the work-hardening rate. The strain to satisfy plastic instability condition can be influenced by several factors in fine grain-size regime: (I) The yield stress increases with decreasing grain size without any accompanying increase in work-hardening rate, so the strain to satisfy plastic instability condition will be reduced; (II) The level of inhomogeneous flow increases with decreasing grain size and over this Lüders strain the flow stress is constant and global work hardening-rate is zero. Of course on a micro level work hardening does occur, since plastic flow is happening at the front of the Lüders band and work hardening occurs locally to stabilize the reduced specimen cross section. Both factors result in the condition being satisfied at reduced strain. As shown in Fig. 14 (a), when the grain size becomes smaller than 4.17 μm, the uniform elongation of Al-2.5Mg samples decreases with decreasing the grain size, whereas the Lüders strain increases with decreasing the grain size. At the grain size around 0.69 μm, the Lüders strain becomes nearly the same as uniform elongation. It is expected that the Lüders strain will continue to increase when

the grain size becomes smaller than 0.69 μm and finally overtakes the uniform elongation, leading to a drastic drop in the uniform elongation. It has been verified in sample with grain size of 0.47 μm, the local strain exceeds the uniform elongation at the inflection point of the stress-strain curve, as indicated in Fig. 14. The present results suggest that the way localized strain is accommodated has a strong influence on the uniform elongation. Comparing to 2N Al, adding Mg to Al matrix can postpone the occurrence of dramatic drop in uniform elongation with decreasing the grain size, retaining enough uniform elongation in UFG Al-2.5Mg samples. This is because the work-hardening ability increases with increasing Mg content, which can alleviate the strain localization and accommodate large plastic strains. It can be concluded that the abrupt drop of uniform elongation in Al-Mg alloys is due to the rapidly increased localized strain, which is caused by the discontinuous yielding behavior, eventually exceeds the uniform elongation with decreasing grain size.

2.4.5 Effect of solute Mg on work hardening

It is noted that the addition of solute Mg can postpone the occurrence of sudden drop in uniform elongation with decreasing the grain size (2.13 (a)). This is because the work hardening is enhanced, as shown in Fig 14 (b). The difference in the work-hardening behaviors suggests that the dislocation motion associated with deformation in these materials is different. But what is the mechanism of enhanced work hardening with Mg addition? The most frequently quoted explanation is based on a viewpoint of stacking fault energy (SFE). Due to the high SFE of pure Al (150 mJ/m^2 [37]), dynamic recovery can easily take place through the cross slip of dislocations and the dislocation cell structure forms during deformation [10,38]. This cell structure has a low dislocation storage capacity [10], that's why pure Al exhibits low work hardening during tensile deformation (Fig. 14 (b)). Many investigations had been carried out on the microstructure

evolution and work hardening in Al-Mg alloys [39,40], and it had been revealed that the addition of solute Mg could inhibit cell structure formation. The conventional view considers that the SFE decreases with increasing Mg content, which results in the recombination of partial dislocations becoming difficult, thus limiting dislocation cross slip [2,10,41,42]. However, a comparative study on the work hardening of Al-Mg and Al-Cu alloys questioned the role of Mg in decreasing SFE because no significant difference in dislocation structures and work hardening behaviors were detected, in spite of the opposite effects of Mg and Cu on the SFE of Al [43]. If the explanation based on SFE is established, adding Cu should increase the SFE of Al and therefore well-defined cell structures would form in Al-Cu alloy. But the dislocation structure in Al-Cu alloy is very similar to that observed in Al-Mg alloy. Thus, an alternative interpretation is proposed that the microstructure evolution in Al alloys is controlled by solute-dislocation interactions rather than the stacking fault-induced barriers for dislocation cross slip. The solute-dislocation interactions are particularly enhanced in Al-Mg alloys due to the large atomic size mismatch (12%) between Al and Mg atoms which arises severe lattice distortion. As a result, the Peierls potential for dislocation motion can be largely fluctuated and the lattice friction becomes very large [44]. Solute effects increase the friction stress and thereby hinder dislocation cross slip, like lowering the SFE. It is considered that Mg atoms play a vital role in the accumulation of dislocations and therefore the work-hardening rate in Al-Mg alloys because of solute-dislocation interactions.

2.5 Conclusions

Fully recrystallized Al-2.5, 5, 7.5 and 10Mg alloys with different mean grain sizes ranging from 0.24 μm to 134 μm were fabricated by HPT/cold rolling and subsequent annealing. The combined effects of grain size and Mg contents on the mechanical properties and strengthening mechanisms

in Al-Mg alloys were systematically investigated by quasi-static tensile tests at room temperature. The main conclusions are summarized as follows:

(1) In all the Al-Mg alloys, the yield strength significantly increases with refining the grain size. Meanwhile, the yielding behavior changes from continuous yielding to discontinuous yielding with Lüders deformation, with decreasing the grain size.

(2) Two-stage Hall-Petch relationship was obtained in each Al-Mg alloy, where extra hardening phenomenon accompanying with discontinuous yielding were observed in the fine-grained alloys. The extra hardening phenomenon is generally induced by the shortage of mobile dislocations in recrystallized grains.

(3) The addition of Mg atoms contributes not only to solid solution hardening but also to enhanced grain boundary strengthening manifested by an increase in the Hall-Petch slope. Grain boundary segregation of solute Mg can alter the nature of grain boundaries and enhance the grain boundary resistance against plastic deformation, but the Mg content at grain boundaries may have already reached saturation in Al-2.5Mg alloy.

(4) The relatively strong grain size dependence of Hall-Petch slope mainly reflects the difficulty in initiating plastic flow and Lüders band propagation, and the influence of grain size on the flow stress is lower at strains beyond yield. In Al-2.5, 5 and 7.5Mg alloys, the constant value of Hall-Petch slope indicates that locked dislocation sources continue to determine the grain boundary resistance even after considerable plastic deformation. Whereas in Al-10Mg alloy, the Hall-Petch slope increases with strain due to high work hardening.

(5) The drastic loss of uniform elongation is attributed to the enhanced early plastic instability associated with the occurrence of discontinuous yielding behavior in the ultrafine-grained

Al-Mg alloys. The work-hardening rate increases with increasing Mg content, which can alleviate strain localization and therefore postpone the occurrence of early necking while decreasing the grain size. Strength-ductility synergy in Al-Mg alloys could be achieved through combining optimized grain refinement with Mg addition.

References

[1] M. Jobba, R.K. Mishra, M. Niewczas, Flow stress and work-hardening behaviour of Al–Mg binary alloys, Int. J. Plast. 65 (2015) 43–60.

[2] Y. Liu, M. Liu, X. Chen, Y. Cao, H.J. Roven, M. Murashkin, R.Z. Valiev, H. Zhou, Effect of Mg on microstructure and mechanical properties of Al-Mg alloys produced by high pressure torsion, Scr. Mater. 159 (2019) 137–141.

[3] H. Aboulfadl, J. Deges, P. Choi, D. Raabe, Dynamic strain aging studied at the atomic scale, Acta Mater. 86 (2015) 34–42. https://doi.org/https://doi.org/10.1016/j.actamat.2014.12.028.

[4] D.H. Jang, Y.B. Park, W.J. Kim, Significant strengthening in superlight Al-Mg alloy with an exceptionally large amount of Mg (13 wt%) after cold rolling, Mater. Sci. Eng. A. 744 (2019) 36–44. https://doi.org/https://doi.org/10.1016/j.msea.2018.11.132.

[5] J.E. Hatch, Aluminum: properties and physical metallurgy, Am. Soc. Met. Met. Park. Ohio 44073, U. S. A, 1984. 424. (1984).

[6] E.L. Huskins, B. Cao, K.T. Ramesh, Strengthening mechanisms in an Al–Mg alloy, Mater. Sci. Eng. A. 527 (2010) 1292–1298. https://doi.org/https://doi.org/10.1016/j.msea.2009.11.056.

[7] N. Tsuji, Y. Ito, Y. Saito, Y. Minamino, Strength and ductility of ultrafine grained aluminum and iron produced by ARB and annealing, Scr. Mater. 47 (2002) 893–899. https://doi.org/https://doi.org/10.1016/S1359-6462(02)00282-8.

[8] Y.Z. Tian, S. Gao, L.J. Zhao, S. Lu, R. Pippan, Z.F. Zhang, N. Tsuji, Remarkable transitions of yield behavior and Lüders deformation in pure Cu by changing grain sizes, Scr. Mater. 142 (2018) 88–91.

https://doi.org/https://doi.org/10.1016/j.scriptamat.2017.08.034.

[9] S. Gao, M. Chen, S. Chen, N. Kamikawa, A. Shibata, N. Tsuji, Yielding Behavior and Its Effect on Uniform Elongation of Fine Grained IF Steel, Mater. Trans. 55 (2014) 73–77. https://doi.org/10.2320/matertrans.MA201317.

[10] B.-H. Lee, S.-H. Kim, J.-H. Park, H.-W. Kim, J.-C. Lee, Role of Mg in simultaneously improving the strength and ductility of Al–Mg alloys, Mater. Sci. Eng. A. 657 (2016) 115–122. https://doi.org/https://doi.org/10.1016/j.msea.2016.01.089.

[11] M. Zha, X.-T. Meng, H.-M. Zhang, X.-H. Zhang, H.-L. Jia, Y.-J. Li, J.-Y. Zhang, H.-Y. Wang, Q.-C. Jiang, High strength and ductile high solid solution Al–Mg alloy processed by a novel hard-plate rolling route, J. Alloys Compd. 728 (2017) 872–877. https://doi.org/https://doi.org/10.1016/j.jallcom.2017.09.017.

[12] E.O. Hall, The Deformation and Ageing of Mild Steel: III Discussion of Results, Proc. Phys. Soc. Sect. B. 64 (1951) 747–753. https://doi.org/10.1088/0370-1301/64/9/303.

[13] N.J. Petch, The cleavage strength of polycrystals, J. Iron Steel Inst. 174 (1953) 25–28.

[14] X. Huang, N. Hansen, N. Tsuji, Hardening by Annealing and Softening by Deformation in Nanostructured Metals, Science (80-.). 312 (2006) 249 LP – 251. https://doi.org/10.1126/science.1124268.

[15] N. Tsuchida, Y. Tomota, K. Nagai, K. Fukaura, A simple relationship between Lüders elongation and work-hardening rate at lower yield stress, Scr. Mater. 54 (2006) 57–60. https://doi.org/10.1016/j.scriptamat.2005.09.011.

[16] 紙川尚也, 繰り返し重ね接合圧延 (ARB) による構造用金属材料の結晶粒超微細化, (2006).

[17] N. Kamikawa, X. Huang, N. Tsuji, N. Hansen, Strengthening mechanisms in

nanostructured high-purity aluminium deformed to high strain and annealed, Acta Mater. 57 (2009) 4198–4208. https://doi.org/https://doi.org/10.1016/j.actamat.2009.05.017.

[18] S. Gao, M. Chen, M. Joshi, A. Shibata, N. Tsuji, Yielding behavior and its effect on uniform elongation in IF steel with various grain sizes, J. Mater. Sci. 49 (2014) 6536–6542. https://doi.org/10.1007/s10853-014-8233-0.

[19] Y.Z. Tian, Y.P. Ren, S. Gao, R.X. Zheng, J.H. Wang, H.C. Pan, Z.F. Zhang, N. Tsuji, G.W. Qin, Two-stage Hall-Petch relationship in Cu with recrystallized structure, J. Mater. Sci. Technol. 48 (2020) 31–35. https://doi.org/https://doi.org/10.1016/j.jmst.2019.12.023.

[20] S. Khamsuk, N. Park, S. Gao, D. Terada, H. Adachi, N. Tsuji, Mechanical Properties of Bulk Ultrafine Grained Aluminum Fabricated by Torsion Deformation at Various Temperatures and Strain Rates, Mater. Trans. 55 (2014) 106–113. https://doi.org/10.2320/matertrans.MA201321.

[21] N. Hansen, The effect of grain size and strain on the tensile flow stress of aluminium at room temperature, Acta Metall. 25 (1977) 863–869. https://doi.org/https://doi.org/10.1016/0001-6160(77)90171-7.

[22] D.J. Lloyd, S.A. Court, Influence of grain size on tensile properties of Al-Mg alloys, Mater. Sci. Technol. 19 (2003) 1349–1354. https://doi.org/10.1179/026708303225006088.

[23] R.W. Armstrong, Hall–Petch Relationship: Use in Characterizing Properties of Aluminum and Aluminum Alloys, Encycl. Alum. It Alloy. GE Tott. M. Tiryakioglu, Ed. (2016).

[24] K. Nakanishi, H. Suzuki, Analysis of the Grain Size Dependence of the Yield Stress in Copper-Aluminum and Copper-Nickel Alloys, Trans. Japan Inst. Met. 15 (1974) 435–440. https://doi.org/10.2320/matertrans1960.15.435.

[25] F. Jiang, T. Masumura, T. Tsuchiyama, S. Takaki, Effect of Substitutional Element

Addition on Hall-Petch Relationship in Interstitial Free Ferritic Steels, ISIJ Int. 59 (2019) 1929–1931. https://doi.org/10.2355/isijinternational.ISIJINT-2019-100.

[26] D. Akama, N. Nakada, T. Tsuchiyama, S. Takaki, A. Hironaka, Discontinuous yielding induced by the addition of nickel to interstitial-free steel, Scr. Mater. 82 (2014) 13–16. https://doi.org/https://doi.org/10.1016/j.scriptamat.2014.03.012.

[27] R.L. Fleischer, Solid-solution hardening, Strength. Met. (1964) 93–140.

[28] R. Labusch, A Statistical Theory of Solid Solution Hardening, Phys. Status Solidi. 41 (1970) 659–669. https://doi.org/10.1002/pssb.19700410221.

[29] J. Zander, R. Sandström, L. Vitos, Modelling mechanical properties for non-hardenable aluminium alloys, Comput. Mater. Sci. 41 (2007) 86–95. https://doi.org/https://doi.org/10.1016/j.commatsci.2007.03.013.

[30] K. Takeda, N. Nakada, T. Tsuchiyama, S. Takaki, Effect of Interstitial Elements on Hall–Petch Coefficient of Ferritic Iron, ISIJ Int. 48 (2008) 1122–1125. https://doi.org/10.2355/isijinternational.48.1122.

[31] H.A. Murdoch, C.A. Schuh, Estimation of grain boundary segregation enthalpy and its role in stable nanocrystalline alloy design, J. Mater. Res. 28 (2013) 2154–2163. https://doi.org/DOI: 10.1557/jmr.2013.211.

[32] P. Lejček, M. Šob, V. Paidar, Interfacial segregation and grain boundary embrittlement: An overview and critical assessment of experimental data and calculated results, Prog. Mater. Sci. 87 (2017) 83–139. https://doi.org/https://doi.org/10.1016/j.pmatsci.2016.11.001.

[33] D. McLean, A. Maradudin, Grain boundaries in metals, PhT. 11 (1958) 35.

[34] X.-Y. Liu, J.B. Adams, Grain-boundary segregation in Al–10%Mg alloys at hot working

temperatures, Acta Mater. 46 (1998) 3467–3476. https://doi.org/https://doi.org/10.1016/S1359-6454(98)00038-X.

[35] R.K. Koju, Y. Mishin, Atomistic study of grain-boundary segregation and grain-boundary diffusion in Al-Mg alloys, Acta Mater. (2020). https://doi.org/https://doi.org/10.1016/j.actamat.2020.10.029.

[36] J.C.M. Li, Petch relation and grain boundary sources, Trans. Metall. Soc. AIME. 227 (1963) 239.

[37] M.J. Mills, P. Stadelmann, A study of the structure of Lomer and 60° dislocations in aluminium using high-resolution transmission electron microscopy, Philos. Mag. A. 60 (1989) 355–384. https://doi.org/10.1080/01418618908213867.

[38] J. Gubicza, N.Q. Chinh, Z. Horita, T.G. Langdon, Effect of Mg addition on microstructure and mechanical properties of aluminum, Mater. Sci. Eng. A. 387–389 (2004) 55–59. https://doi.org/https://doi.org/10.1016/j.msea.2004.03.076.

[39] D.A. Hughes, Microstructural evolution in a non-cell forming metal: Al□Mg, Acta Metall. Mater. 41 (1993) 1421–1430. https://doi.org/https://doi.org/10.1016/0956-7151(93)90251-M.

[40] G.W.J. Waldron, A study by transmission electron microscopy of the tensile and fatigue deformation of aluminum-magnesium alloys, Acta Metall. 13 (1965) 897–906. https://doi.org/https://doi.org/10.1016/0001-6160(65)90081-7.

[41] T.C. Schulthess, P.E.A. Turchi, A. Gonis, T.-G. Nieh, Systematic study of stacking fault energies of random Al-based alloys, Acta Mater. 46 (1998) 2215–2221. https://doi.org/https://doi.org/10.1016/S1359-6454(97)00432-1.

[42] T. Morishige, T. Hirata, T. Uesugi, Y. Takigawa, M. Tsujikawa, K. Higashi, Effect of Mg

content on the minimum grain size of Al–Mg alloys obtained by friction stir processing, Scr. Mater. 64 (2011) 355–358. https://doi.org/https://doi.org/10.1016/j.scriptamat.2010.10.033.

[43] N.Y. Zolotorevsky, A.N. Solonin, A.Y. Churyumov, V.S. Zolotorevsky, Study of work hardening of quenched and naturally aged Al–Mg and Al–Cu alloys, Mater. Sci. Eng. A. 502 (2009) 111–117. https://doi.org/https://doi.org/10.1016/j.msea.2008.10.010.

[44] S. Yoshida, T. Bhattacharjee, Y. Bai, N. Tsuji, Friction stress and Hall-Petch relationship in CoCrNi equi-atomic medium entropy alloy processed by severe plastic deformation and subsequent annealing, Scr. Mater. 134 (2017) 33–36. https://doi.org/https://doi.org/10.1016/j.scriptamat.2017.02.042.

Chapter 3 Role of Mg atoms in the work-hardening ability of Al-Mg alloys

3.1 Introduction

Work hardening is one of the most important factors in the evaluation of plastic deformation, and it is critical for the stability of plastic flow against strain localization. The tensile strength and ductility of materials are closely related to the work hardening capacity [1]. Therefore, a thorough understanding of the work-hardening behavior in terms of the fundamental mechanisms has attracted tremendous interest for its importance in advanced manufacturing processes and novel alloy design. In chapter 2, the results of tensile tests have shown that increasing Mg contents can effectively enhance the yield strength and work-hardening capacity of Al-Mg alloys, leading to improved strength-ductility synergy. However, the mechanism for the enhanced work-hardening ability with increasing Mg content is still not perfectly clarified yet. It has been believed that work hardening is governed by the evolution of dislocation structures and the extent of work hardening with increments in the dislocation density ρ can be well described by the Bailey-Hirsch relationship [2]:

$$\sigma = \sigma_0 + \alpha M \mu b \rho^{1/2} \qquad (3-1)$$

where σ is flow stress, σ_0 is the friction stress, α is a constant, M is the Taylor factor, μ is the shear modulus and b is the magnitude of Burgers vector. The dislocation density is determined by two competing processes: one is athermal storage of forest dislocations and the other is dynamic recovery due to thermally activated dislocation rearrangements and annihilation. The effects of Mg atoms on the work hardening of Al-Mg alloys should be attributed to their effect on these two processes.

It is well known that pure Al is a kind of high stacking fault energy (SFE) material, dynamic recovery can easily take place through the cross slip of dislocations during deformation, facilitating

the formation of dislocation cell structure [3–5]. For materials with such cell structures, the dislocations generated during further deformation do not accumulate within the cells but sink into the cell boundaries when encountered with dislocations with opposite Burgers vectors on the same glide plane. That's why pure Al exhibits low work hardening during tensile deformation. Intensive investigations have been carried out on the microstructure evolution and work hardening in Al-Mg alloys [5–8]. The addition of Mg atoms can inhibit cell structure formation and result in a higher work hardening rate, which is often considered to be attributed to Mg addition reduces the SFE [3,9–11]. Such an effect of SFE reduction is established for many alloys such as Cu-Al [12] and Cu-Zn [13] alloys when dislocations are considerably dissociated. However, in Al-Mg alloys deformed under quasi-static tensile test at room temperature, the dislocation dissociation is so weak that no direct evidence has ever been provided to show remarkable difference. Different from the conventional views, some experimental results questioned the role of SFE in the tensile properties of Al-Mg alloys. For example, an investigation on work hardening of Al-Mg and Al-Cu alloys revealed no remarkable difference in dislocation structures and work hardening behaviors, in spite of the opposite effects of Mg and Cu on the SFE of Al matrix [4,9]. These experimental evidence suggest that the reduction of SFE may not be the main cause that is responsible for the high work-hardening ability of Al-Mg alloys.

In this chapter, a comparative study of Al-Mg alloys with different Mg contents will be conducted to investigate the mechanical properties and the microstructure evolution that relates to work-hardening behavior, aiming to deepen our understanding of the role of Mg atoms in the high work-hardening ability of Al-Mg alloys.

3.2 Materials and experimental methods

3.2.1 Materials and processing

In this study, Al-2.5, 5 and 7.5Mg (wt.%) alloys were selected as model alloys. The as-received materials were firstly homogenized at 500 ℃ for 2 hours and then quenched in water, in order to obtain super-saturated solid solutions with single-phase structure. After homogenization, these alloys were rolled to a final thickness of 1 mm at room temperature. Disks with 30 mm in diameter and 0.8 mm in thickness were cut from the cold-rolled sheets by electrical discharge machining and then heavily deformed by HPT process at room temperature. All the disks were processed up to 5 rotations under an imposed pressure of 2 GPa at a speed of 0.2 rotation per minute. After HPT, the disks were annealed in a salt bath at temperatures ranging from 325 ℃ and 350 ℃ for 1.8 ks to produce recrystallized microstructures, and then immediately quenched in water. The annealing temperature was determined individually for each alloy, in order to obtain recrystallized microstructure with similar grain size.

3.2.2 Microstructural characterizations

After annealing, microstructures were characterized by a JEOL JSM7100F scanning electron microscope (SEM) equipped with an EDAX OIM electron backscattering diffraction (EBSD) system operated at an accelerating voltage of 15 kV. Microstructural characterization by EBSD was conducted on the transverse section (containing the shear direction SD and the normal direction ND) of the HPT disks. The microstructures were observed at the areas of which distance from the center was larger than 3 mm to avoid microstructural inhomogeneity. The observed position corresponded to the gauge part of the tensile samples. The data collection of EBSD measurement was conducted using the software provided by TSL solution, and the OIM analysis software was used to analyze the collected data. The mean grain sizes of these samples were measured by a line intercept method on SEM-BSE images. The samples for microstructural observation were mechanical polished by using SiC abrasive grinding papers and then electrically

polished to a mirror finish in an electrolyte of 10% $HClO_4$ and 90% CH_3OH at 20 V for 60 s at about −30 ℃.

The interrupted tensile samples were prepared for observing the deformation microstructures. The deformed samples were mechanically grinded to a thickness of ~100 μm using 4000 grit SiC abrasive grinding papers and the foils for transmission electron microscopy (TEM) observation were then punched from the gauge part of the tensile samples. The thickness was further reduced by a standard twin-jet electropolishing method using a Struers Tenupole-3 device in a solution of 30% HNO_3 and 70% CH_3OH at −30°C and a voltage of 15 V. TEM observation of dislocation structures was conducted on a JEM-2100F TEM operated at 200 kV.

3.2.3 Tensile tests

The tensile properties were evaluated by uniaxial tensile tests. Tensile samples with gauge length of 2 mm, width of 1 mm and thickness of 0.5 mm were cut from the HPT disks. Tensile tests were conducted on a universal tensile test machine (Shimadzu, AG-100KN X plus) with a quasi-static strain rate of 8.3×10^{-4} s^{-1} at room temperature, and two samples were tested for each condition to verify the reproducibility of stress-strain behavior. The tensile strains were precisely measured by using the DIC method. Surfaces of the tensile samples were decorated with finely sprayed black and white paint speckles which act as markers to track local displacement during deformation for the DIC analysis. A CCD camera was used to acquire digital images at an acquisition rate of 10 frames per second during the tensile tests. After tensile tests, the captured images were analyzed using VIC-2D commercial software to calculate the tensile strain.

3.2.4 In-situ synchrotron X-ray diffraction measurements

The structural evolution of Al-Mg alloys during tensile deformation was investigated by using in-situ synchrotron X-ray diffraction (XRD) measurements. The in-situ synchrotron XRD

measurements were performed at beamline BL46XU of the Super Photon Ring-8 GeV (SPring-8) in Hyogo, Japan. Fig. 3.1 shows the schematic illustration of the in-situ synchrotron XRD measurement system. The energy of the incident X-ray beam was 30 keV (corresponding to a wavelength of 0.0413 nm) and the beam size was 2 mm × 0.5 mm (in the horizontal and vertical directions, respectively). The tensile testing machine was set on a goniometer (HUBER) so that the normal direction was parallel to the incident X-ray beam. Tensile samples with gauge length of 11 mm, width of 3 mm and thickness of 0.5 mm were machined from the HPT-processed disks. Prior to a tensile test, the incident X-ray beam was positioned at the center of the gauge part of the tensile sample. Tensile tests were conducted under constant crosshead speed with an initial strain rate of 8.3×10^{-4} s^{-1} at room temperature. The diffracted X-ray beam was detected by an array of six MYTHEN detectors which were positioned 22.5° from the transmission direction. This detection system enabled us to simultaneously acquire diffraction peaks over a wide range of diffraction angles with high angular resolution, with a maximum time resolution of 1.0 second. Peak broadening quantified by the full width at half maximum (FWHM) of the reflection was analyzed to evaluate the evolutions of dislocation density and dislocation arrangement as a function of tensile strain. Profile fitting of the obtained diffraction peaks was performed using the Voigt function, and the diffraction peak angle and the FWHM were obtained. The instrumental contribution to peak broadening was calibrated using a standard CeO_2 sample and subtracted from the measured peak profiles. The XRD line profiles were analyzed by using the classical Williamson-Hall method and modified Warren-Averbach method to obtain the evolutions of dislocation density and dislocation arrangement during tensile deformation.

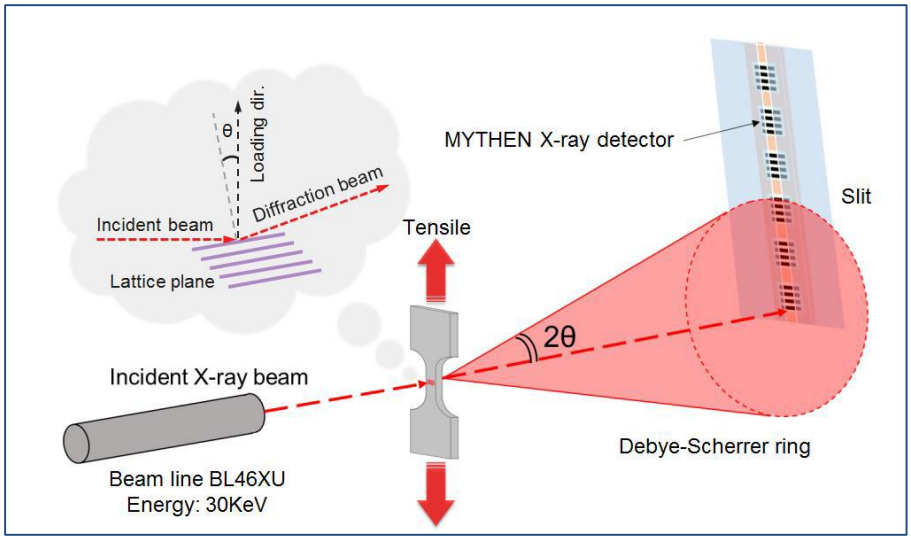

Fig. 3.1 The schematic illustration of the in-situ synchrotron XRD measurement system.

3.3 Results

3.3.1 Microstructures after annealing

Fig. 3.2 shows the inverse pole figures (IPF) and grain average misorientation (GAM) maps obtained by EBSD analysis for the Al-2.5Mg, Al-5Mg and Al-7.5Mg samples. The stereographic triangle for the IPF maps and the gradation for the GAM maps are shown in the inset. Fig. 3.2 (a) – (c) show the IPF maps for the Al-2.5, 5 and 7.5Mg samples after annealing, respectively. It can be seen that all the annealed samples consist of equiaxed grains and the microstructures are relatively homogeneous. No strongly preferred orientations were detected, indicating that the recrystallized Al-Mg samples show weak texture. It was also confirmed by the use of XRD and EBSD that all the samples showed FCC single-phase structure. Fig. 3.2 (d) – (f) show the corresponding GAM maps for the Al-Mg samples. Low-angle grain boundaries with misorientation angles (θ) between 2° and 15° and high-angle grain boundaries with $\theta \geq 15°$ are displayed as green lines and black lines, respectively. The measurements show an average high-angle grain boundaries spacing of around 10 μm and the mean grain sizes are indicated in each figure. The degree of misorientation in each grain can be evaluated from the GAM map, which is

the average misorientation angle among all pairs of adjacent points in a grain. The higher GAM value corresponds to the higher misorientation within the grain, suggesting the existence of deformation structures accompanied with larger number of dislocations. The GAM maps in Fig. 3.2 (d) – (f) shows that most of the recrystallized grains exhibit low GAM values, indicating that the average misorientation within the grains is quite low and the samples are fully recrystallized. Fully recrystallized Al-2.5Mg, Al-5Mg and Al-7.5Mg samples having similar grain size of about 10 μm were successfully fabricated by HPT and subsequent annealing process.

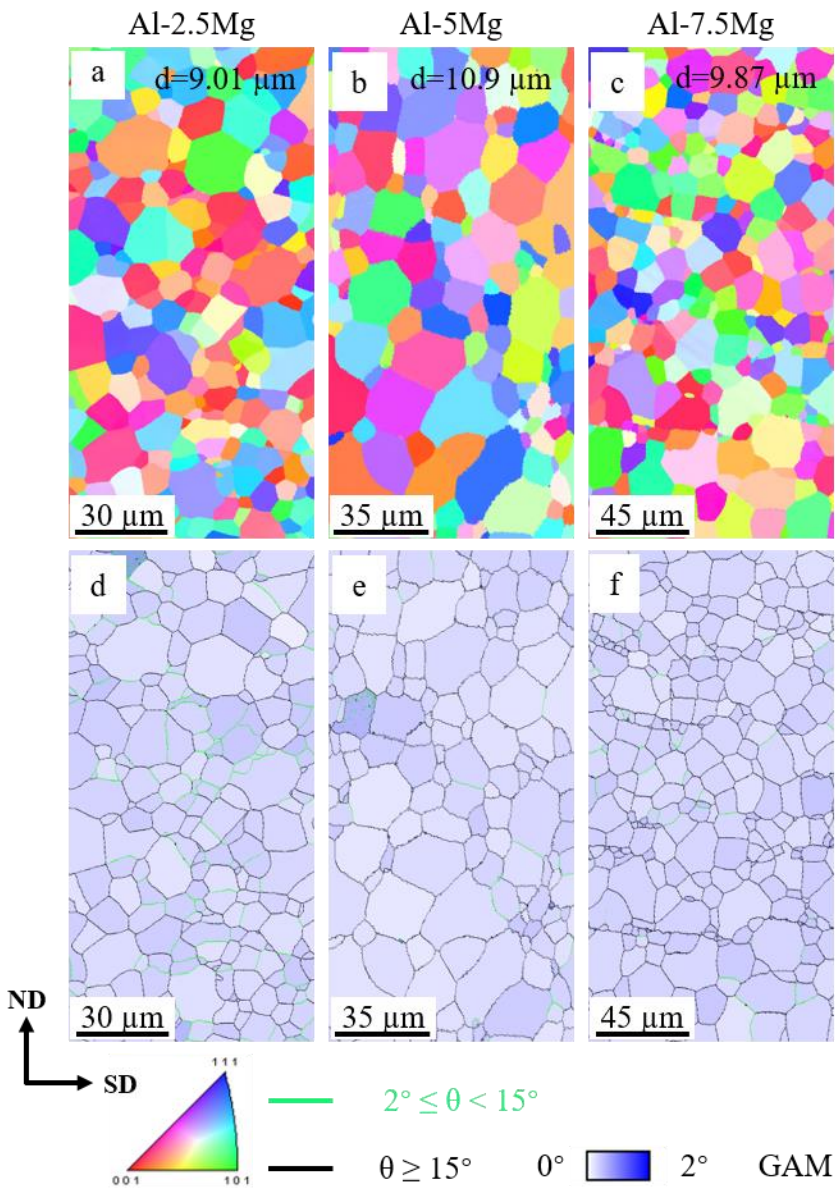

Fig. 3.2 EBSD inverse pole figures (a–c) and grain average misorientation maps (d–f) of the Al-2.5, 5 and 7.5Mg samples. (a) and (d) HPT + 325 ℃ for 1.8 ks; (b) and (e) HPT + 350 ℃ for 1.8 ks; (c) and (f) HPT + 325 ℃ for 1.8 ks. High-angle grain boundaries with misorientation larger than 15° are shown as black lines, and low-angle grain boundaries with misorientation between 2° and 15° are shown as green lines.

3.3.2 Mechanical properties and work-hardening behavior

Fig. 3.3 (a) exhibits the nominal stress-strain curves of Al-Mg alloys with similar grain size but different Mg content. For comparison, the tensile response of 2N Al sample with mean grain size

of 11.2 μm (prepared by accumulative roll-bonding process and subsequent annealing [14]) is also plotted. As demonstrated in the figure, the yield strength and ultimate tensile strength increase with increasing Mg content, but the ductility does not change significantly. It is apparent that the stress-strain curves for the Al-Mg alloys exhibit serrated flow, which corresponds to dynamic strain aging caused by the interaction between moving dislocations and solute atoms. The stress-strain curve for Al-7.5Mg alloy shows a yield-point phenomenon and Lüders deformation. All these phenomenon are typical of what is expected in Al-Mg alloys [15]. The key point of this figure is that the Al-Mg alloys with higher Mg content show enhanced tensile strength, while maintaining a high ductility.

The work-hardening rate, which represents by the derivative of the true stress with respect to the true strain, is shown in Fig. 3.3 (b) as a function of true stress. The area below the point $d\sigma/d\varepsilon = \sigma$ reveals the region in which necking is predicted to occur according to Considre's criterion. Note that the yield-point behavior, occurring in Al-7.5Mg alloy at small strains, was not considered when plotting the work-hardening curve here. Obviously, the work-hardening rate increases with increasing Mg content. The strain to satisfy Considère criterion decreases slightly with the increase in the Mg content till 2.5% and then increases gradually thereafter. It can be seen that the work-hardening rate of Al-7.5Mg alloy remains relatively high over a range of strains, while that of 2N Al decrease rapidly. As a result, the uniform elongation of Al-7.5Mg alloy is even larger than that of 2N Al despite its high yield strength. Higher work-hardening rate can relieve strain localization and promote the uniform elongation in Al-Mg alloys. This feature has been widely used to design stronger Al-Mg alloys. In general, the strength and the ductility are inversely related; hence, these experimental results are especially interesting and noteworthy. The enhanced work hardening as well as improved strength-ductility synergy by increasing Mg content should stem from the

microstructural changes associated with the addition of Mg atoms. In order to reveal the intrinsic mechanisms governing the work-hardening behavior in Al-Mg alloys, the changes of dislocation density and dislocation arrangement during tensile deformation will be investigated in the following sections.

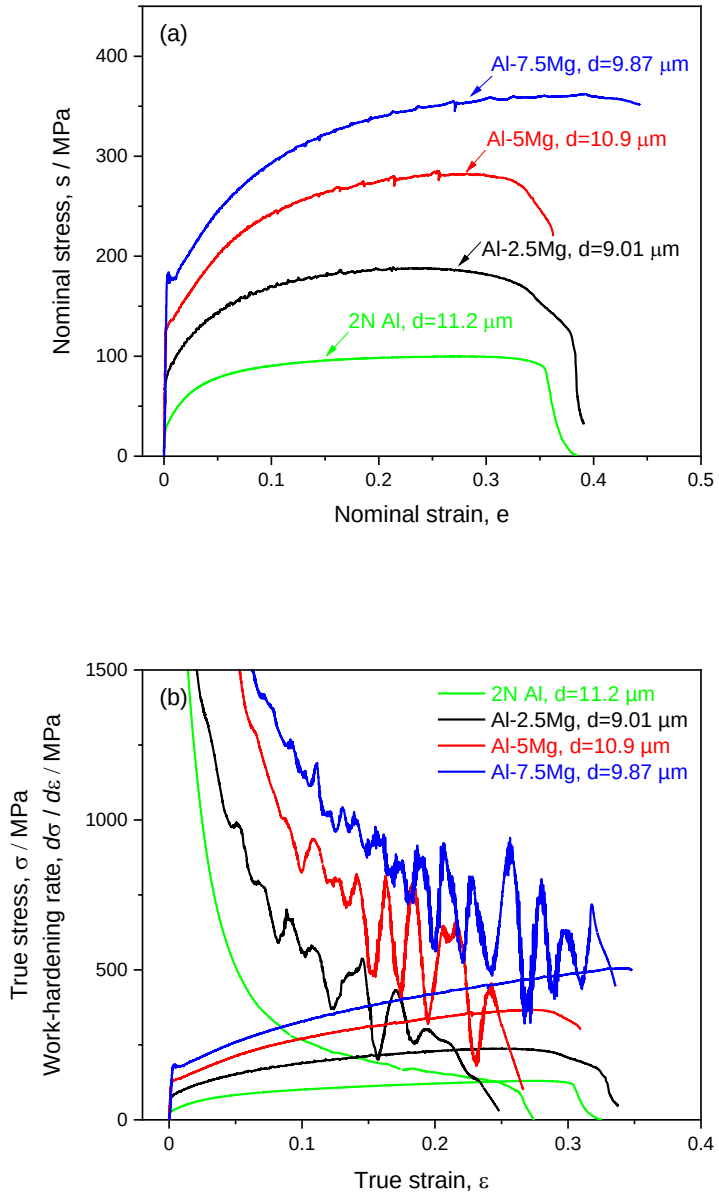

Fig. 3.3 (a) Nominal stress-strain curves of 2N Al, Al-2.5Mg, Al-5Mg and Al-7.5Mgalloys. (b) True stress-strain curves and corresponding work-hardening curves.

3.3.3 Dislocation density changes during tensile deformation

In order to understand the enhanced work-hardening rate accompanying with increasing Mg content, in-situ synchrotron XRD measurements were applied to evaluate the dislocation density evolution during tensile deformation. Fig. 3.4 shows the nominal stress-strain curves for Al-2.5Mg, Al-5Mg and Al-7.5Mg samples obtained during in-situ synchrotron XRD measurements. The strains are calculated from the displacement of the crosshead of the tensile testing machine, and therefore include not only the deformation of the tensile samples but also any deformation of the apparatus. In addition, the size of tensile sample is different from those used in micro tensile test. Therefore, the stress-strain curves obtained at the synchrotron facility are not the exactly same as those in Fig. 3.3 (a).

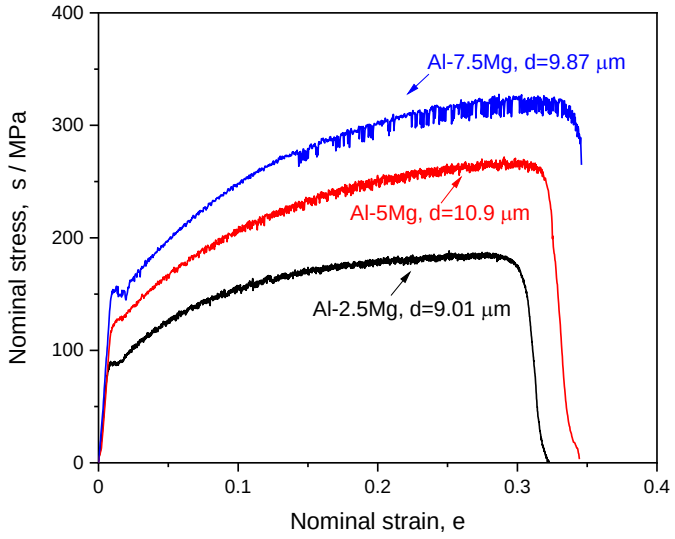

Fig. 3.4 Nominal stress-strain curves for the Al-2.5Mg, Al-5Mg and Al-7.5Mg samples having similar grain size during in-situ synchrotron XRD measurements.

The dislocation density is determined from the XRD profiles based on estimations using the Williamson-Hall analysis [16]:

$$\frac{\Delta 2\theta \cos\theta}{\lambda} = \frac{0.9}{D} + \frac{2\varepsilon \sin\theta}{\lambda} \qquad (3-2)$$

where Δ2θ is the FWHM of the diffraction peak, θ is the diffraction angle, λ is the wavelength of the incident X-ray, ε is the heterogeneous strain, and D is the crystallite size. Note that in order to improve the accuracy of calculated dislocation density, the peak broadening induced by XRD instrument is subtracted from the measured peak profiles. A plot of Δ2θcosθ/λ as a function of 2sinθ/λ for each diffraction peak will make it possible to determine the heterogeneous strain from the slope and the crystallite size from the vertical-axis intercept. Fig. 3.5 shows a Williamson-Hall plot for the Al-2.5Mg alloy at a tensile strain of 0.05 as an example. It is clear that Eq. (3-2) fits well with the data points since Al has weak elastic anisotropy.

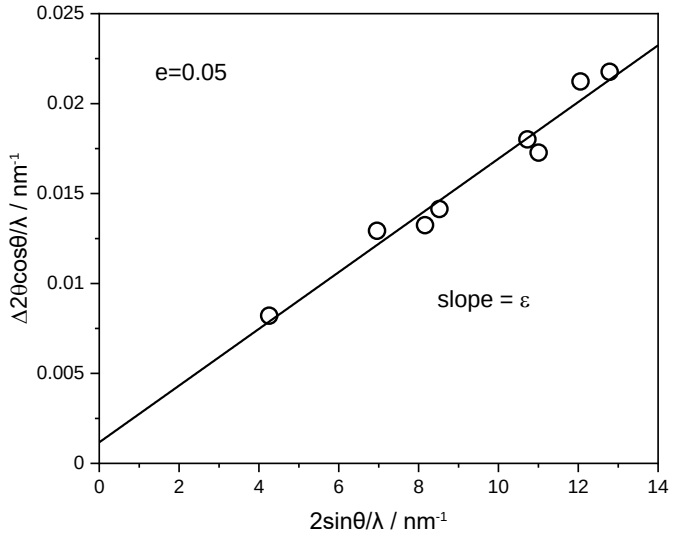

Fig. 3.5 Williamson-Hall plot of the Al-2.5Mg alloy at 0.05 plastic strain.

Afterward, the dislocation density ρ can be calculated by substituting the heterogeneous strain ε into the following equation [16] :

$$\rho = \frac{K\varepsilon^2}{b^2} \qquad (3-3)$$

where b is the magnitude of the Burgers vector, and K is a constant depending on the crystal structure. In this study, K = 16.1 for the FCC structure [16] is used. The changes in dislocation density during tensile deformation can be derived from the changes in the slope of the Williamson-Hall plot with strain by repeating the above procedures.

Fig. 3.6 (a) – (c) shows the calculated dislocation density as a function of nominal strain for the Al-2.5Mg, Al-5Mg and Al-7.5Mg samples, respectively. It should be pointed out that due to the severe splitting of XRD peaks at small strains, the dislocation density was evaluated from a strain of 0.05 for all samples. Although the dislocation density calculated by using the classical Williamson-Hall method could be higher than the true value due to its overestimation nature, the trend of dislocation density evolution during tensile deformation can be captured by in-situ XRD measurements. Thus, a rough comparison can be made to show the discrepancy induced by increasing Mg content. The dislocation density changes can be discussed in conjunction with the stress-strain curves of Fig. 3.4. As exhibited in Fig. 3.6 (a), the dislocation density of Al-2.5Mg alloy increased with increasing macroscopic strain until the applied stress reached the ultimate tensile strength and then decreased as necking occurred, which was consistent with the observed stress-strain behavior. Similar behavior of increase and decrease in dislocation density during tensile deformation can also be observed in Al-5Mg alloy (Fig. 3.6 (b)) and Al-7.5Mg alloy (Fig. 3.6 (c)). Furthermore, one can find that the Al-Mg alloys show distinguishable dislocation density after the same level of tensile deformation, the Al-Mg alloys with higher Mg content possess higher dislocation density. For example, at a strain of 0.25, the dislocation density of Al-2.5, 5 and 7.5Mg alloys is 1.47×10^{15} m^{-2}, 1.99×10^{15} m^{-2}, and 2.91×10^{15} m^{-2}, respectively. The dislocation density of Al-7.5Mg alloy is about 2 times that of Al-2.5Mg alloy at the strain of 0.25. Such a large difference should be related to the difference in Mg content since the grain size effects are expected to be

small. The results shown above suggest that for Al-Mg alloys having similar grain size, increasing Mg content can significantly accelerate the dislocations accumulation during deformation. And according to the Bailey-Hirsch relationship (Eq. (3-1)), a higher rate of dislocation accumulation should contribute to a higher work-hardening rate.

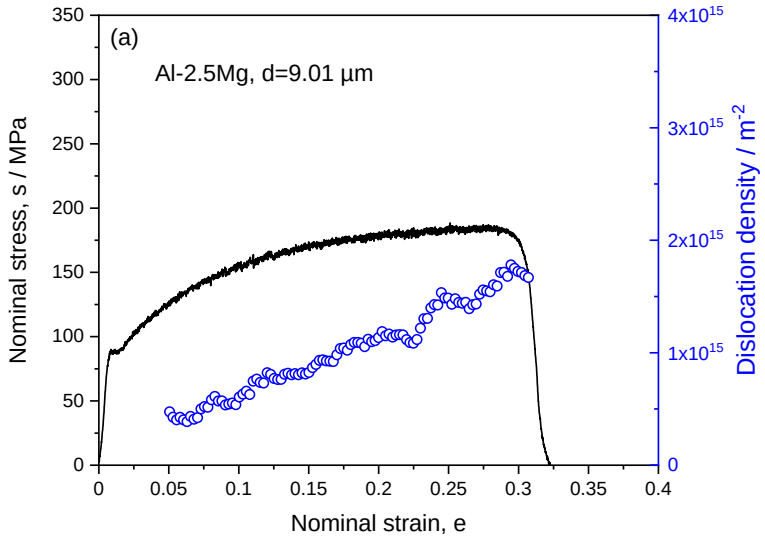

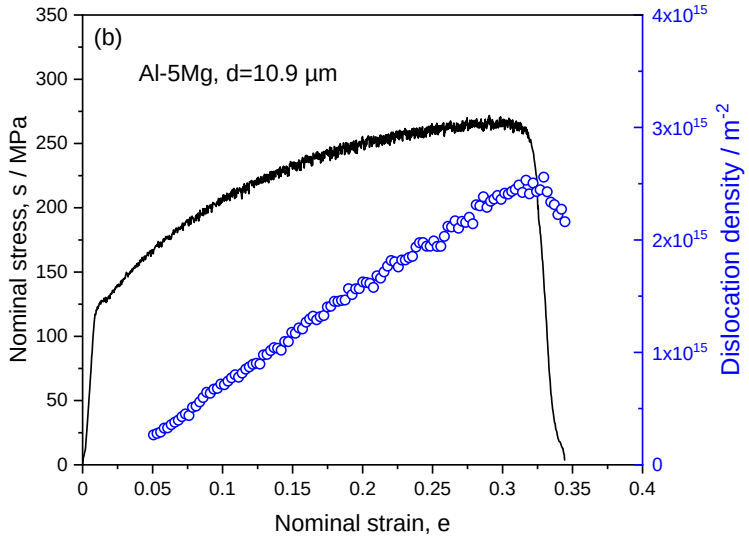

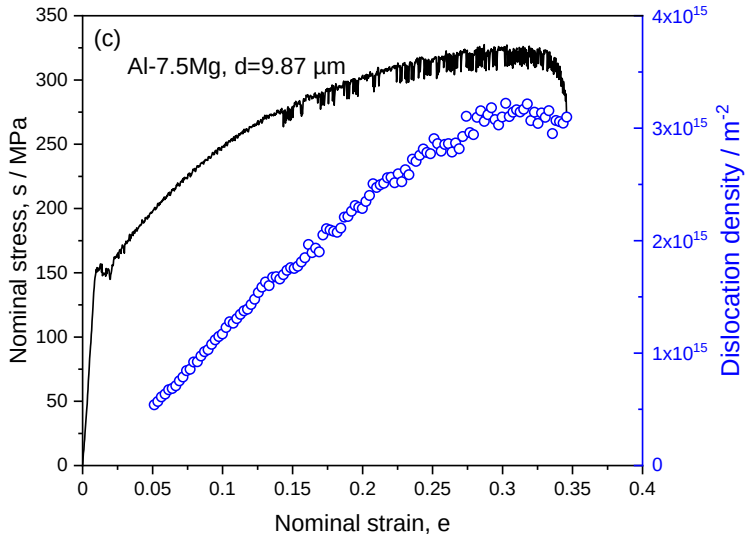

Fig. 3.6 Evolution of the dislocation density as a function of nominal strain for the Al-Mg alloys, obtained by in-situ synchrotron XRD measurements and Williamson-Hall analysis. (a) Al-2.5Mg alloy, (b) Al-5Mg alloy and (c) Al-7.5Mg alloy, respectively.

3.3.4 Dislocation arrangements from modified Warren-Averbach analysis

As shown in Fig. 3.6, the increase in Mg content can accelerate the dislocation accumulation in Al-Mg alloys, which is speculated to be related to the change in the dislocation arrangement since the dislocation density has a strong correlation with the dislocation arrangement. Wilkens [17] introduced a dimensionless parameter (M value) to display the dislocation arrangement, which could be obtained from the Fourier coefficients by applying the modified Warren-Averbach procedure [18]:

$$\ln A(L) = \ln A^S(L) - \frac{\pi b^2}{2} \cdot \rho L^2 \cdot \ln\left(\frac{R_e}{L}\right)(K^2\bar{C}) + O(K^2\bar{C})^2 \qquad (3-4)$$

where A(L) is the real part of Fourier coefficients of structural profile, $A^S(L)$ is the size component of Fourier coefficients, L is the Fourier length, R_e is the effective cut-off radius of dislocations, b

is the magnitude of the Burgers vector, K=2sinθ/λ, $\bar{C}$ is the average contrast factor. The dislocation arrangement parameter M is expressed by the following equation:

$$\mathrm{M} = R_e \times \rho^{1/2} \qquad (3-5)$$

The dislocation arrangement parameter M describes the strength of the dipole character of dislocations: a small or large value of M indicates that the dipole character and the screening of the displacement field of dislocations are strong or weak, respectively. When M > 1, the interaction between dislocations is weak and the dislocations are loosely distributed. By contrast, M < 1 indicates a stronger interaction between dislocations, and the dislocation are rearranged toward the configuration where the dipole character becomes strong, e.g. forming dislocation cell structures [19].

Fig. 3.7 shows the changes in M value for different Al-Mg samples as a function of strain. For all Al-Mg alloys, the M value decreases with the progress of tensile deformation, which suggests that the interaction between dislocations becomes stronger and the dislocations arrange themselves into an energetically stable configuration. It is evident that at the same strain levels, the M value is larger for the Al-Mg alloy with higher Mg content. It is noteworthy that all M values are larger than 1 to the extent of strain studied here. These results suggest that the interactions between solute Mg atoms and dislocations can significantly affect the rearrangement of dislocations during tensile deformation at room temperature. This difference can be explained by the pinning effect of solute Mg atoms on dislocations which hinders their rearrangement into low-energy configurations.

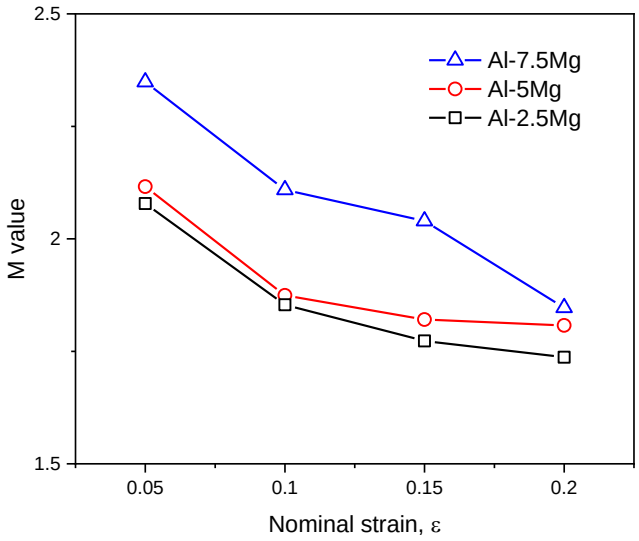

Fig. 3.7 Changes in dislocation arrangement parameter M as a function of nominal strain in different Al-Mg alloys.

3.3.5 Dislocation structures after tensile testing to specified strain

In order to confirm the difference in dislocation density and dislocation arrangement, the deformation structures of the Al-Mg alloys after tensile testing to a strain of 0.1 have been examined by TEM. Fig. 3.8 (a) – (c) shows the bright-field TEM micrographs for Al-2.5Mg, Al-5Mg and Al-7.5Mg samples, respectively. Obviously, radically different dislocation microstructures are developed in the Al-Mg alloys at close strain. In the case of Al-2.5Mg alloy, as shown in Fig. 8a, the deformation promoted the formation of weakly developed cell-like structure. The distribution of wavy dislocations is relatively heterogeneous and most dislocations are clustered in high density regions adjacent to areas which are almost dislocation free. This kind of microstructure is penetrable to the incoming dislocations and corresponds to the relatively low work-hardening rate in Al-2.5Mg alloy. For Al-5Mg alloy (Fig. 3.8 (b)), the dislocation structure changes gradually with increasing Mg content, such that the formation of dislocation cell structure is suppressed and the distribution of dislocations becomes more homogeneous. Fig. 3.8 (c) shows TEM micrographs of the microstructure developed in Al-7.5Mg alloy, it's noteworthy that the

dislocation structure changes significantly with a further increase in Mg content, with the dislocations becoming more planar and forming dislocation network structures. Overall, the dislocation configuration becomes more planar and the distribution becomes more homogeneous with increasing Mg content at close strain levels, which is in good agreement with the trend of dislocation arrangement parameter M evaluated from the XRD data. These TEM micrographs demonstrate that the addition of solute Mg atoms can strongly influence the evolution of dislocation structure during deformation, by inhibiting cell structure formation and promoting a transition from wavy slip to planar slip.

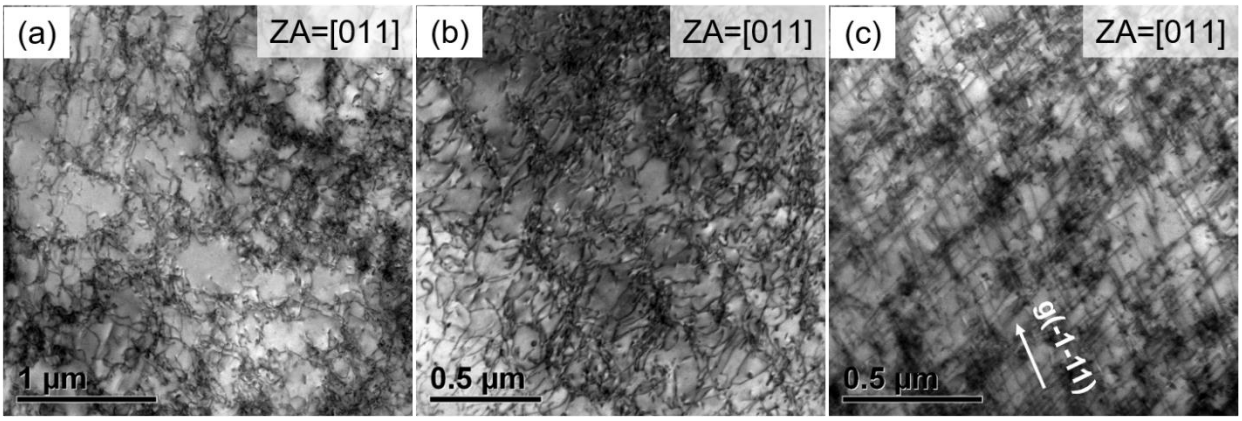

Fig. 3.8 Bright-field TEM micrographs showing the dislocation morphologies of the (a) Al-2.5Mg alloy, (b) Al-5Mg alloy and Al-7.5Mg alloy, respectively.

3.4 Discussions

3.4.1 Flow stress and dislocation density

In agreement with results reported in the literature, Mg content has a significant effect not only on the level of flow stress, but also on the work-hardening rate. As mentioned before, the increase in flow stress is induced by the increase in dislocation density as deformation proceeds. A more detailed analysis is required to establish the relationship between the microstructure evolution and the work-hardening behavior and, in particular, to separate the contributions of athermal hardening

and dynamic recovery. A number of models for the work-hardening behavior have been proposed to describe dislocation density evolution [20,21]. It has been proven that these models are applicable to the work-hardening behavior of Al alloys [22]. The work hardening can be described based on the single parameter, i.e. the dislocation density ρ using the Kocks-Mecking-Estrin model where the flow stress is solely controlled by the dislocation density [20,21,23]:

$$\frac{\mathrm{d}\rho}{\mathrm{d}\varepsilon} = k_1\rho^{1/2} - k_2\rho + \frac{k_3}{d} \qquad (3-6)$$

where d is the grain size, k_1 and k_2 are parameters related to the athermal work-hardening limit and dynamic recovery, respectively. In a polycrystalline material, the grain boundaries lead to additional accumulation of dislocations. Note that the additional accumulation of dislocations induced by grain boundaries could be roughly taken as making equal contribution because the grain size is controlled to be similar. Fig. 3.6 has shown that the net rate of dislocation accumulation with imposed strain increases with increasing Mg content. Namely, the term on the left-hand side of Eq. (3-6) increases with increasing Mg content. As regards the athermal hardening, it is apparent that solute-dislocation interaction is always capable of increasing to some extent the multiplication rate of forest dislocations and, thus, the rate of athermal hardening. In Al-Mg alloys at room temperature, the movement of dislocations is inhibited by solute Mg atoms which is indicated by the occurrence of serrated flow on stress-strain curves. The effect of enhancing the work hardening is greatly increased at the dynamic interaction of the solute atoms with dislocations [24]. In addition, the interaction should also hinder dynamic recovery so that the rate of annihilation of dislocations is reduced. Accelerated dislocation accumulation (enhanced work hardening) is therefore expected in Al-Mg alloys with increasing Mg content.

In practice, the dislocation density and the flow stress show similar evolutions as a function of strain and the saturation tensile strength is related to the maximum dislocation density, as shown

in Fig. 3.6. In order to examine the Bailey-Hirsch relation, the flow stresses of Al-Mg alloys were plotted in Fig. 3.9 as a function of the square root of the dislocation density. It can be concluded that the flow stress follows a linear relationship with the square root of dislocation density despite of experimental errors. The continuously increase of dislocation density leads to the work hardening of the Al-Mg alloys during plastic deformation. Work hardening in Al-Mg alloys is verified to be caused and solely controlled by the increase of dislocation density. The rate of dislocation accumulation in the Al-Mg alloys with higher Mg content is much faster than in those with low Mg contents, probably as a result of interactions between the dislocations and Mg atoms.

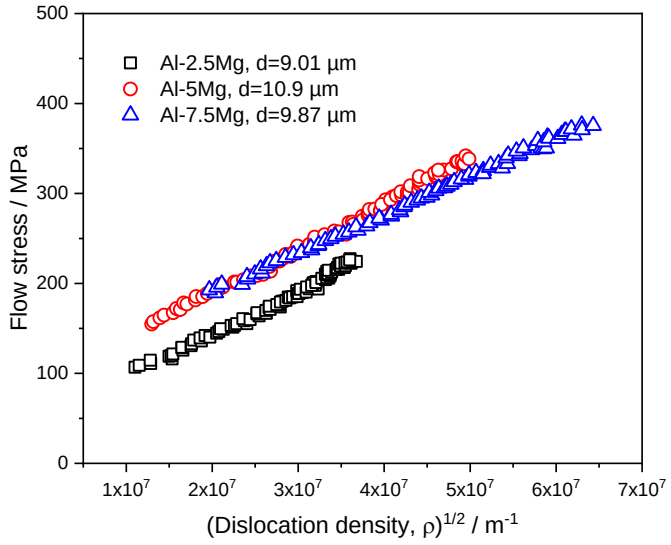

Fig. 3.9 The flow stress of Al-Mg alloys as functions of the square root of the dislocation density.

3.4.2 Origins of high work hardening in Al-Mg alloys

As exhibited in Fig. 3.3, increasing Mg content can improve both yield strength and ultimate tensile strength of Al-Mg alloys without significantly sacrificing the ductility. This is because the work-hardening rate increases with increasing Mg content, which can relieve strain localization and hence postpone the occurrence of necking. But what is the origin of enhanced work hardening with increasing Mg content? It is generally accepted that the work hardening is governed by the

microstructure evolution during deformation. The in-situ synchrotron XRD results (in Fig. 3.6 and Fig. 3.7) have revealed that increasing Mg content can remarkably accelerate dislocation accumulation and decrease the extent of dislocation rearrangement in Al-Mg alloys having similar grain size during tensile deformation. In parallel, TEM observations have confirmed the changes in dislocation structures from weakly developed dislocation cell structures to homogeneously distributed planar dislocation arrays, as shown in Fig. 3.8, which suggests that increasing Mg content can hinder the cross slip of dislocations and promote a transition from wavy slip to planar slip. However, the atomic-scale mechanism for the impeded cross slip induced by Mg addition is still under debate.

The conventional view considers that the reduced SFE is responsible for dislocation planarization accompanying with increasing Mg content. The SFE decreases with increasing Mg content, which results in the recombination of partial dislocations becoming difficult and thus limiting dislocation cross slip. Therefore, the dislocations tend to move along their primary slip planes and form both tangled dislocation and dislocation band structures. It has been widely reported that the plastic deformation mechanisms of FCC materials are sensitive to SFE under quasi-static tensile deformation at room temperature, i.e. dislocations glide in a wavy mode in high SFE materials, in contrast, the dislocation planar slip and deformation twinning prevail in low SFE materials [12,25]. For pure Al, a typical high SFE material, the dislocations can glide easily via cross slip and cell structure forms in the grain interior after imposing specific strains. For materials with such cell structures, the dislocations generated during further deformation do not accumulate within the cells but sink into the cell boundaries when encountered with dislocations with opposite Burgers vectors on the same glide plane. That’s why pure Al exhibits low work hardening during tensile deformation. Many published results proposed that the addition of Mg can reduces the SFE

of Al-Mg alloys [3,9–11]. Note firstly that the judgment on these effects is mainly based on theoretical calculation, while direct experimental data are not available. Secondly, the reduction of the SFE has a significant effect on the deformation mechanism in those cases when dislocations are considerably dissociated. But this conventional view has some limitations. Despite there are many published results showing that stacking faults or micro twins can be observed in some severely plastic deformed Al-Mg alloys [26,27] or shock-loaded Al-Mg alloys at low temperature [28], the dislocation dissociation is so weak that no direct experimental evidence has ever shown stacking faults or deformation twins in Al-Mg alloys under quasi-static deformation at room temperature. The SFE should be still very high because no remarkable difference in the splitting of dislocations is detected in Al-Mg alloys, although the dislocation configuration is clearly different. Moreover, the early data on the SFE obtained from mechanical testing are considered as unreliable because of being based on an inaccurate cross slip model, while the estimations based on the annealing rate of faulted dislocation loops did not show that Mg addition significantly reduced the SFE of Al [29].

Different from the above conventional views, some recent experimental results cast doubts on the role of SFE in the tensile properties of Al-Mg alloys. For example, Zolotorevsky's [4] investigation on Al-Mg and Al-Cu alloys showed that in spite of the opposite effects of Mg and Cu on the SFE of Al matrix, no significant difference in dislocation structures and work hardening behaviors had been observed. If the explanation based on SFE were established, adding Cu should increase the SFE and therefore promoted the formation of well-defined cell structures in Al-Cu alloy. But the dislocation structure in Al-Cu alloy was very similar to that observed in Al-Mg alloy. This supports the idea that the dislocation microstructure evolution in aluminum alloys is controlled by solute-dislocation interaction influencing the motion of dislocations rather than by

overcoming the stacking fault-induced barriers for cross slip of screw dislocations. The dislocation planar slip prevails in Al-Mg alloys with high Mg content due to the high friction stress induced by Mg addition. In general, screw dislocations can switch from one {111} type plane to another if it contains the direction of Burgers vector b. Solute Mg atoms affect the difficulty of cross slip since the dissociated partials of a screw dislocation contain edge components. The edge components of the two partial dislocations are affected by the presence of solute atoms. Cross slip becomes more difficult because the recombination of dissociated partials must overcome the friction stress imposed by the solute atoms. On the other hand, dislocations in metallic materials are usually mixed dislocations containing both edge and screw characters. The solute-dislocation interactions are particularly enhanced in Al-Mg alloys due to the large atomic size mismatch (12%) between Al and Mg atoms which arises severe lattice distortion. As a result, the Peierls potential for dislocation motion can be largely fluctuated and the lattice friction becomes very large [30]. Solute effects increase the friction stress and thereby hinder dislocation cross slip, like lowering the SFE. Note also that the Mg atoms stay preferentially at the dilated region of edge dislocations that leads to decreasing of the stress field around these dislocations. As a result, the dislocations are less clustered to minimize their elastic strain energy. This is explained by the increase of the Mg content which increases the pinning effect of Mg atoms on edge dislocations thus hindering the formation of dislocation cell structure, which is supported by both XRD (Fig. 3.7) and TEM studies (Fig. 3.8). Suppressed cross slip by the high friction stress leads to more stored dislocations hence higher work hardening during deformation. Meanwhile, the dislocation alignment becomes more planar and the distribution becomes more homogeneous with increasing Mg content. Planar dislocations on different slip planes seem to interact and form dislocation networks in Al-Mg alloys with high Mg contents (Fig. 3.8 (c)). The dislocation mean free paths decrease with the

formation of dislocation networks, leading to high work-hardening rate. Planar dislocation arrays can interact with each other and dislocation tangles forms during dislocation-dislocation interactions are obstacles for dislocation motion. Moving dislocations can be trapped by these obstacles and form dislocation pile-ups against these obstacles [31], making local plastic relaxation difficult, which also contributes to a higher work-hardening rate.

The above discussion on the effect of solute Mg on the work-hardening behavior is mainly based on the idea of atomic-scale heterogeneity in Al-Mg alloys. The dislocation cross slip is suppressed in Al-Mg alloys with increasing Mg contents due to the interaction between solute Mg atoms and dislocations. As a result, the dislocations tend to glide on their primary slip planes and promote the formation of planar dislocation arrays. It is noted that the solute Mg-dislocation interaction cannot only affect the dislocation glide in the slip plane. More importantly, the interaction between solute Mg atoms and dislocations can hinder the cross slip of dislocations, resulting in a lower rate of dynamic recovery and therefore a higher rate of dislocation accumulation. Therefore, solute enhanced work hardening has been attributed to the following processes: (1) Solute Mg atoms increase the rate of dislocation multiplication; (II) Solute Mg atoms reduce the rate of dislocation annihilation or the recovery of dislocation structures; (III) Solute Mg atoms also enhance the effectiveness of dislocations as barriers to flow. From all the conclusive experimental evidence, one can draw the conclusion that the solute Mg-dislocation interaction plays the key role in the high dislocation density and hence high work-hardening rate in Al-Mg alloys.

3.5 Conclusions

In summary, fully recrystallized Al-2.5, 5, and 7.5Mg alloys having similar grain size (~10 μm) were prepared by HPT and subsequent annealing. The tensile properties and work-hardening

behaviors of Al-Mg alloys were investigated by quasi-static tensile deformation at room temperature. The correlation between work-hardening behavior and corresponding microstructure evolution during tensile deformation were discussed to clarify the role of Mg atoms in the work-hardening rate of Al-Mg alloys. The main results obtained in this chapter are as follows:

(1) For Al-Mg alloys having similar grain size, the yield strength and work-hardening rate increase with increasing Mg content, resulting in large tensile strength and ductility.

(2) In-situ synchrotron XRD measurement was employed to evaluate the evolution of dislocation density and dislocation arrangement during tensile deformation. The results reveal that the dislocation density increases faster with strain in Al-Mg alloys having higher Mg contents. Moreover, the trend of dislocation arrangement parameter M suggests that the interaction between dislocations and solute Mg significantly affects dislocation rearrangement during deformation. The extent of dislocation rearrangement decreases with increasing Mg content.

(3) Deformation microstructure was characterized by scanning transmission electron microscopy. The addition of solute Mg can suppress dislocation cross slip and promote a transition from wavy slip to planar slip, resulting in a lower rate of dynamic recovery and therefore a higher rate of dislocation accumulation.

(4) Mg atoms play a vital role in the accumulation of dislocations and therefore the work-hardening rate of Al-Mg alloys. Al-Mg alloys with higher Mg contents exhibit higher work-hardening ability because of the important roles of solute-dislocation and solute-solute interactions. Thus, adding Mg could be an effective way to improve the strength-ductility synergy in Al-Mg alloys due to high solid solution strengthening and enhanced work hardening.

References

[1] M.A. Meyers, K.K. Chawla, Mechanical behavior of materials, Cambridge university press, 2008.

[2] J.E. Bailey, P.B. Hirsch, The dislocation distribution, flow stress, and stored energy in cold-worked polycrystalline silver, Philos. Mag. A J. Theor. Exp. Appl. Phys. 5 (1960) 485–497. https://doi.org/10.1080/14786436008238300.

[3] B.-H. Lee, S.-H. Kim, J.-H. Park, H.-W. Kim, J.-C. Lee, Role of Mg in simultaneously improving the strength and ductility of Al–Mg alloys, Mater. Sci. Eng. A. 657 (2016) 115–122. https://doi.org/https://doi.org/10.1016/j.msea.2016.01.089.

[4] N.Y. Zolotorevsky, A.N. Solonin, A.Y. Churyumov, V.S. Zolotorevsky, Study of work hardening of quenched and naturally aged Al–Mg and Al–Cu alloys, Mater. Sci. Eng. A. 502 (2009) 111–117. https://doi.org/https://doi.org/10.1016/j.msea.2008.10.010.

[5] J. Gubicza, N.Q. Chinh, Z. Horita, T.G. Langdon, Effect of Mg addition on microstructure and mechanical properties of aluminum, Mater. Sci. Eng. A. 387–389 (2004) 55–59. https://doi.org/https://doi.org/10.1016/j.msea.2004.03.076.

[6] D.A. Hughes, Microstructural evolution in a non-cell forming metal: Al□Mg, Acta Metall. Mater. 41 (1993) 1421–1430. https://doi.org/https://doi.org/10.1016/0956-7151(93)90251-M.

[7] G.W.J. Waldron, A study by transmission electron microscopy of the tensile and fatigue deformation of aluminum-magnesium alloys, Acta Metall. 13 (1965) 897–906. https://doi.org/https://doi.org/10.1016/0001-6160(65)90081-7.

[8] M. Jobba, R.K. Mishra, M. Niewczas, Flow stress and work-hardening behaviour of Al–Mg binary alloys, Int. J. Plast. 65 (2015) 43–60.

[9] T.C. Schulthess, P.E.A. Turchi, A. Gonis, T.-G. Nieh, Systematic study of stacking fault energies of random Al-based alloys, Acta Mater. 46 (1998) 2215–2221. https://doi.org/https://doi.org/10.1016/S1359-6454(97)00432-1.

[10] T. Morishige, T. Hirata, T. Uesugi, Y. Takigawa, M. Tsujikawa, K. Higashi, Effect of Mg content on the minimum grain size of Al–Mg alloys obtained by friction stir processing, Scr. Mater. 64 (2011) 355–358. https://doi.org/https://doi.org/10.1016/j.scriptamat.2010.10.033.

[11] M. Muzyk, Z. Pakiela, K.J. Kurzydlowski, Ab initio calculations of the generalized stacking fault energy in aluminium alloys, Scr. Mater. 64 (2011) 916–918. https://doi.org/https://doi.org/10.1016/j.scriptamat.2011.01.034.

[12] Y.Z. Tian, L.J. Zhao, N. Park, R. Liu, P. Zhang, Z.J. Zhang, A. Shibata, Z.F. Zhang, N. Tsuji, Revealing the deformation mechanisms of Cu–Al alloys with high strength and good ductility, Acta Mater. 110 (2016) 61–72. https://doi.org/https://doi.org/10.1016/j.actamat.2016.03.015.

[13] P. Zhang, X.H. An, Z.J. Zhang, S.D. Wu, S.X. Li, Z.F. Zhang, R.B. Figueiredo, N. Gao, T.G. Langdon, Optimizing strength and ductility of Cu–Zn alloys through severe plastic deformation, Scr. Mater. 67 (2012) 871–874. https://doi.org/https://doi.org/10.1016/j.scriptamat.2012.07.040.

[14] 紙川尚也, 繰り返し重ね接合圧延 (ARB) による構造用金属材料の結晶粒超微細化, (2006).

[15] D.J. Lloyd, S.A. Court, Influence of grain size on tensile properties of Al-Mg alloys, Mater. Sci. Technol. 19 (2003) 1349–1354. https://doi.org/10.1179/026708303225006088.

[16] G.K. Williamson, R.E. Smallman, III. Dislocation densities in some annealed and cold-

worked metals from measurements on the X-ray debye-scherrer spectrum, Philos. Mag. A J. Theor. Exp. Appl. Phys. 1 (1956) 34–46. https://doi.org/10.1080/14786435608238074.

[17] M. i Wilkens, J.A. Simmons, R. de Wit, R. Bullough, Fundamental aspects of dislocation theory, Natl. Bur. Stand. Spec. Publ. 317 (1970) 1195.

[18] T. Ungár, A. Borbély, The effect of dislocation contrast on x-ray line broadening: A new approach to line profile analysis, Appl. Phys. Lett. 69 (1996) 3173–3175. https://doi.org/10.1063/1.117951.

[19] M. Wilkens, The determination of density and distribution of dislocations in deformed single crystals from broadened X-ray diffraction profiles, Phys. Status Solidi. 2 (1970) 359–370. https://doi.org/10.1002/pssa.19700020224.

[20] U.F. Kocks, H. Mecking, Physics and phenomenology of strain hardening: the FCC case, Prog. Mater. Sci. 48 (2003) 171–273. https://doi.org/https://doi.org/10.1016/S0079-6425(02)00003-8.

[21] U.F. Kocks, Laws for Work-Hardening and Low-Temperature Creep, J. Eng. Mater. Technol. 98 (1976) 76–85. https://doi.org/10.1115/1.3443340.

[22] F. Barlat, M. V Glazov, J.C. Brem, D.J. Lege, A simple model for dislocation behavior, strain and strain rate hardening evolution in deforming aluminum alloys, Int. J. Plast. 18 (2002) 919–939. https://doi.org/https://doi.org/10.1016/S0749-6419(01)00015-8.

[23] C.W. Sinclair, W.J. Poole, Y. Bréchet, A model for the grain size dependent work hardening of copper, Scr. Mater. 55 (2006) 739–742. https://doi.org/https://doi.org/10.1016/j.scriptamat.2006.05.018.

[24] C.G. Schmidt, A.K. Miller, The effect of solutes on the strength and strain hardening behavior of alloys, Acta Metall. 30 (1982) 615–625.

https://doi.org/https://doi.org/10.1016/0001-6160(82)90110-9.

[25] X.H. An, S.D. Wu, Z.G. Wang, Z.F. Zhang, Significance of stacking fault energy in bulk nanostructured materials: Insights from Cu and its binary alloys as model systems, Prog. Mater. Sci. 101 (2019) 1–45. https://doi.org/https://doi.org/10.1016/j.pmatsci.2018.11.001.

[26] M.P. Liu, H.J. Roven, High density hexagonal and rhombic shaped nanostructures in a fcc aluminum alloy induced by severe plastic deformation at room temperature, Appl. Phys. Lett. 90 (2007) 83115. https://doi.org/10.1063/1.2696540.

[27] X.Z. Liao, J.Y. Huang, Y.T. Zhu, F. Zhou, E.J. Lavernia, Nanostructures and deformation mechanisms in a cryogenically ball-milled Al-Mg alloy, Philos. Mag. 83 (2003) 3065–3075. https://doi.org/10.1080/1478643031000152799.

[28] G.T. Gray, Deformation twinning in Al-4.8 wt% Mg, Acta Metall. 36 (1988) 1745–1754. https://doi.org/https://doi.org/10.1016/0001-6160(88)90242-8.

[29] S. Kritzinger, P.S. Dobson, R.E. Smallman, The influence of a dilute magnesium addition on the growth ant shrinkage of dislocation loops in aluminium, Philos. Mag. A J. Theor. Exp. Appl. Phys. 16 (1967) 217–229. https://doi.org/10.1080/14786436708229735.

[30] S. Yoshida, T. Bhattacharjee, Y. Bai, N. Tsuji, Friction stress and Hall-Petch relationship in CoCrNi equi-atomic medium entropy alloy processed by severe plastic deformation and subsequent annealing, Scr. Mater. 134 (2017) 33–36. https://doi.org/https://doi.org/10.1016/j.scriptamat.2017.02.042.

[31] T. Tabata, H. Fujtta, Y. Nakajima, Behavior of dislocations in AL□MG single crystals observed by high voltage electron microscopy, Acta Metall. 28 (1980) 795–805. https://doi.org/https://doi.org/10.1016/0001-6160(80)90156-X.

Chapter 4 Revealing the nature of heterogeneous deformation in Al-Mg alloys

4.1 Introduction

Heterogeneous deformation is commonly observed in metallic materials, such as early necking and Lüders deformation that occur in ultrafine-grained metallic materials, which can be related to grain size and dislocation density [1,2]. Portevin-Le Chatelier (PLC) effect is another frequently observed heterogeneous deformation behavior in metallic materials such as steels and aluminum alloys, manifested by the serrated flow in the stress-strain curve during tensile deformation. The most distinct features of PLC effect are the localized deformation bands and the motion of these bands along the sample with increasing stress [3]. In chapter 2, the tensile results have shown that serrated flow is commonly observed in tensile deformation of Al-Mg alloys and the features of serrated flow exhibit remarkable dependence on grain size and Mg content. Since the localization of strain causes degradation of the inherent structural properties and surface quality of materials, understanding the fundamental features of the PLC effect is crucial for the effective use of Al-Mg alloys. The PLC effect has been studied extensively since its discovery. Experimental observations have shown that PLC bands are of different types. In general, three types of PLC band can be classified based on the type of serrations that appear in the stress-strain curve of polycrystalline materials during constant strain rate tensile tests, assigned as type A, type B, and type C, and their characteristics are well documented [4–6]. Nucleation and propagation behavior of deformation bands are directly related to the morphologies of the serrations in the stress-strain curve [7]. Type A serrations are associated with repetitive continuous propagation of deformation bands along the gauge part of the sample and are often nucleated at one end of gauge part. Type B serrations correspond to a hopping propagation of localized bands in the axial tensile direction of the sample. Type C serrations are characterized by random nucleation of localized non-propagating bands

accompanied by large stress drops [8]. The appearance of the PLC bands can change from type A to type B and then to type C, either with decreasing strain rate or increasing temperature [6,9].

A host of mechanisms have been proposed to explain different kinds of PLC instabilities occurring during plastic flow, these assume various forms of interactions of dislocations with solute atoms and recurrent pinning and depinning of dislocations from the solute atmospheres under increasingly applied stress. Although it has been commonly accepted that the PLC effect corresponds to dynamic strain aging caused by the interaction between moving dislocations and solute atoms [10], the detailed mechanism of the serrated flow is still not perfectly clarified. The PLC effect affects most material properties. Dynamic strain aging has generally been known to cause blue brittleness that deteriorates ductility at high temperatures or low strain rates [11,12]. On the other hand, it has been also well known that work hardening of materials is significantly enhanced under dynamic strain aging conditions [3]. If the serrated flow is properly controlled based on fundamental understanding of its mechanism, good work hardening is expected to be achieved, leading to high strength and large ductility of the material.

Numerous studies have been carried out to clarify the effects of strain rate and temperature on PLC effect, there are very few investigations devoted to the effects of solute content and grain size on the localized deformation behaviors so far. This becomes an important issue since Mg addition and grain refinement are the main methods to further improve the comprehensive mechanical properties of Al-Mg alloys. In this study, the spatiotemporal characteristics associated with heterogeneous deformation in Al-Mg alloys having different Mg contents and grain sizes will be investigated by using uniaxial tensile tests and DIC technique. The aim of the present study is to fundamentally understand the features of heterogeneous deformation in Al-Mg alloys.

4.2 Materials and experimental methods

4.2.1 Materials and processing

Al-xMg (x=2.5, 5, 7.5 and 10 wt.%) alloys were used in this study. For Al-2.5, 5 and 7.5Mg alloys, the as-received materials were firstly heated at 500 ℃ for 2 h and then quenched in water to ensure homogenization. After the homogenization treatment, the materials were cold rolled at ambient temperature by 90% thickness reduction to a final thickness of 2 mm and then annealed for 30 minutes at 400 ℃, 425 ℃ and 400 ℃, respectively, and then immediately cooled in water. The annealing temperature was determined individually for each alloy, in order to obtain recrystallized microstructure with similar grain size. For Al-10Mg alloy, a cylindrical sample was cut from the as-received ingot and then extruded at 400 ℃ with an extrusion ratio of 10.6. After hot extrusion, the extruded rod was heat treated at 450 ℃ for 30 min to remove the Al_3Mg_2 phase, then cold-rolled to 90% thickness reduction, i.e., 1 mm thickness. The cold rolled sheet was then annealed at 380 ℃ for 30 s and quickly cooled in water.

4.2.2 Microstructural characterizations

Microstructural observations were conducted using a field emission scanning electron microscope (FE-SEM; JEOL 7800F) equipped with backscattered electron (BSE) detectors operated at an accelerating voltage of 15 kV. The mean grain sizes of these specimens were measured by a line intercept method. The specimens for microstructural observation were mechanically polished by using SiC abrasive grinding papers and then electrically polished to a mirror finish in an electrolyte of 10% $HClO_4$ and 90% CH_3OH at 20 V for 60 s at about −30 ℃.

The interrupted tensile samples were prepared for observing the deformation microstructures. The deformed samples were mechanically grinded to a thickness of ~100 μm using 4000 grit SiC abrasive grinding papers and the foils for transmission electron microscopy (TEM) observation

were then punched from the gauge part of the tensile samples. The thickness was further reduced by a standard twin-jet electropolishing method using a Struers Tenupole-3 device in a solution of 30% HNO_3 and 70% CH_3OH at −30°C and a voltage of 15 V. TEM observation of dislocation structures was conducted on a JEM-2100F TEM operated at 200 kV.

4.2.3 Tensile tests

Sheet-type tensile samples with a gauge length of 10 mm, width of 5 mm and thickness of 2 mm were machined from the rolled sheets. Tensile tests were conducted on Shimadzu AG-X plus system with an initial strain rate ranging between 8.3×10^{-6} s^{-1} and 8.3×10^{-2} s^{-1} in the temperature range of 25 ℃ to 100 ℃. Temperatures were measured with a thermocouple attached to the surface of the tensile sample. Prior to elevated temperature tensile testing, sample temperatures were stabilized for a minimum of 600 s at each test temperature. Tensile strains during the tensile tests were precisely measured by the DIC technique. Surfaces of the tensile samples were first sprayed in a flat white lacquer and subsequently with random black spots which acted as markers to track local displacement in the DIC analysis. A CCD camera was used to acquire digital images of the sample surfaces during the tensile tests. The captured images were analyzed using VIC-2D commercial software. Localized deformation behaviors during tensile deformation were quantitatively characterized by the DIC analysis.

4.3 Results

4.3.1 Effect of Mg content on serration behavior

To investigate the effect of Mg content on serration behavior, Al-2.5Mg, Al-5Mg and Al-7.5Mg alloys with similar grain size (~35 μm) were prepared. Fig. 4.1 shows the recrystallized microstructures of the Al-2.5Mg, Al-5Mg and Al-7.5Mg alloys obtained by SEM-BSE observations. All the samples were fully recrystallized and homogeneously consisted of equiaxed

grains.

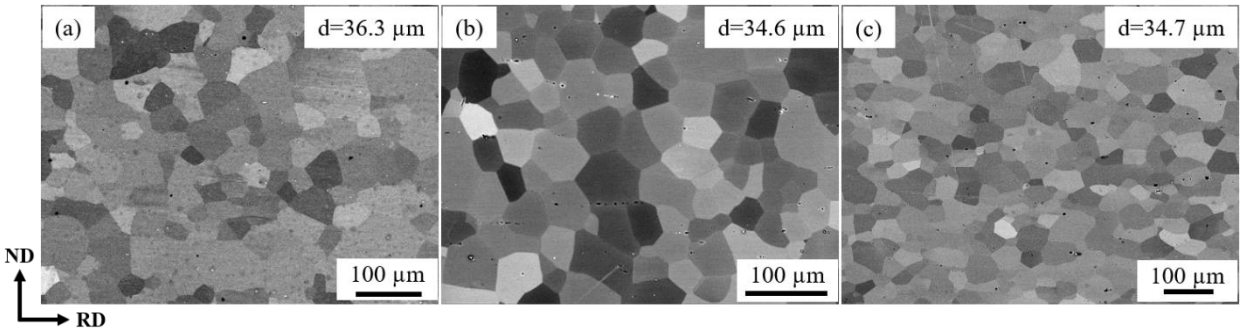

Fig. 4.1 BSE images of Al-2.5Mg, Al-5Mg and Al-7.5Mg samples after cold rolling and subsequent annealing. (a) Al-2.5Mg, 400 ℃ for 30 min, (b) Al-5Mg, 425 ℃ for 30 min, (c) Al-7.5Mg, 400 ℃ for 30 min.

Fig. 4.2 (a) exhibits the nominal stress-strain curves of Al-2.5, 5 and 7.5Mg alloys with similar grain size, obtained by the tensile tests at room temperature. The PLC effect, as manifested by the serrated stress-strain curve, occurs in all the materials used in this study. As shown in Fig. 4.2 (b), the onset of the serrations and the work hardening differ among the Al-Mg alloys due to the difference in Mg contents. For a better view, the stress-strain curves are deliberately shifted along the ordinate axis and enlarged in Fig. 4.2 (c) and Fig. 4.2 (d). It is evident that the morphology of serrations varies with global strain as well as Mg content. For Al-2.5Mg alloy, typical type A serration appears in the beginning and then it transits into a mixed type A and type B serrations at intermediate strains and finally evolves into type B serration at large strains. For Al-5Mg alloy, it is noted that with increasing strain, there is also a trend of serration types changing from type A to type B. But the transition occurs at relatively lower strains comparing to Al-2.5Mg alloy. In contrast, the serration behavior in Al-7.5Mg alloy is quite different. At small strains there's no pronounced serration at all. The critical strain for the occurrence of serrated flow is around 0.12. The serrations are large stress drops that occur below the general level of the stress-strain curve, which are typical type C serrations. This kind of serrations continues to appear till large strains, but in quick succession. The results above suggest that the characteristics of serrated flow depend

strongly on the Mg content. At intermediate strains, increasing Mg content promotes a transition from type A serration to type B serration and finally to type C serration. Meanwhile, the serration amplitude increases with increasing Mg content.

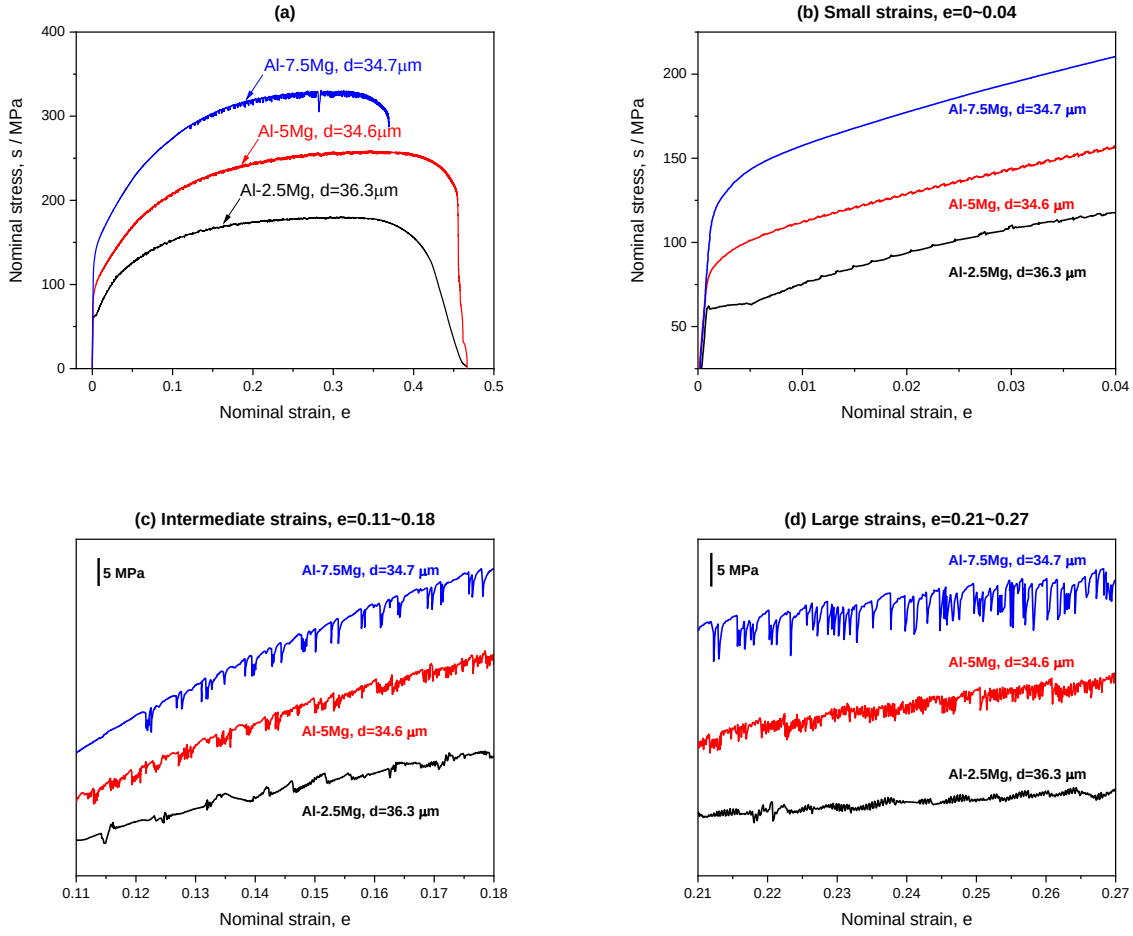

Fig. 4.2 Nominal stress-strain curves of Al-2.5, 5 and 7.5Mg alloys with similar grain size, obtained by the tensile tests at room temperature with a strain rate of 8.3×10^{-4} s^{-1}.

Fig. 4.3 – 4.5 show enlarged parts of the nominal stress-time curves (within similar strain range, as indicated in each figure) and the corresponding local strain rate maps obtained by DIC analysis for Al-Mg alloys, each pair has been synchronized to match the x-axis time scales. Note that the stress-strain and stress-time curve have the same appearance for serration morphologies. The DIC analysis clearly shows that a localized deformation in banded morphology appears and propagates

within the gage part of the tensile sample. The nucleation and propagation of the PLC band correspond well with the serration on the stress-strain curve. Fig. 4.3 shows an enlarged part of the stress-time curve of Al-2.5Mg alloy and corresponding local strain rate maps of the sample obtained by the DIC analysis. The numbers 1~6 indicate at the upper left corners of the strain rate maps correspond to the positions on the stress-strain curve indicated by the same numbers. The PLC bands are recognized as the banded regions having higher local strain rates than the other parts in the gauge section. The DIC strain rate maps clearly shows that the PLC band nucleated at one end of the gauge part followed by continuous propagation along the gage. When the PLC band reaches at the other end in the gage part, the band annihilates. And then a new PLC band nucleates at one end and propagates. Such processes repeatedly happen. The peak positions of serrations on the stress-strain curve, for example, the points 1 and 6, corresponds to the nucleation of the PLC bands in the local strain rate map. Till the nucleation of new PLC band after the annihilation, the flow stress steeply increased. Namely, type A serration corresponds to continuously propagating PLC bands: the sudden stress drop represents the nucleation of a new PLC band; the smooth stage corresponds to the continuous propagation of the PLC band.

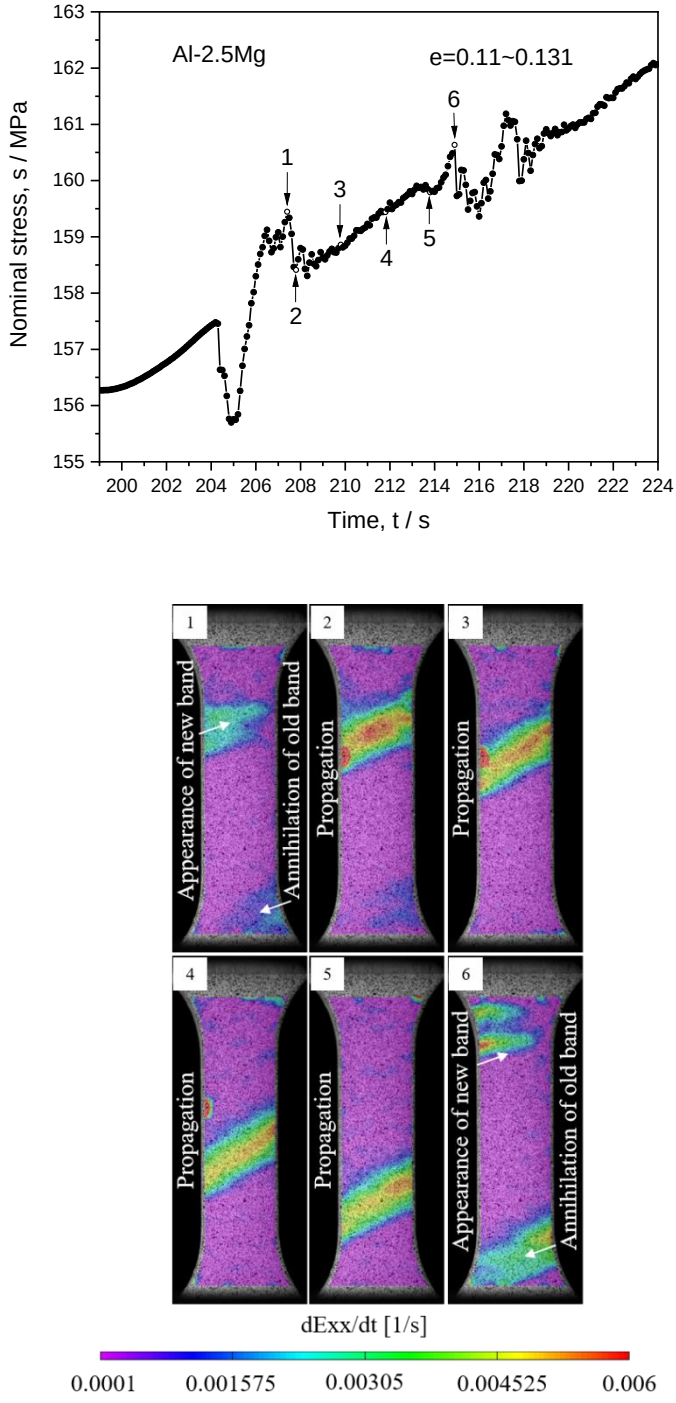

Fig. 4.3 An enlarged part of the nominal stress-time curve for Al-2.5Mg alloy and corresponding local strain rate maps of the sample at selected stages obtained by the DIC analysis.

In contrast, type B serrations occur in Al-5Mg alloy at similar strain level comparing to Al-

2.5Mg alloy, as shown in the magnified stress-time curve in Fig. 4.4. The synchronized strain rate distribution maps show that the nucleation and propagation of the PLC band correspond well with the serrated flow on the stress-strain curve. For example, the peak position of serrations on the stress-strain curve, as indicated by the point 1, corresponds to the nucleation of a PLC band in the local strain rate map. The following oscillations of the stress-time curve correspond to the repeated appearance and disappearance of the PLC band. The potential nucleation sites for the reappearance of the localized deformation band are constrained to occur within the vicinity of the previous deformation band location. Thus, the main characteristic of type B bands is the localized deformation bands are nucleated at gauge part followed by discontinuous short-distance propagation, manifested as hopping propagation. This trend contrasts with the continuous propagation of the band that occurs after the initiation with a type A stress drop.

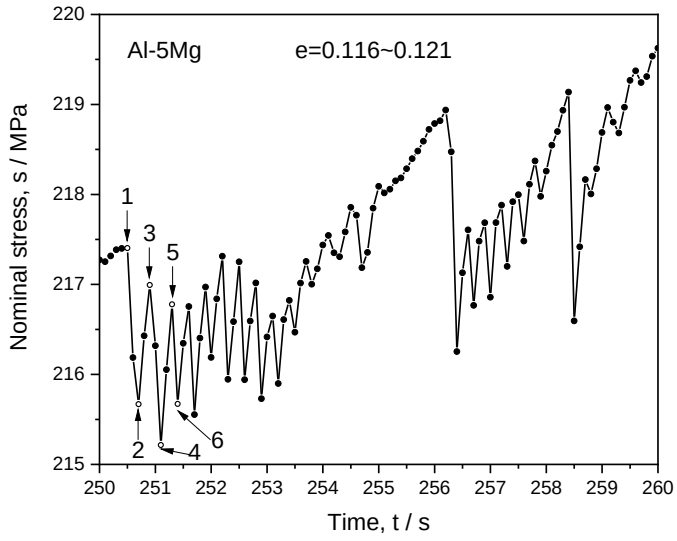

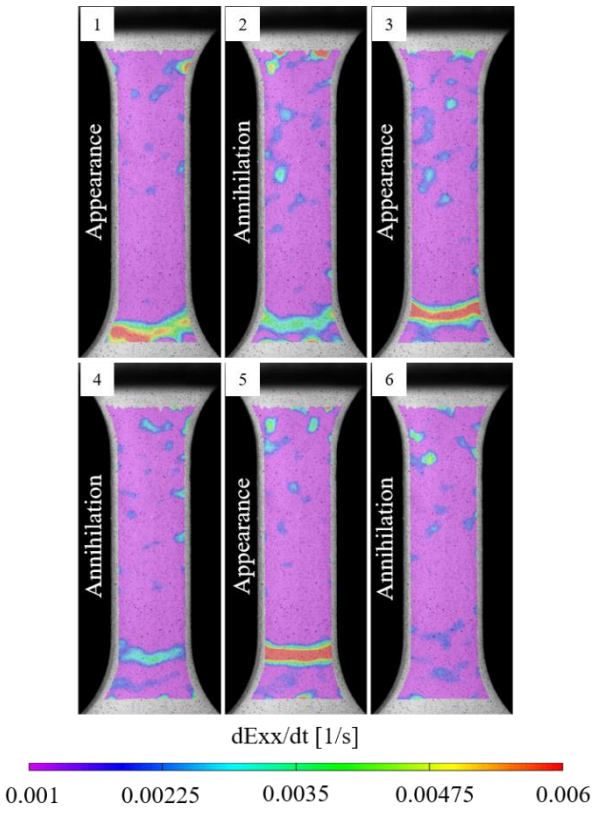

Fig. 4.4 An enlarged part of the nominal stress-time curve for Al-5Mg alloy and corresponding local strain rate maps of the sample at selected stages obtained by the DIC analysis.

As for Al-7.5Mg alloy, the DIC strain rate maps in Fig. 4.5 shows that the PLC band nucleates at the gauge part but the band does not propagate. The nucleation of each non-propagating deformation band corresponds to a large stress drop in the stress-strain curve, as indicated by the numbers 1, 5 and 7. The deformation band annihilates immediately after its nucleation. Thus, type C serrations correspond to the formation of localized non-propagating bands appearing at random locations along the gauge part, each stress drop indicates the formation of a non-propagating deformation band.

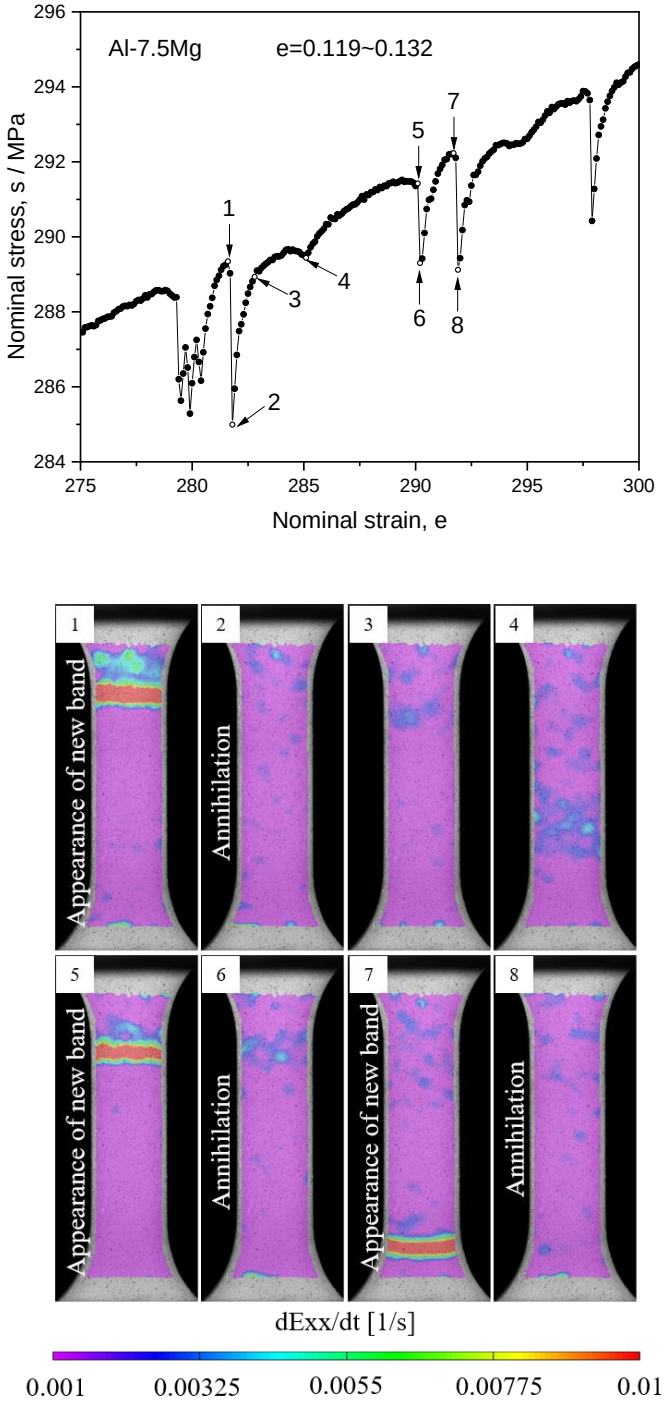

Fig. 4.5 An enlarged part of the nominal stress-time curve for Al-7.5Mg alloy and the corresponding local strain rate maps of the sample at selected stages obtained by the DIC analysis.

In this section, the strain localization associated with various band behaviors were observed

both spatially and temporally by using DIC technique. The DIC analysis clearly shows that, at similar strain level, three notably different types of localized deformation behaviors occur in Al-Mg alloys with different Mg contents. What these localized deformation behaviors have in common is that the sharp increase in flow stress happens after the annihilation of a PLC band and the flow stress gets alleviated at the nucleation of a new PLC band, indicating that lack of mobile dislocations may be one of origins to cause the serrations. Apparently, the characteristics of PLC plastic instabilities depend strongly on the Mg content, increasing Mg content promotes a transition of PLC band from type A to type B and finally to type C. Detailed discussions relating the observations above to interpretations of changes in localized deformation bands and solute-dislocation interactions will be included in the discussion section.

4.3.2 Effect of grain size on serration behavior

Fig. 4.2 has shown that type A and type B serrations can appear in a same sample (Al-2.5Mg or Al-5Mg) during tensile deformation, the only difference is the stain level or dislocation density they occur. This reminds us to consider the role of dislocation density in the serration behavior. To verify this, Al-2.5Mg samples with different grain sizes were selected as model materials since fine-grained sample possesses higher dislocation density at same strain level. Fig. 4.6 shows the representative nominal stress-strain curves obtained from tensile testing on Al-2.5Mg samples with different grain sizes. The mean grain size for each sample is indicated in the figure. It can be seen that grain refinement promotes a transition of serration types. Typical type A serrations are observed in coarse-grained sample, while type B serrations are mainly found in fine-grained sample. The magnitude of the stress drops also increases with decreasing grain size. The tensile response indicates that the occurrence and nature of the serration behavior in Al-Mg alloy also shows remarkable grain size dependence.

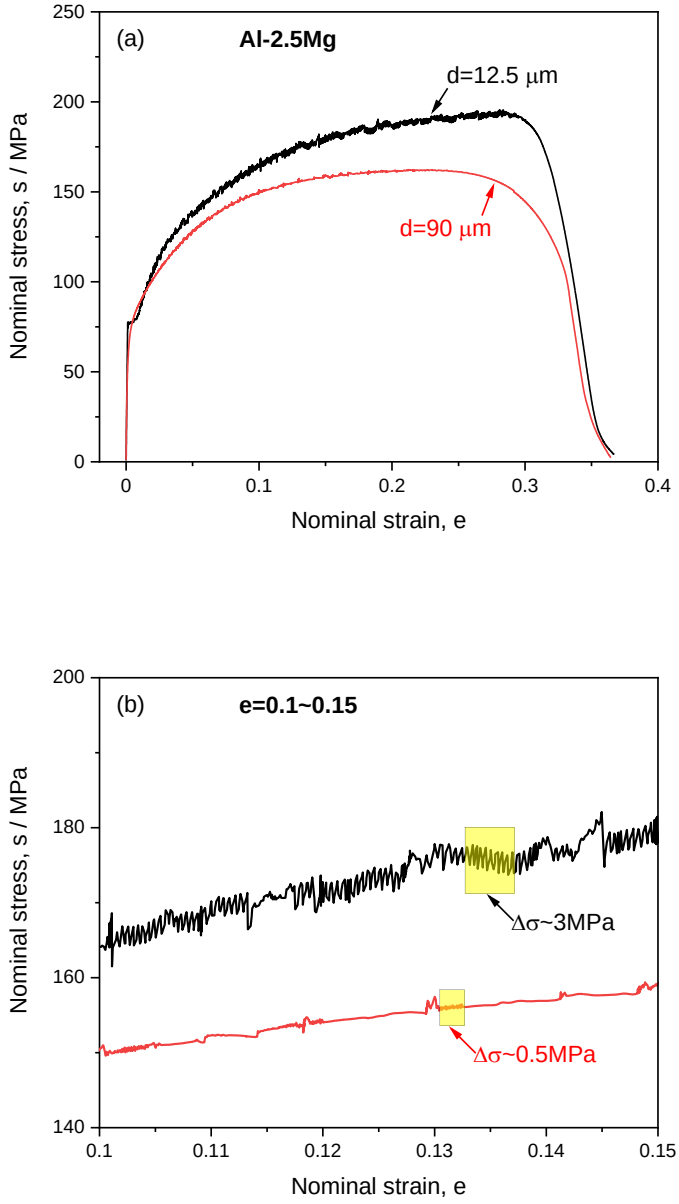

Fig. 4.6 (a) Nominal stress-strain curve of the Al-2.5Mg samples with different grain sizes in the tensile test at room temperature with a strain rate of 8.3×10^{-4} s^{-1}. (b) Enlarged sections of the stress-strain curves.

Similarly, type A and type B bands were observed to exist as continuously propagating bands and hopping bands on the gauge part, respectively. This is consistent with the observations in previous section. The local strain rate inside the PLC band is accurately measured by DIC analysis and plotted as a function of global strain, as shown in Fig 4.7. It can be seen that the local strain

rate inside the band is about several times higher than the global strain rate and increases with global strain in both samples. The local strain rate in the PLC band is much higher in the fine-grained sample than that in the coarse-grained sample, indicating that the deformation behavior becomes more heterogeneous with decreasing grain size. It can be concluded from the results shown above that the grain size has a strong effect on the heterogeneous deformation behaviors of the Al-2.5Mg sample, higher dislocation densities achieved through grain refinement likely aid the transition of PLC band types.

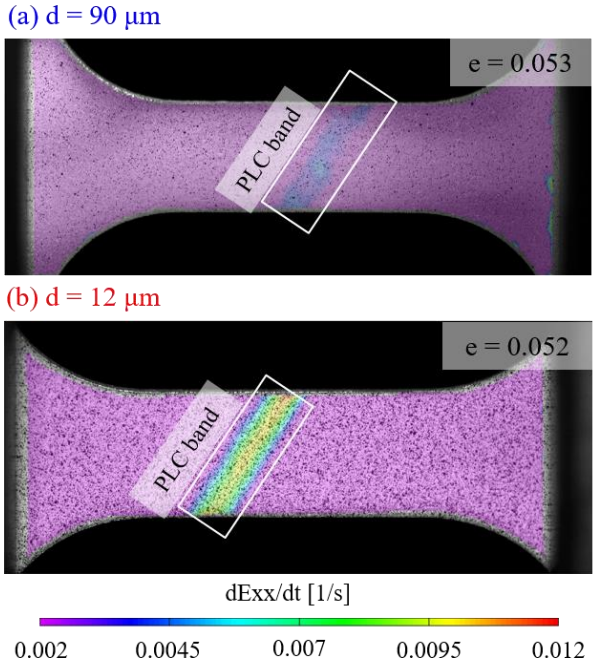

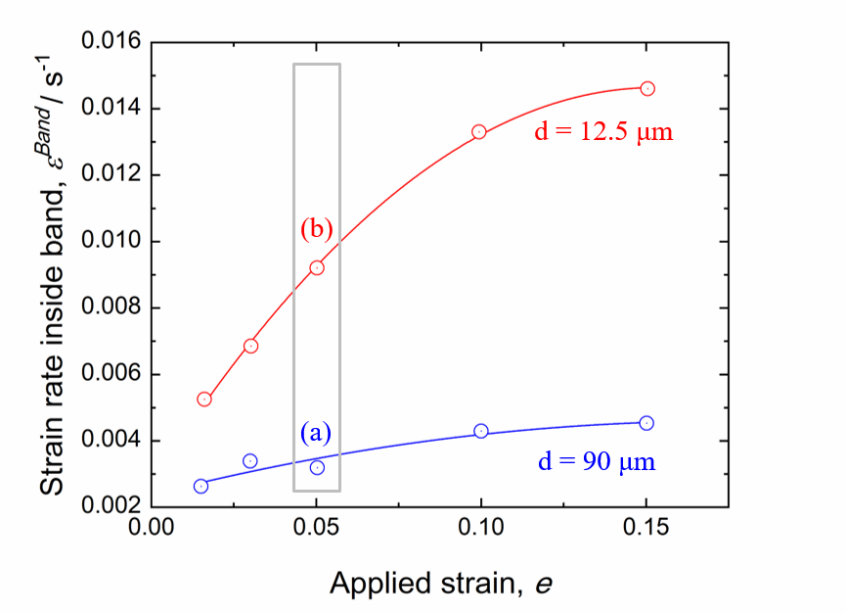

Fig. 4.7 Local strain rate within a PLC band in Al-2.5Mg samples as a function of global strain.

4.3.3 Peculiar deformation behaviors in Al-10Mg alloy

As exhibited by the tensile results in Chapter 2, the serration behavior changes with increasing Mg content. Especially when the Mg content increases to 10 wt.%, pronounced serrated flow only occurs at the late stage of tensile deformation. The deformation behavior seems to be quite different with Al-Mg alloys having lower Mg contents. In this section, it is of interest to investigate the deformation behavior in Al-10Mg alloy. Fig. 4.8 shows the nominal stress-strain curve of Al-10Mg alloy having grain size of 10.4 μm, obtained by tensile tests at room temperature. No pronounced serration behavior occurs at small and intermediate strains, which suggests that the deformation in this stage appears to be relatively homogeneous. Serration behavior associated with large stress drops only appears at the late stage of tensile deformation and the frequency is quite low comparing to Al-Mg alloys with lower Mg contents. It is expected that increasing Mg content may enhance dynamic strain aging effect and thus exhibit more pronounced serration behavior. However, the experimental result indicates that deformation behavior in Al-10Mg alloy may be much more complicated.

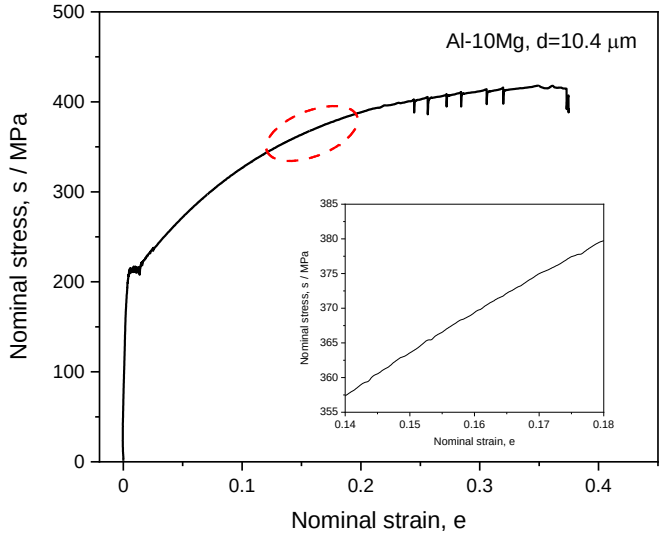

Fig. 4.8 Nominal stress-stain curve for Al-10Mg sample deformed at room temperature with a strain rate of 8.3×10^{-4} s^{-1}. The inset shows enlarged sections of the stress-strain curve.

The stress-strain curve obtained by tensile test shows only the average material response, in which the local information is hidden. In order to get more details about the deformation behavior in the early stage, a DIC measurement was performed to further process the strain rate distribution maps during deformation. The corresponding results, exhibited in Fig. 4.9, show a series of strain rate maps for the selected stages. It clearly shows that the deformation in the early stage is actually heterogeneous, even though the stress-strain curve seems to be smooth. No well-formed PLC band is detected, many island-like deformation regions appear at random locations on the gauge part and disappear quickly. The plastic deformation is mainly carried out through these island-like deformation regions whereas on average it yields a global deformation response that appears to be homogeneous. That is, the plastic deformation of Al-10Mg alloy at small and intermediate strain levels is heterogeneous on local scale whereas homogeneous on global scale.

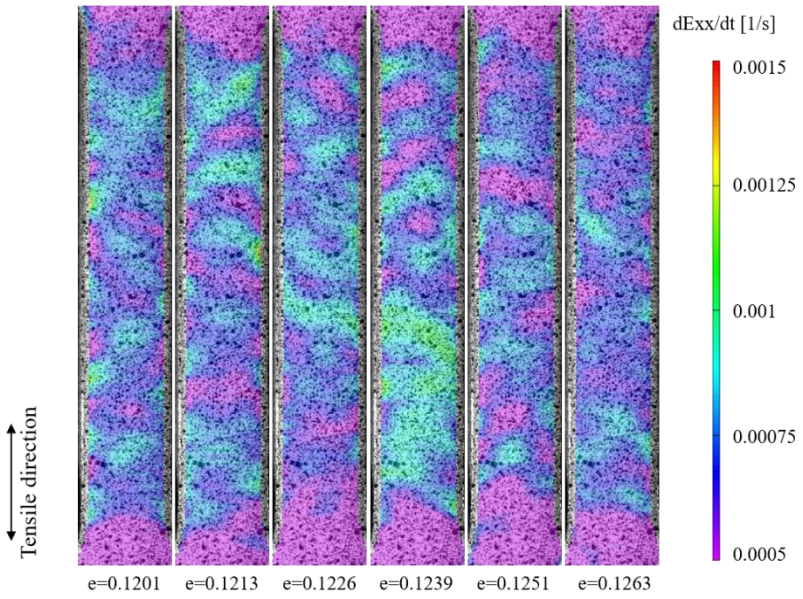

Fig. 4.9 The strain rate maps for Al-10Mg alloy at selected deformation stage. Island-like deformation regions appear at random positions on the gauge part.

As for the serrated flow appears at large strains, DIC analysis was conducted to link local and heterogeneous characteristics to the global deformation response. Fig. 4.10 shows an enlarged part of the nominal stress-time curve (corresponding to the strain range of 0.233 ~ 0.34 in Fig. 4.9) and the strain rate distribution maps obtained by the DIC analysis. The numbers 1 ~ 9 indicated at the synchronized strain rate maps correspond to the positions on the stress-strain curves indicated by the same numbers. The DIC strain rate maps clearly shows that type C band nucleates at one end of the gauge part and then disappears quickly, manifested by a sudden stress drop in the stress-strain curve as indicated by point 1 and 2. Soon after the annihilation of type C band, a type A band nucleates at the region where type C band has just annihilated during reloading. In contrast to previous studies, type A band nucleates during reloading and does not contribute to a stress drop. Then, the type A band propagates continuously on the gauge part and annihilates at the central region of the gauge part. The appearance of next type C band and the annihilation of type A band happen almost simultaneously (as indicated by point 8 and 9, the time interval between these two

points is 0.2 s). Type C and type A bands appear alternately and this process repeatedly happens till fracture. To our knowledge, these peculiar deformation behaviors have never been reported in Al-Mg alloys with lower Mg contents before. Together with the island-like heterogeneous deformation behavior mentioned above, these results indicate that the heterogeneous deformation behaviors in Al-10Mg alloy are somehow special. The detailed mechanisms that are responsible for the island-like heterogeneous deformation and the alternate appearance of type C and type A bands will be discussed in the next section.

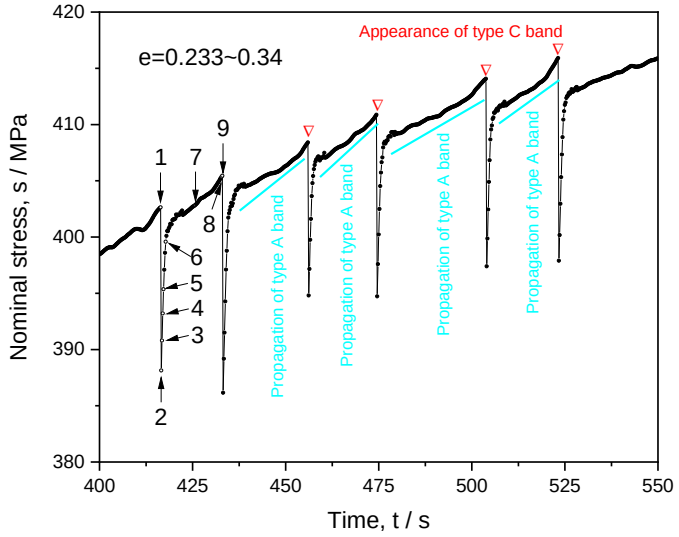

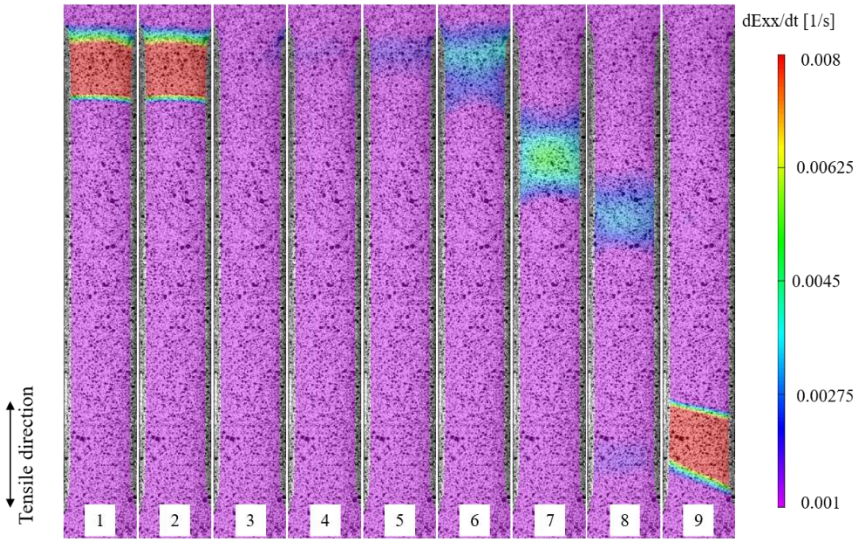

Fig. 4.10 An enlarged part of the nominal stress-time curve for Al-10Mg alloy and corresponding local strain-rate maps of the sample at selected stages obtained by the DIC analysis. Type C and type A bands appear alternately.

4.4 Discussion

4.4.1 The mechanism for the PLC effect in Al-Mg alloys

As a starting point for the discussion, it is necessary to revisit the traditional mechanism for PLC effect. The most commonly accepted explanation for the origin of the PLC effect is based on a model called dynamic strain aging [13–15], which is defined as interaction between the moving dislocations and diffusing solute atoms. The mobile dislocations act as carriers of the plastic deformation according to this mechanism, and move unsteadily among the obstacles formed by other defects. There are two main solute-dislocation interaction models for dynamic strain aging in substitutional alloys: (I) PLC effect occurs with the fast long-range diffusion (lattice diffusion) of solute atoms at a rate faster than the speed of the moving dislocations so as to catch and lock them [16]; (II) Another consideration is that the diffusion of solute atoms might occur along the dislocation core (pipe diffusion) during the residence time of dislocations at obstacles [17–19]. It is hypothesized that the change of serration morphologies and corresponding localized deformation behaviors are due to transitions in operative dynamic strain aging mechanisms based on relative differences between the diffusion rate of the solute atoms and the velocity of the mobile dislocations throughout the dynamic strain aging regime. Nevertheless, the dislocation-solute interaction models suggest that the Mg content does play a role in serrated flow. The experimental results in current study have shown that PLC bands are of different types, and the transition between band types occurs upon changes in Mg content.

However, the traditional dynamic strain aging mechanism by the simple diffusion of solute atoms through lattice or dislocation pipes cannot explain the observations in the present alloys. Because the diffusion rates of solute Mg atoms are extremely low in Al-Mg alloys at room

temperature. For a more detailed consideration, the possibility that substitutional solutes can catch up moving dislocations is calculated by simple lattice diffusion in the Al-Mg alloys. The diffusion coefficients of Mg elements in Al matrix can be obtained for selected temperatures of 20 ℃, by employing the Arrhenius relation:

$$D = D_0 exp\left(\frac{-Q}{RT}\right) \qquad (4-1)$$

where D_0 is diffusion constant (D_0=6.23×10^{-4} m^2/s for Mg in Al matrix), Q is the activation energy of diffusion (Q=1.19 eV), R is the gas constant, and T is the absolute temperature. Based on Eq. (4-1), the average diffusion speed for Mg atoms in Al matrix at room temperature is 3.6 × 10^{-12} m/s. Apparently, Mg diffusion rate in Al matrix is too slow to account for dynamic strain aging effects observed in Al-Mg alloys at room temperature. Although moving dislocations could be obstructed by intersecting other dislocations or slowed down by passing the strong repulsion or attraction from other dislocations and have a waiting time for solute atoms coming, the waiting time is still very far below that for the long-range solute diffusion in the lattice. In addition, the average activation energy for pipe diffusion along the core is about 75% of the bulk value [18], which means the diffusion rate is still extremely low. Thus, the explanation based on long-range lattice/pipe diffusion cannot account for the PLC effect in the present study.

To explain the PLC effect observed in the present alloys, the cross-core diffusion model [20] has to be taken into account. According to cross-core diffusion theory, the Mg diffusion controlling dynamic strain aging occurs inside the dislocation core, from the compression side to the tension side of the dislocation slip plane. The cross-core diffusion has both a larger thermodynamic driving force and a reduced diffusion activation enthalpy relative to regions outside the core (the activation energy is 0.97 eV [20]). The diffusion rate calculated by cross-core diffusion model is 2.8 × 10^{-10} m/s, much higher that of lattice diffusion. Therefore. the diffusion can happen quickly within the

core region. The cross-core diffusion model could be applied as a partial mechanism to explain the PLC effect observed in Al-Mg alloys because solute atoms in or near the dislocation cores are able to make rearrangement and pin dislocations in a very short period of time. Instead of taking the long-range diffusion route for solute atoms to move through the lattice or forest dislocation cores and catch moving or impeded dislocations, the cross-core diffusion mechanism requires only the local rearrangement of the solute atoms around cores of dislocations.

Discussion at multiple length scales is considered for the discussion below, trying to relate solute atom-dislocation interactions to localized deformation behaviors. During deformation of individual grains, dislocation pile-ups at grain boundaries increase the flow strength of the grain, increase the dislocation density, and generate an internal stress which is applied to and activates dislocation sources in neighboring grains. Fig. 4.11 shows a schematic illustration of a deforming tensile sample and the Frank-Read source pile-up at band front. Localized deformation bands from dynamic strain aging are macroscopic deformation, so all the grains within a deformation band experience plastic deformation and grains in the rest of the sample are statically loaded (i.e. no plastic deformation) and likely exhibit non-uniform levels of strain aging and stress relaxation. During tensile testing, plastic deformation within a deformation band causes the band to increase in length and decease in cross-sectional area, effectively creating a small localized necking (i.e. stress concentrator) in the tensile sample (as shown in Fig. 4.11). The types of deformation bands observed are dependent on the local flow stress compared to the local stress needed to activate dislocation sources at the band front.

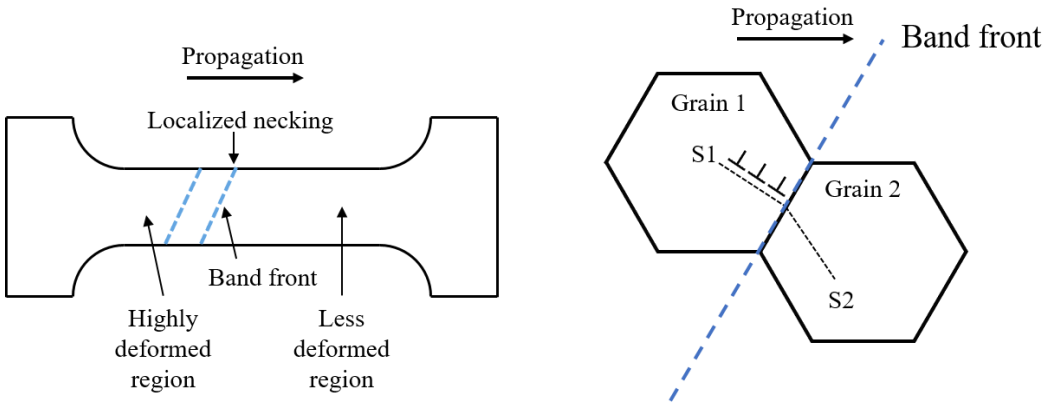

Fig. 4.11 Schematic illustration of a deforming tensile sample and Frank-Read source pile-up at the band front.

In this study, continuous propagation and non-propagation band behaviors are generally associated with low and high Mg contents, respectively. The transition from continuous propagation to hopping propagation and to nucleation of deformation bands is related to the speed that the solute atoms can pin mobile dislocations. In Al-2.5Mg alloy, under constant strain rate, the relatively low Mg content leads to a longer time required for the internal stresses to relax. As a result, the stress concentration effect of the deformation band front causes the internal stress of the deforming grains to exceed the critical stress needed to activate dislocation sources in the grains just ahead of the band front, which is characterized as continuous propagation of localized deformation band, i.e. type A band. This band continues to propagate until a new band nucleates at some other location. The gradual strain distribution along gauge length leads to work hardening during band propagation, which is the distinct feature of type A band.

For type B bands, the potential nucleation sites of the hopping bands are constrained to occur within the vicinity of the previous deformation band location. The hopping propagation behavior of localized deformation bands involves local internal stress concentrations in the breakaway process. The breakaway of a single dislocation initiates the rapid multiplication of dislocations and the activation of neighboring previously aged dislocation groups, i.e. triggers the next avalanche.

Small groups of dislocations in pileup configuration waiting in front of obstacles can produce local stress concentrations, although these dislocation groups are probably spread over a set of adjacent glide planes, rather than being strictly coplanar. The balance between the required relaxation time of internal stresses with available reloading time (measured between two consecutive stress drops) determines the spatial characteristics of deformation bands. Type B bands with its hopping characteristics arises when the internal stresses are not totally relaxed and favors the nucleation of a new band close to the previous one [21,22]. Klose et al. [23,24] also attempted to explain type B band based on a dislocation mechanism approach. They suggested that the hopping propagation of deformation bands involves local internal stress concentrations. Such local stress concentrations arise from small groups of dislocations in a pile-up configurations held by obstacles. This idea is supported by direct TEM observations [25] suggesting the occurrence of a pileup-induced dislocation breakaway process during PLC instability.

In Al-7.5Mg alloy, where non-propagating type C bands were observed, solute Mg atoms have a high concentration. Based on the cross-core diffusion model, a higher Mg content can provide more abundant solute atoms for re-pinning dislocations and can pin mobile dislocations at a much higher rate. During nucleation behaviors, the dislocation avalanches are immediately arrested by obstacles after the deformation band forms. The internal stresses induced by strain rate gradient are totally relaxed, which makes the band propagation difficult and therefore the band annihilates. Higher stress concentrations are required for next dislocation avalanche and the possible nucleation site is dependent on the distribution of the total strain throughout the gauge length. Location with the lowest amount of total strain has the lowest flow stress along the gauge length and therefore the highest probability of nucleating the next deformation band. Therefore, the next band will emerge at a random position on the gauge part and the spatial correlation of bands will

be lost.

The results in Fig. 4.6 and Fig. 4.7 indicate that grain size also have strong influence on the occurrence and nature of the PLC effect. Grain size reduction favors a transition of PLC band propagative feature and increases the magnitude of the stress drop as well as local strain rate within PLC band. The propagation behavior of PLC band on the gauge part of a sample can be related to dislocation pileups in front of grain boundaries. The grain boundaries and dislocations could be obstacles for the motion of PLC band. An increasing PLC band strain rate suggests that the number of mobile dislocations involved in band formation is also increasing. The influence of grain refinement on dynamic strain aging of Al-Mg alloys can be attributed to larger mobile and forest dislocation densities as well as reduced grain boundary spacing, which increase the obstacle density, leading to a longer waiting time of dislocations arrested at obstacles [26]. As a result, the pinning stress exerted by aging solute atoms increases, and that's why the serration amplitude and local strain rate in PLC band increased with decreasing grain size.

A further question is that of what determines the transitions between the three types of PLC bands. As shown in Fig. 4.2, type A and type B bands can occur in the same Al-2.5Mg (or Al-5Mg) sample during tensile deformation, the primary difference between the two conditions is the strain level, and thus the dislocation density. Lower and higher dislocation densities promote the occurrence of type A and type B bands, respectively. For Al-2.5Mg alloy having different grain sizes (as shown in Fig. 4.6), fine-grained sample possesses a higher dislocation density than coarse-grained sample after a constant strain, which also favors a transition from type A to type B bands. Combining the strain and grain size dependence of serration behavior, it is suggested that a certain type of PLC band occurs when a critical value of dislocation density is reached. Type A bands occurs in Al-Mg alloy with low Mg at low global strain values since the dislocation density is low.

The Al-5Mg and Al-7.5Mg alloys have both higher dislocation densities and more abundant Mg atoms available for aging of the dislocations, which promote a transition of band types from type A to type B, and finally to type C. Therefore, the features of PLC bands depend on the amount of obstacles in front of them as well as the speed that the solute atoms can pin mobile dislocations. These results support the arguments that both dynamic strain aging and intensive dislocation interaction are necessary prerequisites to produce the PLC effect [24]. The more detailed mechanisms with deep insights should be clarified after further investigations in the future.

4.4.2 Mechanisms of peculiar deformation behaviors in Al-10Mg alloy

Island-like heterogeneous deformation and alternate appearance of type A and type C bands were detected in Al-10Mg alloy, as shown in Fig. 4.9 and Fig. 4.10, respectively. These heterogeneous deformation behaviors are remarkably different with those observed in Al-Mg alloys with lower Mg contents. It is generally accepted that PLC band is related to dislocation pinning and depinning, and dynamic strain aging region should be within a certain range of strain rate and temperature [27,28]. Numerous studies have shown that the strain rate, temperature and solute concentration have effects on the characteristics of PLC band. Therefore, there should be a critical condition between the appearance of island-like deformation regions and well-formed PLC bands. To understand the mechanism for the occurrence of island-like heterogeneous deformation behavior, the effect of strain rate on serration behaviors in Al-10Mg alloy was investigated as a first step. The plastic behavior of the Al-10Mg alloy deformed at room temperature in the range of strain rates of 8.3×10^{-6} to 8.3×10^{-2} s^{-1} is shown in Fig. 4.12 (a). It's noteworthy that the serration behavior becomes less pronounced and the stress level decreased when the strain rate decreased from 8.3×10^{-4} to 8.3×10^{-6} s^{-1}, indicating a positive strain rate sensitivity. As the strain rate increases from 8.3×10^{-4} to 8.3×10^{-2} s^{-1}, the serration behaviors get enhanced whereas the stress

level decreases. It is noted that with increasing strain rate, there is a trend of serration types changing from type C to type B, and to type A. DIC analysis has confirmed that island-like heterogeneous deformation behavior prevails in Al-10Mg alloy when strain rate $\leq 8.3 \times 10^{-4}$ s^{-1}. In our common understanding of dynamic strain aging, decreasing strain rate is expected to enhance the serration behavior. But it is not the case for Al-10Mg alloy. A hypothesis is proposed to explain this phenomenon: solute Mg atoms around the dislocations may have already reached a saturation value in Al-10Mg alloy, thus decreasing strain rate does not contribute to enhanced PLC effect. In order to verify the hypothesis is correct or not, the serration behaviors in Al-10Mg alloy under different temperatures were also investigated, as shown in Fig. 4.12 (c). Increasing temperature is another way which is expected to enhance dynamic strain aging since it accelerates the diffusion rate of solute atoms. However, the results show that increasing temperature from RT to 50 ℃ does not lead to enhanced serration behavior. For comparison, the serration behaviors in Al-5Mg alloy with similar grain size at different strain rates and temperatures were also investigated, as shown in Fig. 4.12 (b) and Fig. 4.12 (d), respectively. It can be seen that the serration behavior gets enhanced when decreasing the strain rate from 8.3×10^{-4} to 8.3×10^{-5} s^{-1} or increasing the temperature from RT to 50 ℃, which is different with Al-10Mg alloy and therefore indicates the hypothesis is reasonable. It's interesting that characteristics of serrated flow in the stress-strain curves of Al-5Mg alloy at 8.3×10^{-4}, 8.3×10^{-5} and 8.3×10^{-6} s^{-1} are similar to that of Al-10Mg alloy at 8.3×10^{-3}, 8.3×10^{-4} and 8.3×10^{-5} s^{-1}, respectively. It seems that decreasing strain rate could compensate the difference in Mg concentration. Based on the concepts of diffusion controlled models of dynamic strain aging, island-like heterogeneous deformation behavior is expected to be observed in Al-5Mg alloy at low strain rate like 8.3×10^{-5} or 8.3×10^{-6} s^{-1} because a lower strain rate allows atoms to have more time to catch and successfully pin the dislocations.

However, even at the an extremely low strain rate of 8.3×10^{-6} s^{-1}, well-formed PLC bands can be observed, which is quite different with the island-like deformation regions observed in Al-10Mg alloy. These results indicate that the island-like heterogeneous deformation is the intrinsic characteristic of Al-10Mg alloy, which cannot be simply explained by diffusion theory.

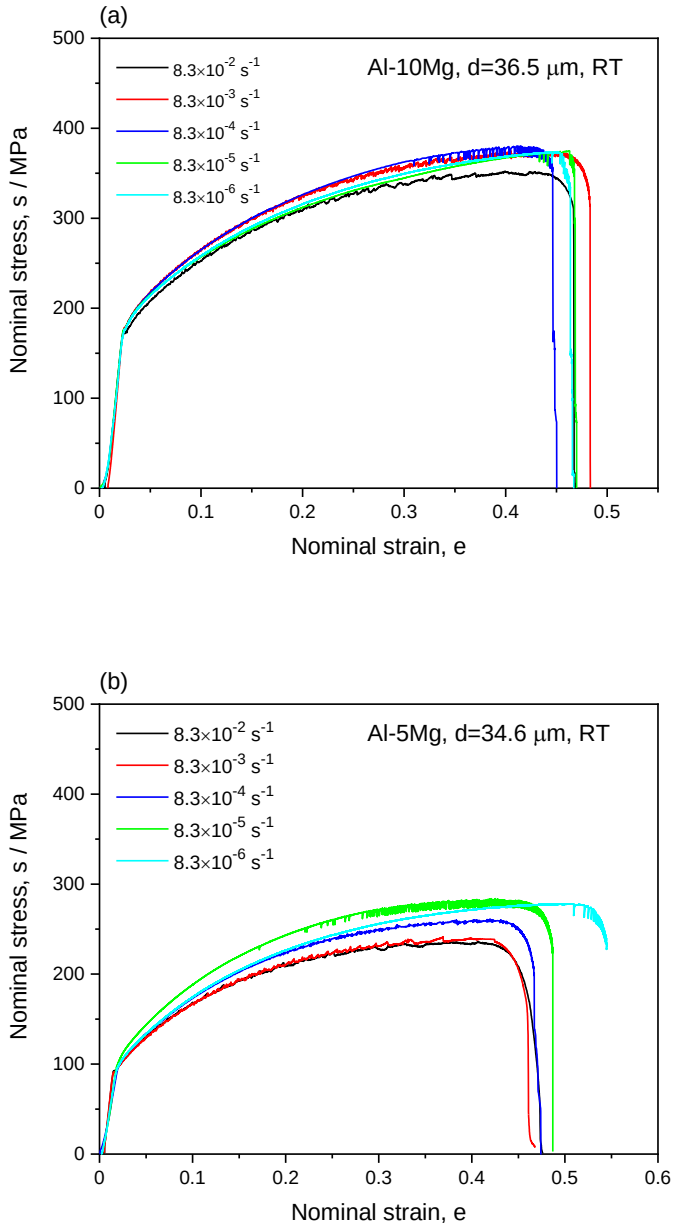

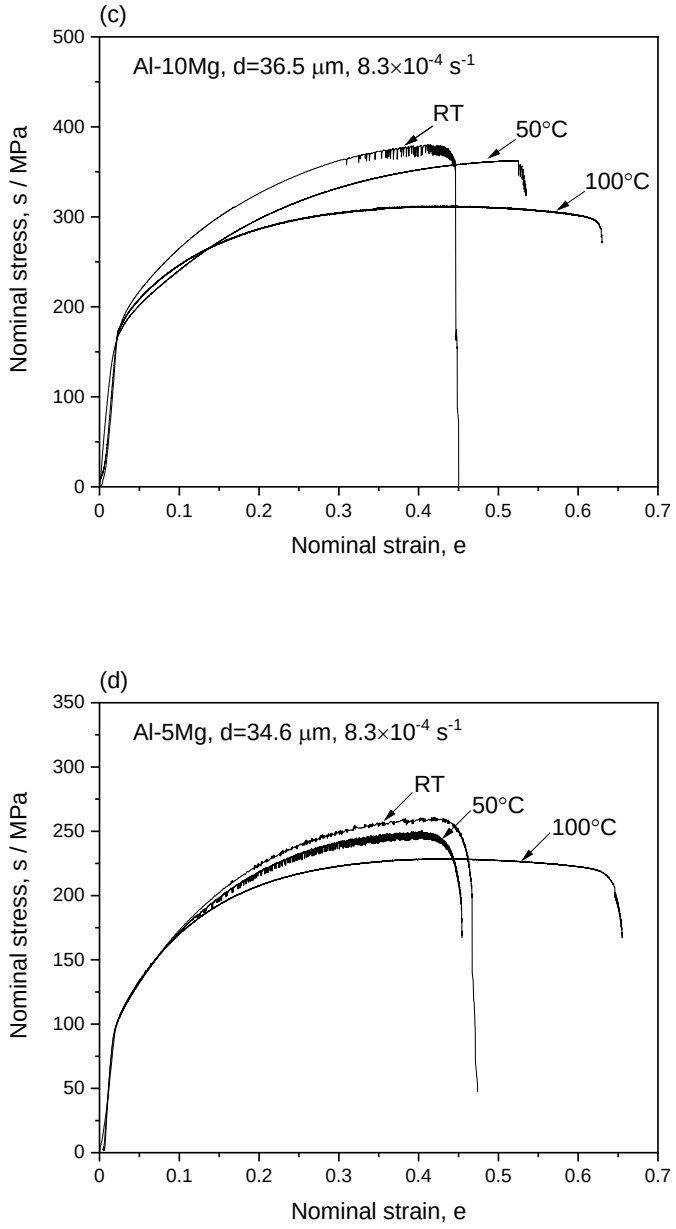

Fig. 4.12 Nominal stress-strain curves of Al-10Mg and Al-5Mg alloys having similar grain size, obtained from tensile testing at various strain rates and temperatures. The strain rates and temperatures are indicated in the figures.

To understand the dynamics of solute atom-dislocation interaction and its influence on the PLC effect, the solute drag on moving dislocations during tensile deformation has to be taken into account. Zhang and Curtin [29] introduced a model that describes solute drag on a moving dislocation in Al-Mg alloy during deformation, taking the cross-core diffusion mechanism into

consideration. They used it to study the magnitude of the solute drag effect as a function of the dislocation velocity, as well as the role of lattice diffusion vs. cross-core diffusion at different dislocation speeds, respectively. In the present study, a comparison of diffusion rate for selected temperatures based on lattice diffusion theory and cross-core diffusion theory has been made, as listed in Table. 4-1. At low dislocation velocities, the core diffusion is too fast to contribute to the drag stress because the core concentration field is nearly in static equilibrium and symmetric around the dislocation core, the solute drag stress is controlled by lattice diffusion. A higher strain rate is needed to generate an asymmetric distribution of Mg around dislocation core. That's why increasing temperature or decreasing strain rate does not contribute to enhanced serration behavior in Al-10Mg alloy, whereas increasing strain rate can promote the occurrence of pronounced serration behavior, which further confirms that the hypothesis is reasonable. For Al-5Mg alloy, in which the Mg concentration is not saturated, lattice diffusion can make more contribution when decreasing strain rate or increasing temperature and therefore lead to enhanced serration behavior. No island-like deformation region was observed in Al-5Mg alloy, even when strained at 8.3×10^{-6} s^{-1}, indicating that interactions between solute Mg atoms and dislocations might not be the only cause for the occurrence of island-like deformation regions and the dislocation structure might play a role.

Table 4-4 Lattice diffusion rate vs. cross-core diffusion rate.

Temperature (℃)	Lattice diffusion (m/s)	Cross-core diffusion (m/s)
20	3.6×10^{-12}	2.8×10^{-10}
50	3.2×10^{-11}	1.67×10^{-9}
100	5.6×10^{-10}	1.7×10^{-8}

To clarify this matter, the deformation structures of the Al-10Mg alloy after tensile testing to

specific strains have been examined by TEM, as shown in Fig. 13. The TEM micrograph in Fig. 4.13 (a) reveals that planar dislocation arrays form in the early stage of plastic deformation, which is quite different with the dislocation structure of Al-Mg alloys having low Mg contents. The planar arrays arise from enhanced dislocation multiplication and suppressed cross slip due to the high friction stress induced by high Mg concentration. As the strain increases to 0.083, the dislocation density increases and planar dislocations on different slip planes seem to interact and form dislocation networks. The dislocation mean free paths decrease with the formation of dislocation network structure. The dislocation tangles form during dislocation-dislocation interactions are obstacles for dislocation motion. Dislocations can be trapped by these obstacles and form dislocation pile-ups against these obstacles. As a result, local stress concentrations arise from small groups of dislocations in a pile-up configurations held by obstacles. These trapped dislocations can overcome the obstacles collectively when the applied stress is increased. Island-like deformation regions might be explained by the sudden bursts of collective dislocation motion, and these mobile dislocations can be arrested by the obstacles nearby quickly. Thus, these isolated deformation regions can't group together to form a localized deformation band. Many island-like heterogeneous deformation regions appear at random locations on the gauge part and this feature makes the microscopic deformation appears to be homogeneous, as reflected by the relatively smooth stress-strain curve at small and intermediate strains.

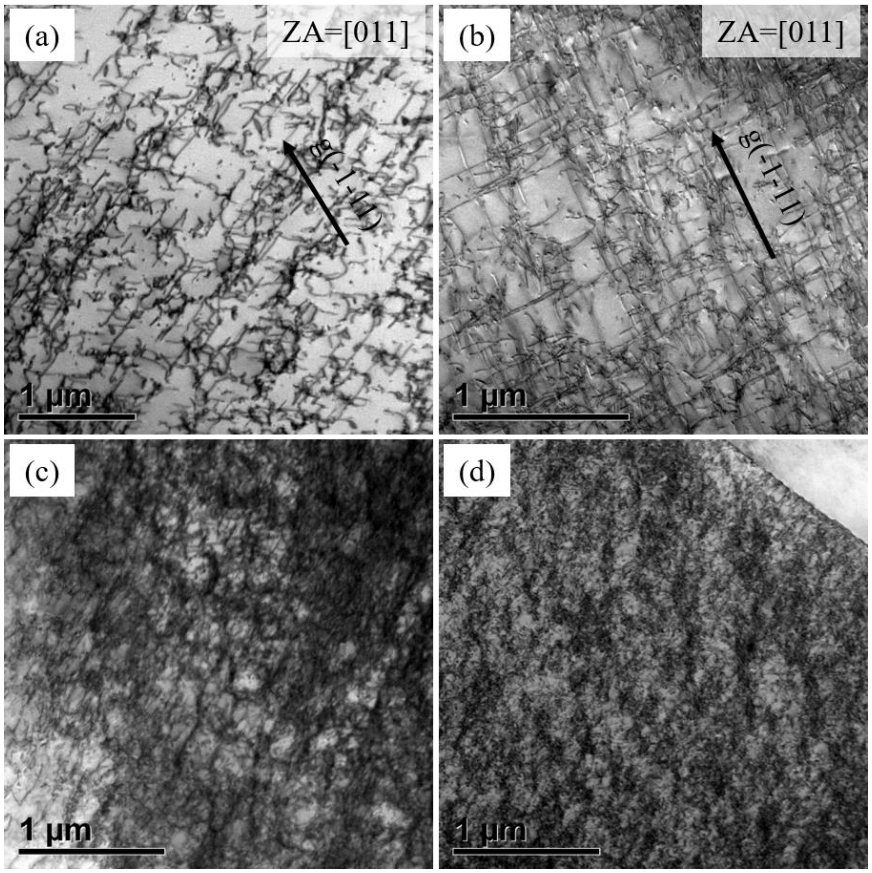

Fig. 4.13 Bright-field TEM micrographs showing the dislocation morphologies of the Al-10Mg alloy at different strain levels. (a) e = 0.036, (b) e = 0.083, (c) e = 0.164, (d) e = 0.237.

The DIC strain rate maps in Fig. 4.10 have shown that type A and type C bands appear alternately at the end of gauge part at large strain levels in Al-10Mg alloy, and the type A bands annihilate at the central region of gauge part. Usually, regions along the gauge length that experienced local plastic deformation have an increased flow stress compared to locations with only elastic deformation and are therefore unlikely to nucleate an additional band until the entire gauge length has experienced localized deformation. However, the actual band motion during plastic deformation would encounter obstacles, such as forest dislocations and grain boundaries. There are waiting times for dislocations to overcome these obstacles by the aid of increased stress. Thus, the alternate appearance of type A and type C bands can be explained by the non-uniform levels of work hardening and strain aging, which result in differences in local flow stress along the

gauge length. For example, as schematically shown in Fig. 4.14 (b), region 2 has longer time of strain aging to influence the local flow stress comparing to region 1. The band propagation behavior observed is dependent on the local flow stress of grains at region 1 and 2 compared to the local stress needed to activate dislocation sources at each region. The longer strain aging time makes it difficult for the type A band to propagate to region 2, that's why type A band annihilates and a new type C band nucleates at the shoulder region of the tensile sample on the other end. Due to the high dislocation density as well as high Mg content in Al-10Mg alloy, the sudden bursts of dislocation motion that corresponds to the formation of type C band were impeded quickly. As for a new type A band nucleates at the region where the type C band had just annihilated during reloading, the reason is still unclear. The above processes repeatedly occur, leading to the alternate appearance of type A and type C bands.

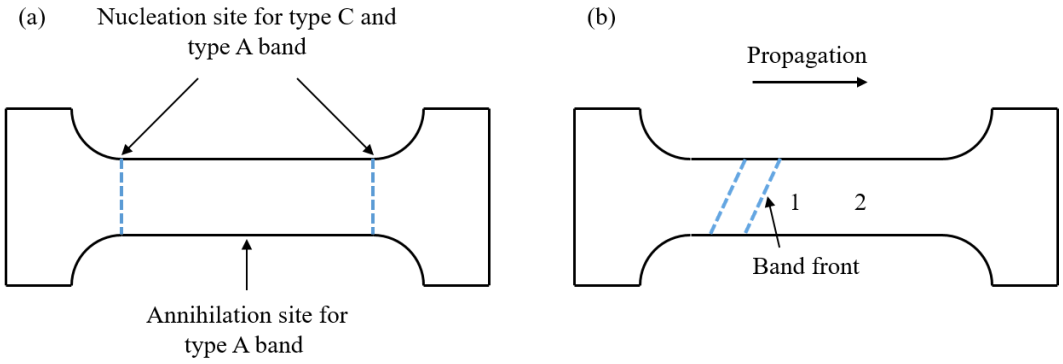

Fig. 4.14 Schematic illustration of the alternate appearance of type A and type C bands in Al-10Mg alloy.

4.4 Conclusions

In this study, a systematic study of the spatiotemporal characteristics associated with heterogeneous deformation behaviors in Al-Mg alloys having different Mg contents and grain sizes has been conducted to reveal the relevant mechanisms. The main conclusions are drawn as follows:

(1) For Al-2.5Mg, Al-5Mg and Al-7.5Mg alloys having similar grain size, the strain localization associated with various band behaviors were observed both spatially and

temporally by using DIC technique. At similar strain level, the characteristics of PLC bands depend strongly on the Mg content, increasing Mg content promotes a transition from continuous propagation (type A) to hopping propagation (type B) and finally to non-propagation (type C) behaviors.

(2) For Al-2.5Mg alloy, the serration behaviors and corresponding localized deformation behaviors exhibit remarkable grain size dependence. Grain refinement facilitates a transition from continuous propagation to hopping propagation behavior. The local strain rate increased with decreasing grain size and the deformation behavior becomes more heterogeneous.

(3) The plastic deformation at small and intermediate strains is heterogeneous in Al-10Mg alloy, even though no pronounced serrated flow occurs in the stress-strain curve. DIC analysis confirms that no PLC band is formed, whereas many island-like deformation regions appear on the gauge part. Type A and type C bands appear alternately at large strains. Solute Mg around dislocations may have reached saturation in Al-10Mg alloy since increasing temperature or decreasing strain rate does not lead to enhanced serration behavior, whereas the serration behavior gets enhanced with increasing strain rate.

(4) TEM observation shows that planar dislocation arrays form in the early stage of plastic deformation in Al-10Mg alloy, as a result, the dislocation mean free paths decrease with the formation of dislocation networks. Island-like heterogeneous deformation might be explained by the sudden bursts of dislocation motion, and these mobile dislocations can be arrested by obstacles nearby quickly. Thus, these isolated deformation regions can’t group together to form a localized deformation band.

(5) The deformation behavior observed was dependent on the speed that the solute atoms can

pin mobile dislocations and the local flow stress of groups of grains within a deformation band due to work hardening. The local rearrangement of Mg atoms by cross-core diffusion could be applied as a partial mechanism to explain the PLC effect observed in Al-Mg alloys, and detailed analysis suggests that both dynamic strain aging and intensive dislocation interactions are necessary prerequisites to produce the PLC effect.

The focus of this work is to fill some gaps in our understanding of the correlation between the nature of serrated flow and the characteristics of band propagation. Although the cross-core diffusion theory can partially explain the dynamic strain aging effect in Al-Mg alloys at atomic scale, quantification of the microscopic formation mechanisms of the bands and the band motion and transition still remains challenging. More theoretical and experimental works on solute-dislocation and dislocation-dislocation interactions are expected to be done in the future to obtain further insights into PLC band formation and propagation events.

References

[1] N. Tsuji, Y. Ito, Y. Saito, Y. Minamino, Strength and ductility of ultrafine grained aluminum and iron produced by ARB and annealing, Scr. Mater. 47 (2002) 893–899. https://doi.org/https://doi.org/10.1016/S1359-6462(02)00282-8.

[2] Y.Z. Tian, S. Gao, L.J. Zhao, S. Lu, R. Pippan, Z.F. Zhang, N. Tsuji, Remarkable transitions of yield behavior and Lüders deformation in pure Cu by changing grain sizes, Scr. Mater. 142 (2018) 88–91. https://doi.org/https://doi.org/10.1016/j.scriptamat.2017.08.034.

[3] A. Yilmaz, The Portevin–Le Chatelier effect: a review of experimental findings, Sci. Technol. Adv. Mater. 12 (2011) 63001. https://doi.org/10.1088/1468-6996/12/6/063001.

[4] P.J. Worthington, B.J. Brindley, Serrated yielding in substitutional alloys, Philos. Mag. A J. Theor. Exp. Appl. Phys. 19 (1969) 1175–1178. https://doi.org/10.1080/14786436908228642.

[5] H. Halim, D.S. Wilkinson, M. Niewczas, The Portevin–Le Chatelier (PLC) effect and shear band formation in an AA5754 alloy, Acta Mater. 55 (2007) 4151–4160. https://doi.org/https://doi.org/10.1016/j.actamat.2007.03.007.

[6] Y. Zhang, J.P. Liu, S.Y. Chen, X. Xie, P.K. Liaw, K.A. Dahmen, J.W. Qiao, Y.L. Wang, Serration and noise behaviors in materials, Prog. Mater. Sci. 90 (2017) 358–460. https://doi.org/https://doi.org/10.1016/j.pmatsci.2017.06.004.

[7] P. Rodriguez, Serrated plastic flow, Bull. Mater. Sci. 6 (1984) 653–663. https://doi.org/10.1007/BF02743993.

[8] Y.L. Cai, S.L. Yang, Y.H. Wang, S.H. Fu, Q.C. Zhang, Characterization of the deformation behaviors associated with the serrated flow of a 5456 Al-based alloy using

two orthogonal digital image correlation systems, Mater. Sci. Eng. A. 664 (2016) 155–164. https://doi.org/https://doi.org/10.1016/j.msea.2016.04.003.

[9] H. Ait-Amokhtar, C. Fressengeas, Crossover from continuous to discontinuous propagation in the Portevin–Le Chatelier effect, Acta Mater. 58 (2010) 1342–1349. https://doi.org/https://doi.org/10.1016/j.actamat.2009.10.038.

[10] P.G. McCormick, The Portevin-Le Chatelier effect in an Al-Mg-Si alloy, Acta Metall. 19 (1971) 463–471. https://doi.org/https://doi.org/10.1016/0001-6160(71)90170-2.

[11] B.J. Brindley, The effect of dynamic strain-ageing on the ductile fracture process in mild steel, Acta Metall. 18 (1970) 325–329. https://doi.org/https://doi.org/10.1016/0001-6160(70)90147-1.

[12] M. Koyama, Y. Shimomura, A. Chiba, E. Akiyama, K. Tsuzaki, Room-temperature blue brittleness of Fe-Mn-C austenitic steels, Scr. Mater. 141 (2017) 20–23. https://doi.org/https://doi.org/10.1016/j.scriptamat.2017.07.017.

[13] A.H. Cottrell, B.A. Bilby, Dislocation Theory of Yielding and Strain Ageing of Iron, Proc. Phys. Soc. Sect. A. 62 (1949) 49–62. https://doi.org/10.1088/0370-1298/62/1/308.

[14] F.R.N. Nabarro, Theory of crystal dislocations, (1967).

[15] G. Gremaud, Overview on dislocation-point defect interaction: the brownian picture of dislocation motion, Mater. Sci. Eng. A. 370 (2004) 191–198. https://doi.org/https://doi.org/10.1016/j.msea.2003.04.005.

[16] A.H. Cottrell, M.A. Jaswon, N.F. Mott, Distribution of solute atoms round a slow dislocation, Proc. R. Soc. London. Ser. A. Math. Phys. Sci. 199 (1949) 104–114. https://doi.org/10.1098/rspa.1949.0128.

[17] R.A. Mulford, U.F. Kocks, New observations on the mechanisms of dynamic strain aging

and of jerky flow, Acta Metall. 27 (1979) 1125–1134. https://doi.org/https://doi.org/10.1016/0001-6160(79)90130-5.

[18] R.C. Picu, D. Zhang, Atomistic study of pipe diffusion in Al–Mg alloys, Acta Mater. 52 (2004) 161–171. https://doi.org/https://doi.org/10.1016/j.actamat.2003.09.002.

[19] J. Schlipf, On the kinetics of static and dynamic strain aging, Scr. Metall. Mater. 31 (1994) 909–914. https://doi.org/https://doi.org/10.1016/0956-716X(94)90501-0.

[20] W.A. Curtin, D.L. Olmsted, L.G. Hector, A predictive mechanism for dynamic strain ageing in aluminium–magnesium alloys, Nat. Mater. 5 (2006) 875–880. https://doi.org/10.1038/nmat1765.

[21] M. Lebyodkin, Y. Brechet, Y. Estrin, L. Kubin, Statistical behaviour and strain localization patterns in the Portevin-Le Chatelier effect, Acta Mater. 44 (1996) 4531–4541. https://doi.org/https://doi.org/10.1016/1359-6454(96)00076-6.

[22] M. Lebyodkin, L. Dunin-Barkowskii, Y. Bréchet, Y. Estrin, L.P. Kubin, Spatio-temporal dynamics of the Portevin–Le Chatelier effect: experiment and modelling, Acta Mater. 48 (2000) 2529–2541. https://doi.org/https://doi.org/10.1016/S1359-6454(00)00067-7.

[23] F.B. Klose, A. Ziegenbein, F. Hagemann, H. Neuhäuser, P. Hähner, M. Abbadi, A. Zeghloul, Analysis of Portevin-Le Chatelier serrations of type Bin Al–Mg, Mater. Sci. Eng. A. 369 (2004) 76–81. https://doi.org/https://doi.org/10.1016/j.msea.2003.10.292.

[24] F.B. Klose, J. Weidenmüller, A. Ziegenbein, P. Hähner, H. Neuhäuser §, Plastic instabilities with propagating deformation bands in Cu–Al alloys, Philos. Mag. 84 (2004) 467–480. https://doi.org/10.1080/14786430310001610320.

[25] T. Tabata, H. Fujtta, Y. Nakajima, Behavior of dislocations in AL□MG single crystals observed by high voltage electron microscopy, Acta Metall. 28 (1980) 795–805.

https://doi.org/https://doi.org/10.1016/0001-6160(80)90156-X.

[26] S. Zhao, C. Meng, F. Mao, W. Hu, G. Gottstein, Influence of severe plastic deformation on dynamic strain aging of ultrafine grained Al–Mg alloys, Acta Mater. 76 (2014) 54–67. https://doi.org/https://doi.org/10.1016/j.actamat.2014.05.004.

[27] S. Serajzadeh, H. Sheikh, Investigation into occurring dynamic strain aging in hot rolling of AA5083 using finite elements and stream function method, Mater. Sci. Eng. A. 486 (2008) 138–145. https://doi.org/https://doi.org/10.1016/j.msea.2007.09.021.

[28] C.-W. Tsai, C. Lee, P.-T. Lin, X. Xie, S. Chen, R. Carroll, M. LeBlanc, B.A.W. Brinkman, P.K. Liaw, K.A. Dahmen, J.-W. Yeh, Portevin-Le Chatelier mechanism in face-centered-cubic metallic alloys from low to high entropy, Int. J. Plast. 122 (2019) 212–224. https://doi.org/https://doi.org/10.1016/j.ijplas.2019.07.003.

[29] F. Zhang, W.A. Curtin, Atomistically informed solute drag in Al–Mg, Model. Simul. Mater. Sci. Eng. 16 (2008) 55006. https://doi.org/10.1088/0965-0393/16/5/055006.

Chapter 5 Summary and conclusions

In the present dissertation, the effects of grain size and Mg contents on deformation behavior and strengthening mechanisms in Al-Mg alloys were systematically investigated. In order to achieve a superior strength and ductility balance, the combined effects of grain size and Mg contents on the mechanical properties of Al-Mg alloys were evaluated by room temperature tensile tests. Further investigation was conducted to reveal the effects of Mg contents on the deformation microstructure evolution and the mechanism of enhanced work hardening in Al-Mg alloys. Moreover, the PLC effect was investigated to understand the fundamental features of heterogeneous deformation in Al-Mg alloys, with a special focus on the grain size and Mg content effects. The main conclusions obtained in each chapter are briefly summarized as follows:

In Chapter 1, the background and purpose of the study were introduced.

In Chapter 2, the effects of grain size and Mg contents on mechanical properties and strengthening mechanisms of Al-Mg alloys were systematically investigated. Fully recrystallized Al-2.5Mg, Al-5Mg, Al-7.5Mg and Al-10Mg alloys with various grain sizes ranging from 0.24 μm to 134 μm were fabricated by HPT/cold rolling and subsequent annealing. Systematic tensile tests confirmed the accurate and reliable Hall-Petch relationships, where extra-hardening phenomena accompanying with discontinuous yielding behaviors were observed in the fine-grained regimes. It was found that Mg addition contributed not only to solid solution hardening but also to enhanced grain boundary strengthening. The Hall-Petch slope showed a large increase after adding 2.5 wt.% Mg to Al matrix, but then varied little with further increase in Mg content. The effect of solute Mg on Hall-Petch slope was discussed based on the physical models of the Hall-Petch relationship. It was considered that grain boundary segregation of solute Mg may alter the nature of grain boundaries and enhance the grain boundary resistance against dislocation slip, but the Mg

concentration at grain boundaries may have already reached saturation in Al-2.5Mg alloy. In addition, it was found that the yield point phenomena played an important role in the uniform elongation of Al-Mg alloys. By the DIC analysis, it was confirmed that the drastic loss of uniform elongation was attributed to the enhanced early plastic instability associated with the occurrence of discontinuous yielding behavior in ultrafine-grained materials. The work-hardening rate increases with increasing Mg content, which can alleviate strain localization and thus postpone the occurrence of early necking while decreasing the grain size. Strength-ductility synergy in Al-Mg alloys could be achieved through combining optimized grain refinement with Mg addition.

In Chapter 3, the role of substitutional Mg atoms in the dislocation density evolution and work hardening in Al-Mg alloys was investigated. Fully recrystallized Al-2.5Mg, Al-5Mg and Al-7.5Mg alloys having similar grain size (~10 μm) were fabricated by HPT and subsequent annealing process. The mechanical properties and work-hardening behavior had been investigated after quasi-static tensile deformation. The results showed that the yield strength and work-hardening rate increase with increasing Mg content, resulting in large tensile strength and ductility. In-situ synchrotron XRD measurement was employed to evaluate the evolution of dislocation density and dislocation arrangement during tensile deformation. The XRD results showed that the dislocation density increases faster with strain in Al-Mg alloys having higher Mg contents. Meanwhile, the extent of dislocation rearrangement decreases with increasing Mg content during tensile deformation. TEM observation for deformation structures had confirmed that the addition of solute Mg atoms could hinder dislocation cross slip and promote a transition from wavy slip to planar slip, resulting in a lower rate of dynamic recovery and therefore a higher rate of dislocation accumulation. The present experimental results demonstrated that the Mg atoms played a vital role in the accumulation of dislocations and therefore the work-hardening rate of Al-Mg alloys. Al-Mg

alloys with higher Mg contents possessed much higher dislocation density compared to the low-alloyed Al-Mg alloys because of the important role of solute-dislocation and solute-solute interactions. Thus, adding Mg could be an effective way to improve the strength-ductility synergy of Al-Mg alloys due to high solid solution strengthening and enhanced work hardening.

In Chapter 4, the spatiotemporal characteristics associated with heterogeneous deformation behaviors in Al-Mg alloys were investigated to reveal the relevant mechanisms. It was found that the characteristics of PLC bands depended strongly on the Mg content and grain size. For Al-2.5Mg, Al-5Mg and Al-7.5Mg alloys having similar grain size (~35 μm), increasing Mg content promoted a transition from continuous propagation to hopping propagation and finally to non-propagation behaviors. On the other hand, grain refinement also facilitated a transition from continuous propagation to hopping propagation behaviors in Al-2.5Mg alloy. Through qualitative and quantitative deduction, the traditional dynamic strain aging mechanisms based on long-range lattice/pipe diffusion were disproved. The local rearrangement of the solute atoms by cross-core diffusion could be applied as a partial mechanism to explain the PLC effect observed in Al-Mg alloys, and detailed analysis suggested that that both dynamic strain aging and intensive dislocation interactions were necessary prerequisites to produce the PLC instabilities. The types of deformation bands observed were dependent on the speed that the solute atoms can pin mobile dislocations and the local flow stress within the deformation band.

Detailed DIC analysis showed that island-like heterogeneous deformation and alternate appearance of type A and type C bands occurred in Al-10Mg alloy, which were quite different with the heterogeneous deformation behaviors in Al-Mg alloys with lower Mg contents. For the Island-like heterogeneous deformation at small and intermediate strains, it was considered that solute Mg around dislocations may have reached saturation in Al-10Mg alloy since decreasing the

strain rate from 8.3×10^{-4} to 8.3×10^{-5} s^{-1} or increasing the temperature from room temperature to 50 ℃ did not lead to enhanced serration behavior, whereas increasing strain rate promoted the occurrence of pronounced serration behavior. In contrast, a parallel study on Al-5Mg alloy showed that the serration behavior got enhanced when decreasing the strain rate from 8.3×10^{-4} to 8.3×10^{-5} s^{-1} or increasing the temperature from room temperature to 50 ℃. Therefore, it should be reasonable to consider that solute Mg around dislocations may have reached saturation in Al-10Mg alloy. It was believed that the island-like heterogeneous deformation was the intrinsic characteristic of Al-10Mg alloy and could not be simply explained by diffusion theory because island-like heterogeneous deformation was not observed in Al-5Mg alloy even at an extremely low strain rate of 8.3×10^{-6} s^{-1}. TEM observation showed that planar dislocation arrays form in the early stage of plastic deformation in Al-10Mg alloy, as a result, the dislocation mean free paths decreased with the formation of dislocation networks. Island-like heterogeneous deformation might be explained by the sudden bursts of dislocation motion, and these mobile dislocations could be arrested by obstacles nearby quickly. Consequently, the isolated island-like deformation regions could not group together to form a localized deformation band. As for the alternate appearance of type A and type C bands, the propagation and annihilation of type A band could be explained by the non-uniform levels of work hardening and strain aging; however, the mechanism for a type A band nucleated at the region where type C band had just annihilated during reloading is still unclear.

The results obtained in this study provide new insights into the effects of grain size and Mg contents on deformation behavior and strengthening mechanisms in Al-Mg alloys, and may also contribute to the understanding of work hardening and heterogeneous deformation in other substitutional solid solutions. Further investigation is required to clarify the mechanism of enhanced grain boundary strengthening due to grain boundary segregation and the mechanism of

yielding phenomenon at grain boundary in both ultrafine-grained regimes and coarse-grained regimes. In addition, there's still a gap between atomic-scale dynamic strain aging and macroscopic heterogeneous deformation, quantification of the microscopic formation mechanisms of the bands and the band motion and transition still remains challenging. More theoretical and experimental works on solute-dislocation and dislocation-dislocation interactions are expected to be done in the future to obtain further information on the PLC band formation and propagation events.

Acknowledgements

First and foremost, I would like to express my deepest gratitude to Prof. Nobuhiro Tsuji, for his excellent guidance and constant supports throughout my PhD course. He always encourages me to focus on the important parts of physics problems and to keep the larger context in mind. I sincerely acknowledge his invaluable suggestions and encouragements. My special appreciation goes to Dr. Si Gao for his kind instructions and fruitful discussions. I also acknowledge his patience in proofreading my manuscripts and dissertation. I would also like to express my sincere gratitude to Dr. Myeong-heom Park, Dr. Wu Gong, Dr. Yan Chong and Prof. Akinobu Shibata for their instructions and help. Prof. Yoshikazu Todaka of Toyohashi University of Technology, who kindly providing me the access to their experimental equipment, is also to be thanked.

Moreover, I am indebted to Ms. Akiko Koike, the secretary of Tsuji lab, who always kindly helps me with numerous administrative issues. I am also grateful to the current and former members of Tsuji lab for their kind help and support. I really enjoy the friendly atmosphere in Tsuji lab.

I would also like to express my sincere appreciation to Prof. Hiroshi Okuda and Prof. Hideyuki Yasuda of Kyoto University for evaluating my dissertation and giving their valuable advice.

The scholarship granted by China Scholarship Council, which supported my life during the PhD course, is greatly acknowledged.

Last but not least, I want to thank my family. Without their constant support and love, this work would not have been possible.

List of publications

I. International journal paper

(1) H. Wu, L. Liang, H. Zeng, X. Lan et al. Microstructure and nanomechanical properties of Zr-based bulk metallic glass composites fabricated by laser rapid prototyping. Materials Science and Engineering: A, 765 (2019) 138306.

(2) H. Wu, L. Liang, X. Lan et al. Tribological and biological behaviors of laser cladded Ti-based metallic glass composite coatings. Applied Surface Science, 507 (2020) 145104.

(3) G. Deng, A. Tieu, X. Lan et al. Effects of normal load and velocity on the dry sliding tribological behaviour of CoCrFeNiMo0.2 high entropy alloy. Tribology International, 144 (2020) 106116.

(4) X. Lan, S. Gao, M. Park, A. Shibata, N. Tsuji. Tensile properties of ultrafine-grained Al-2.5mass%Mg alloy fabricated by high-pressure torsion and subsequent annealing processes. (To be submitted)

(5) X. Lan, S. Gao, M. Park, A. Shibata, N. Tsuji. Effects of grain size and Mg contents on the mechanical properties of Al-Mg alloys. (To be submitted)

(6) X. Lan, S. Gao, M. Park, A. Shibata, N. Tsuji. Role of substitutional Mg atoms in the high work-hardening ability of Al-Mg alloys. (To be submitted)

(7) X. Lan, S. Gao, M. Park, A. Shibata, N. Tsuji. Revealing the nature of heterogeneous deformation in Al-Mg alloys. (To be submitted)

II. Presentations in international conference

(1) Xiaodong Lan, Si Gao, Myeong-heom Park, Akinobu Shibata, Nobuhiro Tsuji, Microstructures and tensile properties of ultrafine grained Al-Mg alloys fabricated by high pressure torsion and subsequent annealing. The 10th Pacific Rim International Conference on Advance Materials and Processing, August 2019, Xi'an, China.

(2) Xiaodong Lan, Si Gao, Myeong-heom Park, Akinobu Shibata, Nobuhiro Tsuji, Mechanical properties and strengthening mechanism of ultrafine grained Al-Mg alloys. Materials Research Meeting 2019, December 2019, Yokohama, Japan

III. Presentations in domestic conference

(1) Xiaodong Lan, Si Gao, Myeong-heom Park, Akinobu Shibata, Nobuhiro Tsuji, Deformation behavior and strengthening mechanisms in ultrafine-grained Al-2.5Mg. 日本金属学会 2018 年秋期講演大会，2018 年 9 月，仙台市。

(2) 蘭 小東，高 斯，朴 明験，柴田 曉伸，辻 伸泰，超微細粒 Al-Mg 合金の特徴的な力学特性と DIC 解析。軽金属学会第 135 回秋期大会，2018 年 11 月，東京都。

(3) Xiaodong Lan, Si Gao, Myeong-heom Park, Akinobu Shibata, Nobuhiro Tsuji, Mechanical properties and strengthening mechanisms of ultrafine grained Al-Mg alloy. 日本金属学会 2019 年春期講演大会，2019 年 3 月，東京都。

(4) 蘭 小東，高 斯，朴 明験，柴田 曉伸，辻 伸泰，Al-2.5mass%Mg 合金の引張変形時に生じるセレーションの解析。軽金属学会第 136 回春期大会，2019 年 5 月，富山市。

(5) 朴 明験，Xiaodong Lan，Sukyoung Hwang，辻 伸泰，粒径の異なる Al-Mg 合金におけるセレーション挙動解明。日本金属学会 2019 年秋期講演大会，2019 年 9 月，岡山市。

(6) Xiaodong Lan, Si Gao, Myeong-heom Park, Akinobu Shibata, Nobuhiro Tsuji, Mechanical properties and strengthening mechanisms of ultrafine-grained Al-Mg alloys. 軽金属学会関西支部若手研究者・院生による研究発表会，2019 年 12 月，吹田市。

(7) Xiaodong Lan, Si Gao, Myeong-heom Park, Akinobu Shibata, Nobuhiro Tsuji, Tensile properties and microstructures of ultrafine-grained Al-Mg alloys with different Mg contents. 日本金属学会 2020 年春期講演大会，2020 年 3 月，東京都。